CHEMICAL REVIEWS

Review

Cite This: Chem. Rev. 2020, 120, 3261−3295

pubs.acs.org/CR

Applications of Infrared Multiple Photon Dissociation (IRMPD) to the Detection of Posttranslational Modifications

Philippe Maitre,*[,†] Debora Scuderi,[†] Davide Corinti,[‡] Barbara Chiavarino,[‡] Maria Elisa Crestoni,[‡] and Simonetta Fornarini*[,‡]

[†]Laboratoire de Chimie Physique (UMR8000), Université Paris-Sud, CNRS, Université Paris Saclay, 91405, Orsay, France

[‡]Dipartimento di Chimica e Tecnologie del Farmaco, Università di Roma "La Sapienza", I-00185 Roma, Italy

ABSTRACT: Infrared multiple photon dissociation (IRMPD) spectroscopy allows for the derivation of the vibrational fingerprint of molecular ions under tandem mass spectrometry (MS/MS) conditions. It provides insight into the nature and localization of posttranslational modifications (PTMs) affecting single amino acids and peptides. IRMPD spectroscopy, which takes advantage of the high sensitivity and resolution of MS/MS, relies on a wavelength specific fragmentation process occurring on resonance with an IR active vibrational mode of the sampled species and is well suited to reveal the presence of a PTM and its impact in the molecular environment. IRMPD spectroscopy is clearly not a proteomics tool. It is rather a valuable source of information for fixed wavelength IRMPD exploited in dissociation protocols of peptides and proteins. Indeed, from the large variety of model PTM containing amino acids and peptides which have been characterized by IRMPD spectroscopy, specific signatures of PTMs such as phosphorylation or sulfonation can be derived. High throughput workflows relying on the selective fragmentation of modified peptides within a complex mixture have thus been proposed. Sequential fragmentations can be observed upon IR activation, which do not only give rise to rich fragmentation patterns but also overcome low mass cutoff limitations in ion trap mass analyzers. Laser-based vibrational spectroscopy of mass-selected ions holding various PTMs is an increasingly expanding field both in the variety of chemical issues coped with and in the technological advancements and implementations.

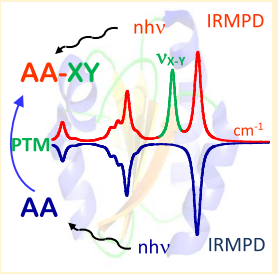

CONTENTS

1. INTRODUCTION

A posttranslational modification (PTM) is a covalent modification occurring downstream after DNA has been

Special Issue: Bond Specific Spectroscopy of Peptides and Proteins

Received: June 21, 2019
Published: December 6, 2019

DOI: 10.1021/acs.chemrev.9b00395
Chem. Rev. 2020, 120, 3261−3295

Table 1. Selected PTMs of Amino Acid Side Chains

PTM	Amino acid(s)	reactant functional group	PTM product group
phosphorylation	serine threonine tyrosine	−OH	$-OPO_3H_2$
O-sulfation	serine threonine tyrosine	−OH	$-OSO_3H$
hydroxylation	proline	−C−H	−C−OH
thiol oxidation	cysteine	−S−H	$-S-OH/-SO_2H/-SO_3H$
S-nitrosation	cysteine	−S−H	−S−NO
thioether oxidation	methionine	$-S-CH_3$	$-S(=O)-CH_3$
nitration	tyrosine	$-C_6H_4(OH)$	$-C_6H_3(OH)(NO_2)$
N-acetylation	lysine	>N−H	$>N-C(=O)CH_3$
N-methylation	lysine arginine	>N−H	$>N-CH_3$
O-glycosylation	serine threonine	−OH	-O-glycan
deamidation	glutamine asparagine	$-C(=O)NH_2$	−C(=O)OH
iodination	tyrosine	$-C_6H_4(OH)$	$-C_6H_3(OH)I$

transcribed into RNA and translated into proteins.[1] PTMs typically affect the side chain of amino acid residues. The introduction of various chemical moieties, not present in proteinogenic amino acids, typically leads to changes in hydrophilicity and more generally in the interactions of the protein with its environment, and thus in its reactivity. The impact of a PTM on a local protein conformation often spurs signaling initiation. PTMs may occur at one or more protein sites, forming the basis for a wide proteome expansion and enlarging the inventory of side chains distributed in a protein. With the posttranslational modification of proteins being a dynamic process, the proteome diversity is enormous and continuously changing in time in each cell. PTMs are usually controlled by enzyme activity. Indeed a protein is not thoroughly characterized unless PTMs such as phosphorylation, sulfation, acetylation, methylation, glycosylation, and disulfide bond formation are not identified and localized. The vast landscape of PTMs has represented a cutting-edge topic in recent years, and various types of PTMs have been discovered and outlined.[1−7] The large number of major and minor groupings of PTMs leads to an enormous variety of proteins possibly existing in a single cell, setting a giant analytical problem. Considerable effort is obviously devoted to develop strategies to evaluate such a rich and varied landscape and to contribute to build an integrated systems biology vision. In this regard, mass spectrometric approaches are playing an increasingly recognized role, relying on the higher sensitivity with respect, for example, to nuclear magnetic resonance (NMR) spectroscopy. On the other hand, NMR spectroscopy is endowed with superior performance in molecular structural characterization. Other currently adopted methodologies include light and electron microscopy, Fourier transform IR spectroscopy, and chip experiments; however, mass spectrometry has become by far the major asset.

Mass spectrometry (MS) basically yields information on the mass to charge ratio (m/z) of the sampled species, and comparison of the experimental and theoretical isotopic patterns allows for the determination of the chemical or molecular formula. High mass resolution allows for readily monitoring any change in m/z, induced for example by the presence of a PTM. Structural information can be derived from fragmentation mass spectra, resulting from the activation of mass-selected molecular ions through ion-neutral collisions. However, this collisional activation allows only indirect structural information to be derived. There is thus a need for structure-selective or even specific fragmentation techniques in order to derive the structural formula.

As developed in greater detail in section 1.2, dissociation methods based on electron attachment on molecular ions provide structurally informative fragmentation patterns. Since the emergence of these techniques with the electron capture dissociation (ECD), multiple methods have been proposed not only limited to Fourier transform ion cyclotron resonance (FT-ICR) instruments but also on more easily available quadrupolar or linear ion traps. UV photodissociation[8−11] and electron photodetachment dissociation[12,13] also provide fragmentation patterns which can be directly related to the ion molecular structure.

Direct information on the molecular structure can be derived from the so-called infrared (IR) fingerprint where IR bands are specific of a functional group and its interaction with the environment. Following the first evidence for the so-called infrared multiple photon dissociation (IRMPD),[14] it has been realized that wavelength selective or even specific ion activation could be performed using IR lasers. Fixed wavelength lasers were first exploited.[15−17] IR spectroscopy in the NH and OH stretching region was then explored with relatively limited intensity table-top lasers, providing a wealth of information on the hydrogen bonding network of microsolvated protonated water or ammonia clusters, in particular.[18,19] It is at the turn of this century that highly intense and widely tunable free electron lasers (FELs) were used for deriving IRMPD spectra of molecular ions under mass spectrometric conditions.[20−37] Because resonant absorption of IR photons depends on molecular vibrations, the subsequent fragmentation event is highly structure specific, revealing characteristic functional groups of the molecule. Obviously, if the functional group (such as the one delivered by a PTM) is embedded in a large biomolecule, spectral congestion prevents a highly detailed structural analysis. It is thus not surprising

DOI: 10.1021/acs.chemrev.9b00395
Chem. Rev. 2020, 120, 3261−3295

that most IRMPD evidence on PTMs has emerged from the study of single amino acids (the minimal model) or small peptides. However, mode specific photon absorption, enabling efficient fragmentation in the presence of the PTM, combined with characteristic fragmentation paths, involving the PTM itself, has allowed fruitful analytical applications on larger systems.[38] Analytical methods take advantage from increasingly widespread IR lasers, tunable over a rather wide range, and on the ultrahigh sensitivity of mass spectrometry. The use of computational resources to supply theoretical IR spectra renders the methodology apt for reference free identification of unknown analytes.[39,40]

1.1. Presence and Function of Common Posttranslational Modifications (PTMs)

This section summarizes PTMs in amino acids and peptides that have been specifically addressed by IRMPD spectroscopy methods, and an inventory of the described PTMs is listed in Table 1.

Phosphorylation is one of the most common types of covalent addition to protein residues, affecting mainly serine, threonine, and tyrosine.[41] This reversible and dynamic process regulates protein functions and plays key roles in prominent cellular processes such as cell growth, differentiation, and apoptosis. Over 100.000 phosphorylation sites are estimated to be present in the human proteome. A large family of enzymes, protein kinases, is in charge of protein phosphorylation.[42] In this process a neutral −OH group is converted into an $-OPO_3H_2$ acidic group, deprotonated at physiological pH. Abnormal phosphorylation levels are related to cell pathologies, and their detection is important for diagnostics purpose in human diseases.[41,43−45]

Beside the phosphoryl group also the sulfuryl group is an inorganic moiety that may be conveyed on the side chain of an amino acid residue.[46] The active agent delivering $-SO_3H$ is 3′-phosphoadenosine-5′-phosphosulfate, which converts an −OH group into a strongly acidic group mainly found as $-OSO_3^-$ at physiological pH. The presence of the anionic tyrosine sulfate, $TyrOSO_3^-$, modification is related to recognition processes,[2] and sulfate moieties in serine, threonine, and tyrosine may be involved in multiple functions including protein assembly, signal transduction, and antithrombotic activity.[47−49]

One category of oxidative PTM is enzyme mediated hydroxylation. The C−H oxidation into C−OH onto the five-member ring of a proline residue is required for proper organization of collagen fibrils.[50] This reaction, involving unactivated C−H bonds, occurs with high regio- and stereospecifity under control of iron based non heme enzymes.[2]

Oxidative conversion of cysteine sulfhydryl (or thiol) groups (−SH) to form −S−S− bridges is a common way to achieve cross-linkages in proteins and peptides.[51,52] For example, disulfide links turn the redox-active tripeptide glutathione (GSH) to its oxidized form (GSSG). However, a cysteine −SH may also undergo oxidation to sulfenic, sulfinic, or sulfonic acid (−SOH, $-SO_2H$, $-SO_3H$, respectively). Reactive oxygen species such as hydrogen peroxide (H_2O_2) and superoxide (O_2^-) stimulate these oxidative PTMs affecting the thiolate side chain of Cys, tuned by the surrounding redox environment.[53,54] Sulfenylation, long considered noxious damage, has in fact emerged as a key step in redox signaling.[55] Sulfenic acid, −SOH, is known to be highly reactive and unstable and likely occurs as transient intermediate. It represents a reversible PTM while further oxidation to $-SO_2H$ and to $-SO_3H$ is largely irreversible.[54]

The thioether functional group of methionine (Met) is also a common target of biologically relevant oxidants. Methionine sulfoxide is a readily formed product. The thioether to sulfoxide change causes a modification in the electron density on sulfur, altering for example Met ligation activity.[56]

The thiolate and thiyl radical from the side chain of cysteine may also react with other reactive molecules such as NO, delivered by NO donors, yielding an S-nitroso derivative. The process is reversible and its regulation is exploited by cells for signaling purposes.[52,57,58] S-Nitrosated glutathione (GSNO) is considered as a key intermediate in the formation and degradation of S-nitrosated proteins.[59] In many cases, S-nitrosation of proteins and altered protein function is associated with pathological states.[60]

Also the nitrogen atom of the indole side chain of tryptophan may become a nitrosation target, depending on the cell redox state. Nitrosation may occur at physiological pH only when the amino group is N-blocked, as in N-acetyltryptophan. The so-formed N-nitroso function may behave as NO carrier, acting in a similar way as S-nitroso thiols in modulating physiological functions such as vaso-relaxation and inhibition of platelet aggregation.[61]

The highly activated phenolic ring of tyrosine is also a target of nitration, mainly performed by NO-derived oxidants in biological systems.[62,63] A nitro group is added in the 3-position, and the ensuing altered physicochemical properties affect enzymatic activity and sensitivity to proteolytic degradation.

Acetylation of the N-terminal side chain (ε-amino group) of lysine is a reversible PTM. In particular, lysine residues in histone proteins undergo acetylation and deacetylation processes that are considered an integral part of the epigenetic code regulating gene transcription.[2,64,65]

N-Methylation is the most studied among methylation processes of protein side chains and is complementary to acetylation involving lysine and arginine on histone tails. It represents a mechanism of epigenetic regulation.[2,66,67]

Covalent glycosylation is the most common PTM,[43,68] and over 50% of all proteins are estimated to be glycosylated.[69] Covalently bound glycans exert an appreciable influence on the physicochemical properties of the protein, including folding, aggregation, and propensity to degrade by protease activity.[70] The glycan chain performs biological roles such as recognition of hormones and toxins, embryonic development, and cell to cell interaction. There are two main types of protein glycosylation, namely N-glycosylation, in which the saccharide is bound to an asparagine residue via an N-acetylglucosamine residue, and O-glycosylation, in which the saccharide is attached to serine or threonine side chains. O-Glycosylation usually involves shorter saccharide units than N-glycosylation.[2,71]

Deamidation is a pH dependent reaction involved in protein degradation. It is due, for example, to the action of bacterial toxin enzymes. It is thought to intervene in cell signaling and metabolic mechanisms and to perform as molecular clock for biological processes.[2,72,73]

The phenolic ring on the side chain of tyrosine is also susceptible to undergo substitution of one or more hydrogen atoms with iodine. Iodination is a PTM essential for thyroid hormonogenesis and iodine storage. Multiple iodination sites

DOI: 10.1021/acs.chemrev.9b00395
Chem. Rev. 2020, 120, 3261−3295

are known to occur on proteins produced by the thyroid gland, consistently involving modification at tyrosine residues.[74,75]

1.2. Problems in the Detection and Localization of PTMs. A Challenge for MS/MS

Detection and analysis of PTMs in peptides and proteins relies on several biochemical wet techniques and on MS-based methods. It is obviously a nontrivial task in consideration of the typically minor change conveyed by a PTM on a usually large protein. Both established methods and continuously devised and upgraded novel approaches have their own strengths and drawbacks, so that a certain target may require diverse and complementary strategies. In the biochemical armory, Western Blot is a powerful technique widely used for the analysis and identification of proteins in biological samples. However, its application to the detection of PTMs is problematic due to the typically low abundance of modified proteins and suffers from the limited number of suitable antibodies.[76]

Several MS-based methods are available to address global and site specific analysis of PTMs.[77−81] PTMs imply a change in the molecular weight of the native protein, and these mass modifications can be detected. However, mass accuracy and mass resolution are crucial aspects in discriminating between native and modified forms of the protein. Alternative approaches are based either on the analysis of peptides obtained by proteolytic digestion of the sampled protein (bottom-up strategy) or on the assay of the intact protein by means of activation toward dissociation using mass spectrometric methods (top-down strategy).

Analysis of proteolytic peptides is achieved by comparing their isotopic patterns to the theoretical ones and performing dissociation experiments to reveal the amino acid sequence and the PTM sites.[82,83] High accuracy mass analyzers have been used exploiting stable isotope labeling in cell culture,[84] chemical derivatization and targeted enrichment,[85] and various procedures to activate the fragmentation of the ionized analyte.[44,86,87] The standard method of fragmentation in tandem mass spectrometry (MS/MS) is collision-induced dissociation (CID). CID relies on the collision of a selected ionic species with a neutral target. The energy of the ion is raised by kinetic to internal energy conversion, and fragmentation may occur. In the CID of peptides fragment ions give information on amino acid nature and sequence, because amide linkages are preferentially cleaved. A few MS/MS studies have reportedly succeeded in the analysis of peptides and proteins, while fragmentations retained the individual PTMs.[88−90]

Generally, though, when a peptide contains a PTM, under CID conditions the preferred fragmentation pattern may be different. Moreover, several PTMs are easily cleaved and neutral loss of the modification may be the prevailing dissociation path. Characteristic neutral losses have a role in identifying glycopeptides and phosphopeptides and also in recognizing oxidized cysteine and methionine residues.[91] Diagnostics of the PTM localization, however, is poor.

A different fragmentation chemistry is observed with methods based on electron transfer. Implemented fragmentation methods widely adopted in proteomics include high-energy collisional dissociation (HCD), electron capture dissociation (ECD), and electron transfer dissociation (ETD).[44,86,92,93] ECD is based on the capture of a low-energy electron (ca. 1 eV) by a multiply charged ion. Following addition of an electron in the π^*_{CO} orbital, radical chemistry results in the peptide backbone, which is preferentially cleaved at the N−Cα bond, rather than at the amide linkage.[93] Because of the very specific radical driven chemistry, ECD is particularly valuable for PTM analysis, achieving fragmentation without loss of labile PTMs, and allows their location to be determined with amino acid resolution.[94−97]

In ETD fragmentation is triggered by an electron transfer event from a molecular anion to multiply protonated peptides and, as observed in ECD, labile PTMs are preserved in the usual fragmentation paths.[98,99] On the negative side, ECD and ETD require multiply charged ions and may not be applied, for example, to singly protonated peptides.[100] ETD and CID provide complementary information for PTM identification.

HCD is used in ion trap mass spectrometers removing a limitation of these instruments, namely the low mass cutoff of fragment ions,[101] and provides increased coverage of peptide sequences.

In UV photon based methods, absorption of a single photon is enough to cause dissociation of a peptide/protein in the gas phase. The photodissociation ensures sequence coverage and fair retention of PTM groups.[102−105]

1.3. Gas Phase IR Spectroscopy of Ions and IRMPD Specificities

It had long been thought that infrared lasers could provide a selective or even specific activation mode of molecular ions. Indeed, if the IR light is provided by a relatively narrowband laser, absorption only occurs if the molecular ion has an IR active mode close to the laser wavelength. This activation mode can thus potentially allow for the specific fragmentation of an ion, depending on the nature of its functional groups and intramolecular interactions.

Fragmentation mass spectra obtained with fixed wavelength IR lasers have been shown to be particularly well suited for distinguishing unmodified from modified (phosphorylated or sulfonated) peptides. This topic is developed in section 4. Using wavelength tunable IR lasers, IR spectra of gas phase molecular ions can be obtained, taking full advantage of the sensitivity, mass accuracy, and mass resolving power of mass spectrometry.

Gas phase infrared spectroscopy is being increasingly used for deriving structural information on molecular ions formed under MS conditions. Its various implementations have been the subject of several reviews addressing the topic from a general viewpoint[22] or focusing on organometallic[23] and biomolecular ions.[26,27,33−35,37] Following a brief introduction of the technique, this section will focus on the experimental set-ups which have been used for obtaining data reported herein on the characterization of PTMs.

The perspectives of the coupling of wavelength tunable infrared lasers with tandem mass spectrometry were drawn in a seminal paper[14] where the first evidence of infrared induced fragmentation of molecular ions trapped in a Penning trap was reported. While mass peak assignment and indirect structural characterization can be derived from MS/MS collision-induced fragmentation, it had been realized for a long time that IR spectroscopy could provide unique direct structural information on molecular ions. The simple measurement of IR absorption spectra,[106] however, is rather difficult due to the low density of trapped ions. In the 1978 paper,[14] it was suggested that gas phase IR spectra of molecular ions could be

DOI: 10.1021/acs.chemrev.9b00395
Chem. Rev. 2020, 120, 3261−3295

derived by monitoring IR induced dissociation as a function of the laser wavelength.

Considering that the energy required for the dissociation of a molecular ion is much greater than that of an infrared photon, the term infrared multiple photon dissociation (IRMPD) was coined. IRMPD relies on the resonant absorption of multiple photons so as to pump vibrational energy into the molecular ion, eventually leading to fragmentation along the lowest energy pathway. Due to the anharmonicity of the vibrational mode, it is generally assumed that the energy pumping proceeds through a noncoherent process, made of cycles of excitation of the resonant vibrational modes and relaxation through relocation of the absorbed IR energy into other vibrational modes, i.e. intramolecular vibrational energy redistribution. IRMPD is thus a slow heating process, very similar to low-energy collisional excitation.[17] Primary fragment ions are comparable with the two processes. Using an ion trap, however, resonant IR activation of these primary fragments may occur, thereby leading to sequential fragmentation. The ensuing IRMPD spectra are thus richer, even for a relatively short irradiation time such as 50 ms, than those obtained with CID driven by radiofrequency ion excitation as performed in a quadrupole ion trap (QIT).[107]

Powerful infrared laser sources are required for driving the IRMPD process. Gas discharge lasers such as CO_2 lasers have first been used. Spectroscopy using these lasers is however limited by their restricted and discontinuous wavelength tunability.[108] Gas phase infrared spectroscopy in the NH and OH stretching mode region was successfully performed exploiting laser sources based on nonlinear optical techniques.[109] These laser sources are typically tunable in the 3 μm region, and valuable information on hydrogen bonding networks can be derived.[109−111] Extension of the spectral range down to 600 cm^{-1} has recently been made available using difference frequency mixing techniques. However, the output power of the table top laser is relatively low and the "messenger technique" is rather taken advantage of.[18,112−115] This sensitive spectroscopic technique relies on the fragmentation of a weakly bound complex formed between the molecular ion and a rare gas atom which can be induced through the absorption of a single IR photon. These complexes are typically formed through addition of rare gas atoms on electrosprayed ions in a cryogenically cooled ion trap, as further illustrated in section 5.

Most of the IRMPD spectra discussed in the present review were recorded using an infrared free electron laser (IR-FEL). IR-FELs have been shown to be particularly well suited for IRMPD spectroscopy of strongly bound molecular ions in the so-called IR fingerprint region. First evidence of IR emission by a FEL was observed at Stanford University.[116] IR-FELs rely on relativistic electron bunches which are generated in the 10−50 MeV range. Photon emission is induced by imposing a sinusoidal trajectory to the electrons when circulating through a series of alternatively poled magnets (undulator) which are placed in the laser cavity. The photon wavelength depends on the electron energy, but when it is fixed, it can rapidly (less than 1s) be tuned by changing the undulator gap. Most of the IRMPD spectra presented here were recorded at the FELIX (Nijmegen, The Netherlands)[117] or CLIO (Orsay, France)[118] facilities. These pulsed lasers run at 10 and 25 Hz, respectively, and deliver so-called macropulses, typically a few microseconds long. Each macropulse consists of a train of picosecond long micropulses, which are spaced by 16 ns at CLIO, and 1 to 40 ns at FELIX. The IR-FEL bandwidth is Fourier transform limited by the duration of the micropulses and typically amounts to 0.5% of the central wavelength.

The overlap between the IR laser beam and the ion cloud is an important issue. Using a QIT,[119] it has been verified that 100% depletion can be achieved with a single IR-FEL macropulse, with a laser beam waist on the order of 1 mm. Ion-laser overlap issues using a QIT have been discussed in detail by Glish and Remes.[120] In a Penning ion trap, however, due to the complex motion of ions, the optimization of the overlap between an IR laser beam and the ion cloud is a more delicate issue. Two different choices have been made at the CLIO and FELIX facilities. In the former, a single pass of the IR-FEL beam is made on the axis of the Penning ion trap of the FT-ICR mass spectrometer. The beam is mildly focused so as to reach a beam waist on the order of 1 mm in the FT-ICR cell.[121] At FELIX, however, a multiple pass configuration has been chosen.[21,35] In either case, the irradiation time is on the order of 100 ms to a few seconds.

IRMPD spectra recorded with a QIT and a FT-ICR mass spectrometer are similar provided that the molecular ions are collisionally thermalized prior to their irradiation.[122] The helium pressure within the ion trap ensures a fast cooling, typically within less than 10 ms.[120] As a result, collisional deactivation of the infrared excited but nondissociated ions occurs between two consecutive macropulses. No such collisional cooling can take place under the low pressure ($<10^{-9}$ mbar) within the FT-ICR cell. Thermalization of the ions has to occur before the transfer to the FT-ICR cell, which can be performed with so-called hybrid FT-ICR mass spectrometers equipped with a quadrupole filter and an argon pressurized linear hexapole ion trap.[121]

It should be noted that revealing weak vibrational bands, especially for strongly bound ions, can be difficult. In such cases, an auxiliary CO_2 laser can be used.[19] In these experiments, a pulsed tunable laser is used to excite the ions and the CO_2 laser is used to provide the ion enough internal energy to dissociate. Alternatively, the already cited messenger technique can be used.[18]

Ultimately, structural assignment of the sampled ion is achieved by comparing its IRMPD spectrum to IR absorption spectra predicted for different candidate structures. Due to the complex multiple photon absorption process, nonlinear effects can be observed, and the relative intensities of the experimental IRMPD bands do not always match with those predicted by theory. These nonlinear effects are typically observed when several IR absorption bands simultaneously overlap with the IR laser. Saturation effects are also observed on resonance with strongly IR active bands. In such cases, better resolved IRMPD bands can be obtained using an attenuated IR-FEL beam. Lower fluence conditions also prevent red-shifts of IRMPD bands.[123]

The "IRMPD intensity" which is plotted as a function of the laser wavenumber to yield an IRMPD spectrum can be defined in different ways.[124] IRMPD is a pseudo-first-order unimolecular dissociation process, and it has been shown that plotting the first-order laser-induced photodissociation rate constant as a function of the laser wavenumber presents several advantages. In particular, compared to photodissociation yield and depletion/appearance methods, a better link with calculated infrared absorption spectra is obtained. Calculations can be performed at different levels of theory, but hybrid

DOI: 10.1021/acs.chemrev.9b00395
Chem. Rev. 2020, 120, 3261−3295

density functional methods such as B3LYP[125,126] have been shown to perform very well.[25,27] Harmonic frequencies usually have to be scaled.[127] While no universal scaling factor value exists, it has been shown that an average absolute difference on the order of 25 cm^{-1} between calculated and experimental IR absorption spectra can be obtained using a dual scaling factor approach.[127] Typically, a scaling factor value on the order of 0.98 can be used for frequencies in the 800−1800 cm^{-1} range, while a lower value (0.95−0.96) has to be used for the more anharmonic CH, NH, and OH stretching bands in the 3000−3800 cm^{-1} range. However, the frequencies associated with several PTM vibrational modes should rather be left unscaled, according to reported evidence.[128−131]

While nonlinear IRMPD effects lead to differences between experimental IRMPD and calculated IR absorption intensities, clear-cut structural conclusions can be made on the comparison of IRMPD spectra with predicted IR spectra of different candidate structures. Indeed, the IRMPD band positions typically match those predicted by theory for the IR absorption spectra. This notion is consistent with the fact that the IRMPD process is triggered only when the IR laser is resonant with an IR active vibrational mode. It should also be emphasized that the isomeric form of the electrosprayed ions typically corresponds to the lowest energy structure.

As said above, ions are thermalized at room temperature through multiple collisions with a rare gas prior to their irradiation by the IR lasers. As a result, multiple low energy isomers may be populated, as revealed by IRMPD spectroscopy in several examples. Different strategies have been developed to overcome these limitations and improve the analytical capabilities of IRMPD. Isomer separation can be achieved based on their ion mobility either using a drift tube device or a differential mobility filter. Isomer specific IR spectroscopy can also be based on double resonance (IR−IR of tagged-ions or UV−IR) of cryogenically cooled ions. Another asset of the tagging approach is that it opens the door for multiplexing IRMPD fragmentation since only detachment of the tag is observed upon IR activation. These topics are discussed in section 5.

2. INDIVIDUAL PTMS REVEALED BY IRMPD SPECTROSCOPY

In the following paragraphs, the present review provides a collection of data about specific functions that are known to perform as PTM in natural peptides and proteins. As mentioned above, most data regard functionalized amino acids that represent minimal models for the PTM placed on a much larger biomolecule. So the much more complex environment faced by the PTM in the biological medium is hardly taken into account. However, the simple modified amino acid constitutes the founding base to rationalize the spectroscopic properties of PTMs in the more complex biological environment. There are still many unresolved challenges involved in the unambiguous determination of the presence and the site of PTMs, and there is a strong quest for innovative strategies capable to localize PTM sites and to release structural information with growing sensitivity, selectivity, and throughput. IRMPD can usefully assist in this search.

2.1. Oxo Forms

The amino acid cysteine is particularly susceptible to redox based modifications whereby the thiol group (−SH) can be progressively oxidized to sulfenic (−SOH), sulfinic ($-SO_2H$), and sulfonic ($-SO_3H$) acid. Intrinsic properties of cysteine sulfenic, sulfinic, and sulfonic acids have been examined by IRMPD spectroscopy in the mid-IR range.[132] The experimental spectra of the deprotonated species ($[CysSO_x\text{-}H]^-$ (x = 1−3), the notation simply indicating the number of S-bonded oxygen atoms with no inference about the actual deprotonation site) have been interpreted in combination with ab initio DFT calculations and molecular dynamics (MD) simulations. The latter method enables conformational dynamics to be assayed and anharmonic effects to be directly integrated in the spectroscopic analysis. The increasing acidity of the $-SO_xH$ functionality with growing number of oxygen atoms bears direct consequence in the IRMPD spectra. In fact, the 750−1900 cm^{-1} fingerprint range explored in the IRMPD spectra reported in Figure 1 encompasses vibrational modes that are highly revealing in terms of structural features.

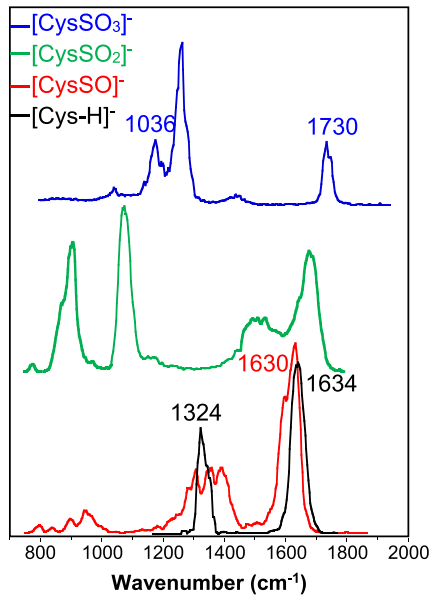

Figure 1. IRMPD spectra of deprotonated cysteine ($[Cys\text{-}H]^-$) and deprotonated cysteine oxo-forms ($[CysSO_x\text{-}H]^-$, x = 1−3). Adapted with permission from ref 132. Copyright 2016 John Wiley and Sons.

The carboxylic group is the deprotonation site in the least acidic sulfenic derivative (pK_a ca. 7.6), as indicated by the highly active antisymmetric stretch of the carboxylate, $-CO_2^-$, at 1630 cm^{-1}, matching the corresponding band in the IRMPD spectrum of deprotonated cysteine, also reported in Figure 1 for comparison purposes.[133,134] On the other end, deprotonation occurs on the highly acidic $-SO_3H$ group of cysteine sulfonic acid (pK_a < 2), leaving the carboxylic acid functionality unaffected, as testified by the characteristic vibrational modes associated to the carbonyl stretching vibration at 1730 cm^{-1} and the in-plane COH bending mode at 1036 cm^{-1}.

The landscape of optimized structures for $[CysSO_x\text{-}H]^-$ (x = 1−3) presents a commonly favored conformer, stabilized by the $S(O_{x-1})O^-\cdots HOCO\cdots HN$ or $S(O_{x-1})OH\cdots {}^-OCO\cdots HN$ network of hydrogen bonding interactions. This pattern of noncovalent interactions is displayed in Figure 2, showing the result of natural bond orbital analysis. A trend in delocalization energy may be recognized along the series $[CysSO\text{−}H]^-$ < $[CysSO_3\text{−}H]^-$ < $[CysSO_2\text{−}H]^-$. The orbitals mainly con-

DOI: 10.1021/acs.chemrev.9b00395
Chem. Rev. 2020, 120, 3261−3295

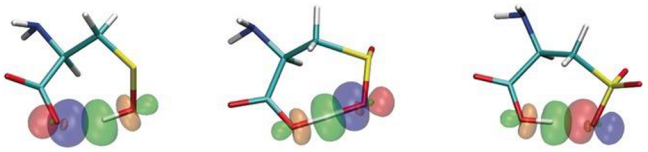

Figure 2. Natural bond orbitals responsible for hydrogen bonding interactions in $[CysSO\text{-}H]^-$, $[CysSO_2{-}H]^-$, and $[CysSO_3{-}H]^-$, from left to right, respectively. The acceptor oxygen lone pair is shown in blue/red and the antibonding O−H orbital in green/orange. Reproduced with permission from ref 132. Copyright 2016 John Wiley and Sons.

tributing to the hydrogen bond are a lone pair orbital on the acceptor oxygen atom and the antibonding, vacant orbital on the donor O−H bond.

One may note that in $[CysSO_2{-}H]^-$ the hydrogen bond interaction appears to be equally partitioned along the CO···H···OS axis and the proton shared between the two oxygen atoms. This finding, consistent with the comparable acidity of the carboxylic and the sulfinic acid groups, renders a static DFT computational approach inadequate to describe deprotonated cysteine sulfinic acid, which is instead well interpreted by ab initio molecular dynamics (MD) simulations. The MD simulations show clearly that the proton is equally shared between the two comparably basic terminals, $-SO_2$ and $-CO_2$, at variance with $[CysSO{-}H]^-$ and $[CysSO_3{-}H]^-$, where the proton is tightly bound to the most basic site. This occurrence explains the failure of any meaningful matching between observed bands and harmonic frequencies obtained by DTF calculations. Table 2 summarizes significant vibrational signatures that are associated to the alteration of cysteine imparted by oxidative PTMs. The S−OH stretching and bending modes of $[CysSO{-}H]^-$ at 794 and 1354/1392 cm^{-1}, respectively, find a counterpart in corresponding modes recorded at 890 and 1100 cm^{-1} in the IRMPD spectrum of an inorganic ion, $S(OH)_3^+$.[135] Likewise, the symm/asymm SO_3 stretching modes of $[CysSO_3{-}H]^-$ at 1036/1258 cm^{-1} find a matching in the corresponding absorbances in the spectra of inorganic cluster ions of HSO_4^-.[136]

Interestingly, while ($[CysSO_2{-}H]^-$ and $[CysSO_3{-}H]^-$ are obtained by negative ESI of the parent acids that are commercial products, cysteine sulfenic acid is a transient species that may not be isolated. However, mass spectrometric procedures allow formation and storage of otherwise fleeting species. Thus, $[CysSO{-}H]^-$ ions have been successfully obtained by collision-induced dissociation of cysteine S-sulfate ions at m/z 200, $[cysS{-}SO_3{-}H]^-$, along a fragmentation path that has been the focus of a recent in depth study.[137]

The thioether group of methionine residues is also an oxidation target. Being converted into sulfoxide form through a reversible reaction, it may act as protective agent against reactive oxygen species. The vibrational signature for the S═O bond was clearly identified in a study exploiting IRMPD spectroscopy to investigate a controversial topic, namely the occurrence of one electron versus two electron oxidation mechanisms of methionine.[131] Figure 3 shows the IRMPD

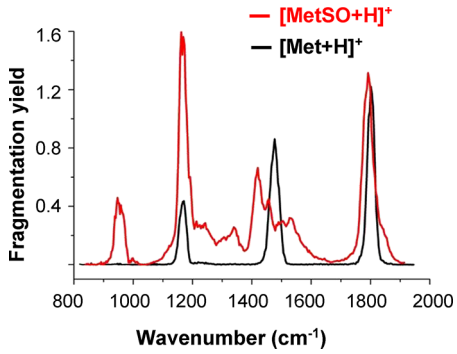

Figure 3. IRMPD spectra of $[Met+H]^+$ and $[MetSO+H]^+$ in the 800−2000 cm^{-1} wavenumber range (depicted in black and red, respectively). Adapted with permission from ref 131. Copyright 2011 Elsevier.

spectra of protonated methionine, $[Met+H]^+$, and protonated methionine sulfoxide, $[MetSO+H]^+$. The first one displays three prominent bands at 1170, 1477, and 1800 cm^{-1} associated to the in plane C−O−H bending, the umbrella mode of the ammonium group, and the C═O stretching

Table 2. Summary of Characteristic Vibrational Modes Associated to Oxidative PTMs of Cys and Met Residues[a]

Functionality	Vibrational mode	Mode assignment	Sample molecule	ref
−SOH	1354/1392(m/m)	SOH bend	cysteine-sulfenic ac.	132
	794 (w)	S−OH stretch	cysteine-sulfenic ac.	
$-SO_3^-$	1036 (w)	symm SO_3 stretch	cysteine-sulfonic ac.	132
	1172 (m)	asymm SO_3 stretch		
	1258 (s)	asymm SO_2 stretch		
$-S(=O)CH_3$	947 (m)	S═O stretch	methionine sulfoxide	131
	1050 (m)	S═O stretch	Met-Lys sulfoxide	131
	ca. 1000 (m)	S═O stretch	Lys-Met sulfoxide	139
	998 (s)	S═O stretch	Met-Trp sulfoxide	140
	1028 (s)	S═O stretch	Trp-Met sulfoxide	140
	1003 (m)	S═O stretch	Met-Val sulfoxide	141
	1024 (m)	S═O stretch	Val-Met sulfoxide	141
	1038 (m)	S═O stretch	Glutathione-$S(O)CH_3$	140
$-S(O_2)CH_3$	1128 (s)	symm SO_2 stretch	methionine sulfone	139
	1307 (m)	asymm SO_2 stretch	methionine sulfone	139
	1127 (m)	symm SO_2 stretch	Glutathione-$S(O_2)CH_3$	140

[a]Experimental features are reported as observed in IRMPD spectra, typically interpreted and substantiated by computational analysis. Qualitative scale of band activity: w (weak), m (medium), s (strong).

DOI: 10.1021/acs.chemrev.9b00395
Chem. Rev. 2020, 120, 3261−3295

mode, respectively. Their position is well matched by the IR spectrum pertaining to the lowest energy conformer of methionine protonated on the amino group, characterized by the S···HNH···O═C hydrogen bonding network. The spectrum of $[MetSO+H]^+$ presents a remarkable difference due to the appearance of a distinct band at 947 cm^{-1}, besides few additional features. This band is ascribed to the stretching mode of the S═O group, and the position of individual features is well interpreted by the S═O···HNH···O═C hydrogen bonding frame of the ground state conformer. In particular, the strong involvement of the S═O group as hydrogen bond acceptor is held responsible for a red-shifted stretching frequency when compared, for example, with the corresponding resonance in dimethylsulfoxide or in protonated sulfuric acid.[138]

In Met-containing peptides, the methionine sulfoxide signature is recognized in the stable oxidation product of the methionine-lysine dipeptide (Met-Lys), extracted from human prion protein sequence, and obtained by γ radiolysis in N_2O atmosphere.[131] The IRMPD spectrum of the protonated dipeptide $[(Met-Lys)+H]^+$ presents in fact a blank region where a prominent band at 1050 cm^{-1} appears in the spectrum of the oxidized species $[(MetSO-Lys)+H]^+$ (Figure 4). The

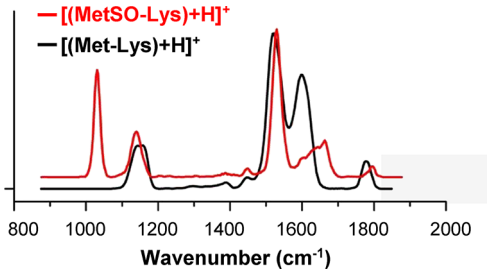

Figure 4. IRMPD spectra of $[(Met-Lys)+H]^+$ (black) and $[(MetSO-Lys)+H]^+$ (red) in the 800−1900 cm^{-1} wavenumber range. Adapted with permission from ref 131. Copyright 2011 Elsevier.

presence of this sharp band, blue-shifted compared to the one from $[MetSO+H]^+$, supports the formation of a sulfoxide function which was found to result both by reaction of hydrogen peroxide and by one electron oxidation by •OH radicals in the presence of catalase, which better mimics the oxidation of a methionine residue after oxidative stress.

The same oxidation procedure applied to the lysine-methionine dipeptide (Lys-Met) yields the expected sulfoxide product together with a decarboxylation product, and IRMPD spectroscopy of the corresponding protonated species, $[(Lys-Met)+H]^+$, $[(Lys-MetSO)+H]^+$, and $[(Lys-Met)+H-CO_2]^+$, has delivered the spectra plotted in Figure 5.[139] Once again, the additional presence of a band around 1000 cm^{-1} testifies oxidation at the thioether function. Bands associated to the carboxylic group, such as the C═O stretching around 1800 cm^{-1} and the COH bending at 1150 cm^{-1}, are missing in the IRMPD spectrum of $[(Lys-Met)+H-CO_2]^+$.

The sulfoxide signature at ca. 1000 cm^{-1} characteristic of the oxidized thiomethyl group of methionine is clearly recognized also in the IRMPD spectrum of the oxidation product of other dipeptides, such as Val-Met, Tyr-Met, and Met-Met.[139] Similarly, a sulfoxide functionality is revealed at 1028 and 998 cm^{-1} in the IRMPD spectra of protonated Trp-Met and Met-Trp bearing an additional O-atom, respectively.[140] Only on the latter dipeptide, though, has the protonated mono-

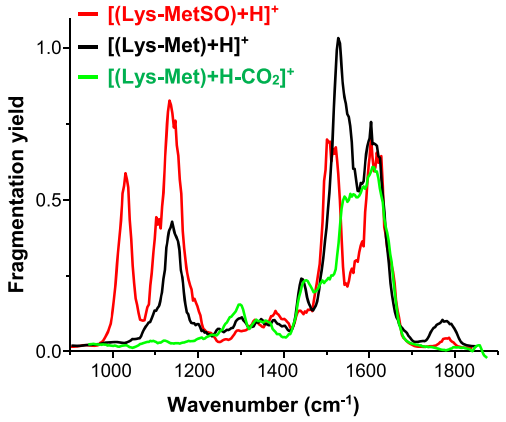

Figure 5. IRMPD spectra of $[(Lys-Met)+H]^+$, $[(Lys-MetSO)+H]^+$, and $[(Lys-Met)+H-CO_2]^+$ in the 800−1900 cm^{-1} wavenumber range. Adapted with permission from ref 139. Copyright 2013 Elsevier.

oxidized form displayed evidence for oxidation occurring also on the aromatic ring of Trp, consistent with a band at 1461 cm^{-1} ascribed to the bending mode of a phenolic COH group.

In the oxidation of methionine in two peptides of reverse sequence, Met-Val and Val-Met, IRMPD spectra were interpreted by static DFT calculations and MD simulations.[141] The stable geometries of the sulfoxo derivatives of the two peptides have taken into account that methionine sulfoxide is chiral. In fact the energy required for stereoinversion at the sulfoxide chiral center is high enough to make the two possible epimers, methionine S-sulfoxide and methionine R-sulfoxide, optically stable at room temperature.[142] Figure 6 reports IRMPD spectra of $[(MetSO-Val)+H]^+$ and $[(Val-MetSO)+H]^+$ together with IR spectra for the most stable conformer, selected as an example out of the rich and thermally populated conformational space. Depicted on the right are the geometries of both epimers, with the R-sulfoxide being slightly more stable. The reverse chirality at sulfur yields very similar calculated IR spectra for the two diastereisomers, at variance with previously reported findings on diastereoisomeric discrimination by IRMPD spectroscopy.[143−146] Once again, a signature for the S═O stretching mode is found at 1003 and 1024 cm^{-1} in the IRMPD spectra of $[(MetSO-Val)+H]^+$ and $[(Val-MetSO)+H]^+$, respectively, in an otherwise blank region in the spectra recorded for the native peptides $[(Met-Val)+H]^+$ and $[(Val-Met)+H]^+$. The lower ν(S═O) value for $[(MetSO-Val)+H]^+$ is accounted for by the somewhat stronger S═O···HN^+ hydrogen bond, as indicated by the shorter distance in the computed structures.[141]

The superior performance of MD simulations becomes evident in Figure 7, showing the IR absorption spectra obtained from the simulations starting from the lowest energy conformers depicted in Figure 6. For both isomers the IR spectrum calculated from the dynamics reproduces quite well the experimental IRMPD spectrum. This finding is verified particularly in the case of the S═O stretching mode at ca. 1000 cm^{-1}, involved in the S═O···HN^+ hydrogen bond.[141]

Based on the collected evidence on oxidation signatures of Met-containing peptides, IRMPD spectroscopy has helped to elucidate a long-range electron transfer mechanism from Tyr to oxidized Met leading to repair of Met and formation of tyrosyl radical, as observed to intervene in Met-Enkephalin peptide.[139]

DOI: 10.1021/acs.chemrev.9b00395
Chem. Rev. 2020, 120, 3261−3295

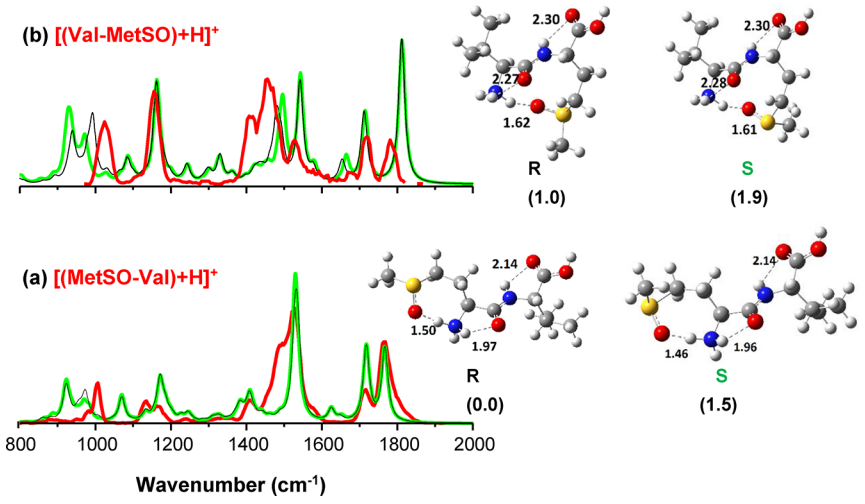

Figure 6. IRMPD spectra (in red) of $[(MetSO{-}Val)+H]^+$ and $[(Val{-}MetSO)+H]^+$ compared with the calculated IR spectra for the most stable conformer of each species in either R or S configuration (black and green trace, respectively). The corresponding structures are shown on the right together with their relative ΔG_{298} (kJ mol^{-1}). H-bond distances are in Å. Adapted from ref 141. Copyright 2017 American Chemical Society.

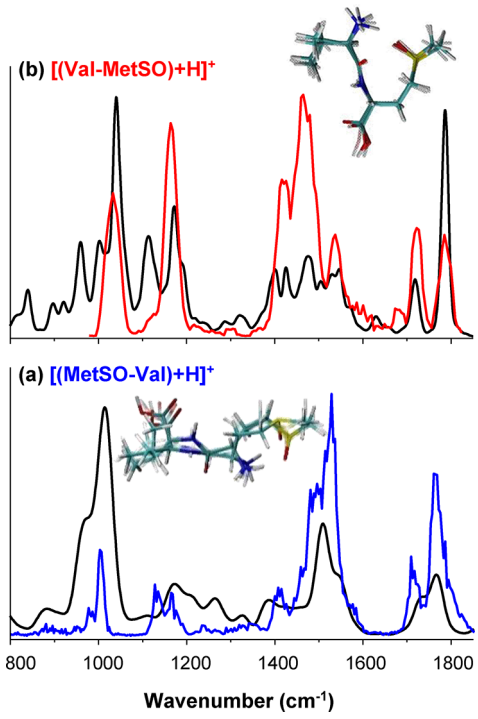

Figure 7. IRMPD spectra of $[(MetSO{-}Val)+H]^+$ and $[(Val{-}MetSO)+H]^+$ ((a) in blue and (b) in red, respectively) compared with MD vibrational spectra. Selected snapshots along the MD trajectory are shown in superimposed molecular structures. Adapted from ref 141. Copyright 2017 American Chemical Society.

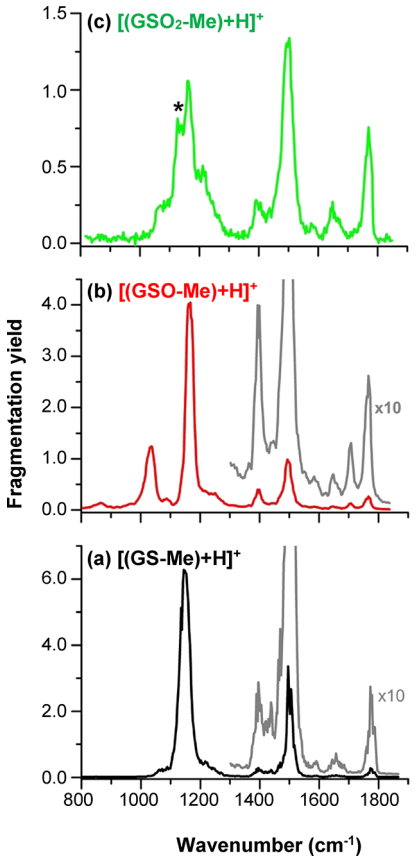

Figure 8. IRMPD spectra of (a) $[(GS\text{-}Me)+H]^+$, (b) $[(GSO\text{-}Me)+H]^+$, (c) $[(GSO_2\text{-}Me)+H]^+$. Adapted from ref 140, with permission from the PCCP Owner Societies.

IRMPD spectroscopy has also enabled us to ascertain the common sulfoxide structure when Met-Val undergoes oxidation by either radiolysis or electrochemistry.[147]

The oxidation of a thioether function has been revealed also on a methyl-modified form of a ubiquitous tripeptide, *S*-methylglutathione (GS-Me).[148] Figure 8a reports the IRMPD spectrum of protonated GS-Me, $[(GS\text{-}Me)+H]^+$, which resembles closely the spectrum recorded for protonated glutathione[149] being characterized by two strong absorptions at 1152 cm^{-1}, associated to the bending of the C−OH groups of the Gly and Glu residues, and at 1505 cm^{-1}, assigned to the NH_3^+ umbrella bending mode and the Cys and Gly amide II modes.[140] The potentially characteristic CH_3−S stretching mode is expected to be weakly active at 660−630 cm^{-1}, thus below the inspected wavenumber range.[150] The oxidized form of GS-Me, containing an additional O atom, presents a distinctive absorption at 1038 cm^{-1}, which is a signature of the sulfoxide functionality, in the spectrum of the protonated species, $[(GSO\text{-}Me)+H]^+$, shown in Figure 8b.[140] Thioether

DOI: 10.1021/acs.chemrev.9b00395
Chem. Rev. 2020, 120, 3261−3295

oxidation can also proceed to the sulfone stage yielding GSO_2-Me, and the band at 1127 cm^{-1}, marked by an asterisk in the spectrum of $[(GSO_2\text{-Me})+H]^+$ reported in Figure 8c, is ascribed to the sulfone vibrational mode. It is in fact consistent with the IRMPD spectrum of protonated methionine sulfone where pronounced features at 1128 and 1307 cm^{-1} are ascribed to the symmetric and asymmetric SO_2 stretching modes, respectively.[139]

2.2. Hydroxo Forms

Hydroxylation of proline involves regiospecific hydroxylation of the native amino acid generating a chiral center. Enzymatic hydroxylation yields (2*S*,4*R*)-4-hydroxyproline (Hyp) while formation of the (2*S*,4*S*)-4-hydroxyproline (hyp) epimer is not observed in natural proteins. Discrimination between protonated species ($HypH^+$ and $hypH^+$) has been achieved using IRMPD spectroscopy.[151]

As shown in Figure 9, the C═O stretching frequency of the carboxylic group at 1750 cm^{-1} for $HypH^+$ is shifted to 1770 cm^{-1} for $hypH^+$. Moreover, the latter diastereoisomer is unique in being characterized by a distinct band at 1333 cm^{-1}, ascribed to a major contribution of COH bending and NH_2 wagging modes. In other words, selective fragmentation of $HypH^+$ and $hypH^+$ can be obtained at 1750 and 1770 cm^{-1}, and specific fragmentation of $hypH^+$ can even be obtained when the laser is on resonance with the IR signature at 1333 cm^{-1}.

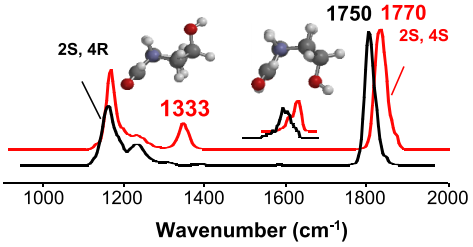

Figure 9. IRMPD spectra in the mid-IR range of protonated (2*S*,4*R*)-4-hydroxyproline ($HypH^+$, black trace) and protonated (2*S*,4*S*)-4-hydroxyproline ($hypH^+$, red trace) and the representative most stable conformer for each species. Adapted from ref 151. Copyright 2012 American Chemical Society.

The experimental IRMPD spectra, both in the mid-IR and in the NH/OH stretching range, are nicely interpreted by the calculated IR spectra of the lowest lying conformers (structures shown in Figure 9), corroborating their major contribution in the sampled ion population. The ionic hydrogen bonds between the protonated amino group and both the hydroxyl and the carboxylic C═O groups are the key factors in explaining the spectral differences. The strongly IR active carboxylic OH at 3551/3556 cm^{-1} for $HypH^+$/$hypH^+$, respectively, can be used as a structural signature using an OPO/OPA. The individual configuration at C(4) is found to determine a preference for $HypH^+$ to attain C(4)-*exo* ring puckering while for $hypH^+$ to rather adopt C(4)-*endo* puckering.[151] This divergent stereochemical preference is responsible for the distinct features in the IRMPD spectra and reflects the same bias observed in the neutral epimers even when part (Hyp) of collagen protein. The end result is the observed chirality induced discrimination in IR spectroscopic behavior.

2.3. Phosphorylation

Hydroxyl groups in the aliphatic or aromatic side chain of serine (Ser), threonine (Thr), or tyrosine (Tyr) are the target of reversible phosphorylation, the most frequently occurring PTM. The presence of the phosphoric ester group is responsible for both characteristic vibrational modes and specific photofragmentation behavior, as described in a comprehensive study on the protonated species of the phosphorylated amino acids ($pSerH^+$, $pThrH^+$, $pTyrH^+$).[128] In the case of $pThrH^+$ and $pSerH^+$, photofragmentation occurs by loss of a 98 Da unit, formally H_3PO_4, while cleavage of a 46 Da unit, formally H_2O+CO, is observed from $pTyrH^+$. Vibrational spectra, both experimental and simulated ones, are displayed in Figure 10. Table 3 summarizes the most significant phosphorylation signatures emerging from IRMPD spectroscopy.

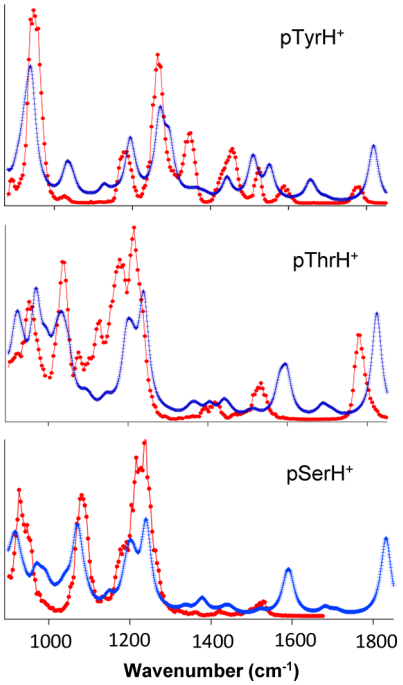

Figure 10. IRMPD spectra (in red) of $pThrH^+$, $pSerH^+$, and $pTyrH^+$ compared with the IR spectra for the Maxwell−Boltzmann weighted conformer population of each species (in blue). Reprinted from ref 128. Copyright 2008 American Chemical Society.

POH bending and P−OH stretching modes of the phosphate group contribute to a pronounced feature in the 920−970 cm^{-1} range in the spectra of $pThrH^+$, $pSerH^+$, and $pTyrH^+$ and to a second major feature at 1040/1080 cm^{-1} in the spectra of $pThrH^+$/$pSerH^+$. This latter band appears instead as a weak absorption at 1026 cm^{-1} in the spectrum of $pTyrH^+$. However, as shown in Figure 10, while the experimental spectra of $pSerH^+$ and $pThrH^+$ are fairly similar, the IRMPD spectrum of $pTyrH^+$ is quite distinct. The difference emerges clearly in the superposition of the spectra for $pThrH^+$ and $pTyrH^+$ displayed in Figure 11. In particular, a noteworthy feature diagnostic of phosphorylation is the P═O stretch which is observed at around 1220/1230 cm^{-1} for $pThrH^+$ and $pSerH^+$ while at 1265 cm^{-1} for $pTyrH^+$. This difference is ascribed to the flexible structure of $pThrH^+$ and $pSerH^+$ which allows the phosphoryl group to be engaged in strong H-bonding with the protonated amino group, causing

DOI: 10.1021/acs.chemrev.9b00395
Chem. Rev. 2020, 120, 3261−3295

Table 3. Summary of Characteristic Vibrational Features Associated to Phosphorylation of Ser, Thr, and Tyr Residues[a]

Vibrational mode	[pSer+H]$^{+}$[b]	[pThr+H]$^{+}$[b]	[pTyr+H]$^{+}$[b,c]	[GlypTyr+H]$^{+}$[d]	[(pTyr+H)·H_2O]$^{+}$[c]
ν(P−OH)/δ(POH)	920−970 (s)	967 (s)	946 (s)	∼950 (s)	
ν(P−OH)/δ(POH)/ν(PO−C)	1080 (s)	1035 (s)			930 (s)
δ(POH)			1026 (w)	∼1000 (s)	1004 (w)
ν(PO−C)					1223 (m)
ν(P═O)	1228 (s)	1216 (s)			1283 (s)
ν(P═O)/ν(PO−C)			1265 (s)	1200−1300 (s)	
ν(C(═O)O−H)			3552 (s)		3558 (s)
ν(PO-H)			3667 (s)		3667 (s)

Vibrational mode	[pSer-H]$^{-}$[e]	[pThr-H]$^{-}$[e]	[pTyr-H]$^{-}$[e]	$H_2PO_4^{-}$[e]	$(C_2H_5O)_2PO_2^{-}$[f]
ν(P−OH)	836 (m)	842 (m)		764 (s)	
$\nu_s(PO_2^{-})$	1028 (w)	1000 (w)	1098 (s)	1106 (m)	1080 (s)
δ(POH)	1108 (m)	1106 (w)	1050 (w)		
$\nu_{as}(PO_2^{-})$	1290 (s)	1300 (s)	1270 (s)	1297 (w)	1280 (s)

[a]Experimental features are reported as observed in IRMPD spectra, typically interpreted and substantiated by computational analysis. Qualitative scale of band activity: w (weak), m (medium), s (strong). [b]Reference 128. [c]Reference 143. [d]Reference 155. [e]Reference 157. [f]Reference 158.

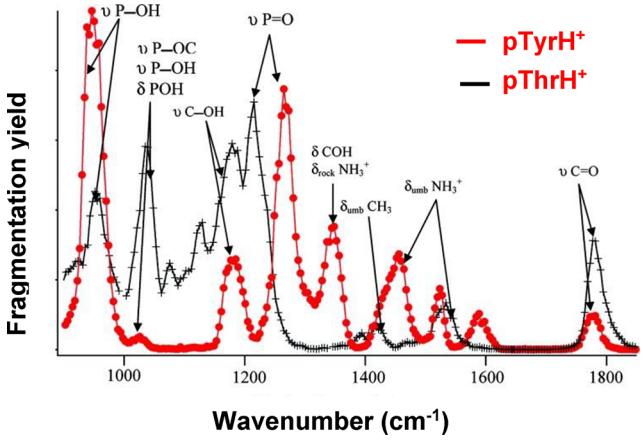

Figure 11. IRMPD spectra of pTyrH^{+}(red) and pThrH^{+} (black). Reprinted from ref 128. Copyright 2008 American Chemical Society.

P═O bond weakening and the P═O stretching frequency to be red-shifted. The same interaction is instead prevented by the rigid aromatic linker in pTyrH^{+}.[128] Two most stable conformers were identified, conforming to similar geometries as reported by IR spectroscopy of protonated native tyrosine.[152] The two conformers lie close in energy (and free energy) and present quite similar IR absorption spectra. In the most favored one the phosphate group and amino acid chain face each other on the same side of the aryl ring. However, although the P═O bond is pointing toward the ammonium group, their distance is too wide for any significant hydrogen bond interaction.[153]

It may be useful to note that the IRMPD spectrum of protonated native serine presents negligible activity in the 1000−1300 cm^{-1} range characteristic of $-OPO_3H_2$ vibrations[129,154] allowing the signature for this PTM to come clearly into sight when comparing the IRMPD spectrum of the native amino acid with the spectrum of the modified species.

While it would be desirable to connect the characteristic P═O stretch frequency to phosphorylation at either Ser/Thr or Tyr residues as a means to discriminate between alternative sites, the just noticed sensitivity to environment makes this expectation hard to fulfill when the amino acid is inserted in a complex peptide or protein network. An example is reported on a 12 residue peptide, YPEFPLSPPKKK, an excerpt of stathmin protein. The doubly protonated phosphorylated peptide, [YPEFPLpSPPKKK+2H]$^{2+}$, presents a few broad absorptions that are missing in the IRMPD spectrum of the native peptide, in particular around 1080 and 1240 cm^{-1}, suggested to be the signature for the presence of phosphorylated serine (pS) (Figure 12).[128]

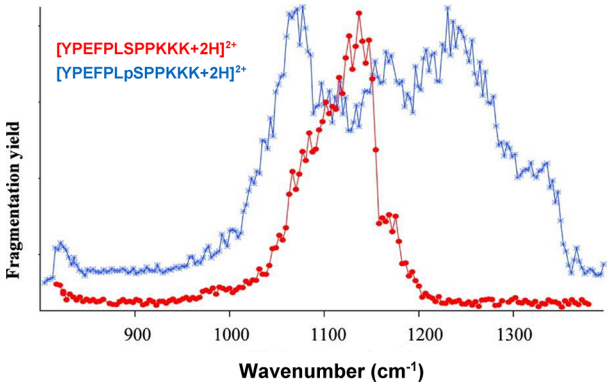

Figure 12. Experimental IRMPD spectra for doubly protonated phosphorylated, [YPEFPLpSPPKKK+2H]$^{2+}$ (blue), and native, [YPEFPLSPPKKK+2H]$^{2+}$ (red), peptides. Reprinted from ref 128. Copyright 2008 American Chemical Society.

The influence of the environment surrounding the $-OPO_3H_2$ group is already remarkable in a simple, exemplary dipeptide, GlypTyr. Protonation on the Gly N-terminus allows [GlypTyr+H]$^{+}$ to attain a folded most stable configuration whereby the phosphoryl oxygen is a potent hydrogen bond acceptor toward the charged ammonium ion.[155] As a consequence, the P═O stretch contribution in the IRMPD spectrum is found to conform to the behavior displayed by pSerH^{+} rather than by pTyrH^{+}, with the latter species lacking any possible P═O involvement in hydrogen bonding.[155]

A similar limited, though highly influential, environmental change is induced by microhydration of pTyrH^{+} by a single water molecule.[153] The IRMPD spectrum in the X−H (X = C, O, N) stretching range is well interpreted by the IR spectrum of the lowest energy structure pointing to the water molecule placed as a bridge between the phosphoryl group and the

DOI: 10.1021/acs.chemrev.9b00395
Chem. Rev. 2020, 120, 3261−3295

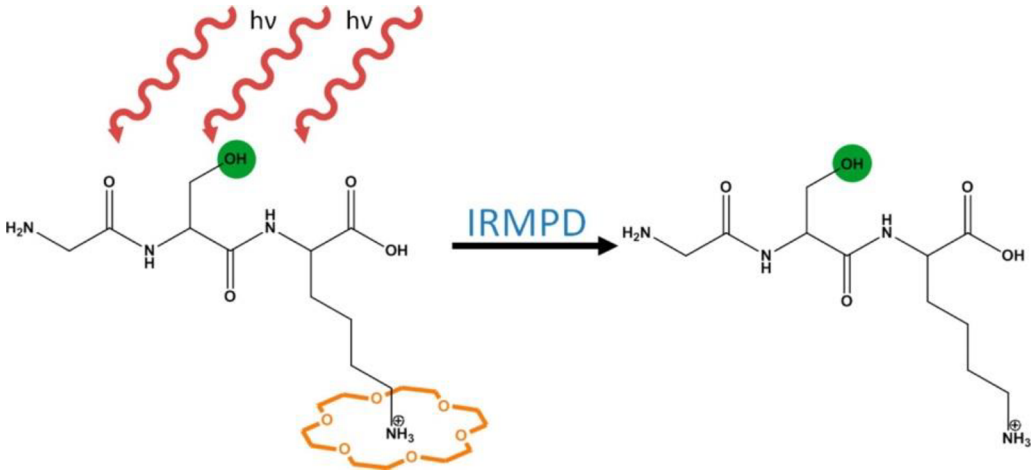

Figure 13. Crown ether 18-crown-6 (18c6), solvating the protonated amino group, is released when the adduct is heated by resonant photon absorption on the serine OH stretch. Reprinted from ref 159. Copyright 2012 American Chemical Society.

protonated amino group. The ensuing network of hydrogen bonds, P═O···H−O(H)···H−N^+, accounts for the broad and red-shifted bands pertaining to the implicated OH/NH stretching modes. In the same range, the PO−H stretching modes display a distinct resonance at 3667 cm^{-1}, at the same frequency as free $pTyrH^+$ (Table 3), summing the contribution of symmetric and antisymmetric $P(OH)_2$ stretches.[153]

Doubly protonated phosphorylated peptide ions, namely $[ApSAAR+2H]^{2+}$ and $[AApSAR+2H]^{2+}$ have been assayed by IRMPD spectroscopy in order to learn about the structure of these species and establish a correlation with ion mobility experiments and observed collisional cross sections.[156] To this end, experiments performed in the mid-IR range, yielding four broad bands ascribed to general peptide modes, were not deemed diagnostic. In the frequency range pertaining to N−H/O−H stretching vibrations, both peptide ions display two sharp absorptions at 3663/3558 and 3662/3560 cm^{-1}, for $[ApSAAR+2H]^{2+}$ and $[AApSAR+2H]^{2+}$, respectively. The band at higher frequency is assigned to the O−H stretching mode of free hydroxyl in the phosphate group while the second one comprises asymmetric stretching modes of the Arg guanidinium ion and the O−H stretch of free carboxylic hydroxyl. However, for both isomeric peptide ions highly informative modes pertain to lower frequency NH/OH stretches involved in H-bond interactions. In this spectral range computational simulations have failed to provide an unambiguous picture, predicting exceptionally high activity and poorly represented frequency values. An improved agreement with the experimental spectrum was shown by the IR absorption spectrum recalculated with second order anharmonic corrections for the NH/OH stretches.[156]

The deprotonated phosphorylated amino acids, $[pTyr-H]^-$, $[pSer-H]^-$, and $[pThr-H]^-$, represent more faithfully the charge state of a phosphorylated amino acid in the biological environment. IRMPD spectroscopy has been performed on these negative ions as well as on free $H_2PO_4^-$ ion as reference.[157] Due to the comparatively strong acidity of the $-OPO_3H_2$ group, deprotonation is found to involve the phosphoric functionality rather than the carboxylic group and the experimental IRMPD spectra are well interpreted by the IR spectra pertaining to the most stable isomer. As already observed on the corresponding protonated species, also in this case the rigid aromatic linker in $[pTyr-H]^-$ ensures spatial separation between the $-OPO_3H^-$ substituent on the aryl ring and the remaining part of the amino acid. Thus, as shown by the data listed in Table 3, the frequencies for symmetric PO_2^- stretch and POH bend are closely matched by the ones pertaining to free phosphate,[157] also listed in Table 3. In contrast, in the case of pSer and pThr, the $-OPO_3H^-$ group is involved in a network of noncovalent interactions, behaving as strong hydrogen bond acceptor in the PO_2^-···HOC interaction and as H-bond donor in the POH···NH_2 contact. These interactions are held responsible for the blue-shifted POH bending mode, at 1108 cm^{-1} for $[pSer-H]^-$ and 1106 cm^{-1} for $[pThr-H]^-$, relative to 1050 cm^{-1} for $[pTyr-H]^-$. Conversely, the PO_2^- symmetric stretching is red-shifted at 1028 cm^{-1} for $[pSer-H]^-$ and 1000 cm^{-1} for $[pThr-H]^-$, to be compared with 1098 cm^{-1} for $[pTyr-H]^-$ and 1106 cm^{-1} for $H_2PO_4^-$ ion. Another appropriate reference is provided by the IRMPD spectrum of deprotonated diethyl phosphate, showing the PO_2^- symmetric/antisymmetric stretching modes at 1080/1280 cm^{-1} (Table 3),[158] in nice agreement with the corresponding frequencies recorded for the free phosphate of $[pTyr-H]^-$. The emerging pattern is consistent, though qualitative in character, in view of the high degree of coupling of vibrational modes pertaining to amino acid frame and phosphate ester group.

The PO−H stretching frequency of the phosphate group[153] reported at 3667 cm^{-1} for $[pTyr+H]^+$ lies at the high energy end of the range typical for OH stretches pertaining to amino acids and peptides. This notion has provided the basis for a diagnostic tool proposed to clearly distinguish between phosphorylated peptides (containing pSer, pThr, and/or pTyr) and native peptides (containing Ser, Thr, and/or Tyr).[34,159] In order to design a practical analytical method that could allow simultaneous detection of (phosphorylated)-peptides in a mixture, a multiplexed IRMPD spectroscopy has been devised based on sampling noncovalent complexes of ionized peptides with crown ether 18-crown-6 (18c6). This molecule is selected for the high binding affinity for protonated amino groups. The procedure is reminiscent of the ion tagging method used in vibrational predissociation spectroscopy as "messenger technique".[109,113] In this way, a common and unique photofragmentation channel is recorded for all analytes, releasing the 18c6 ligand and the protonated peptide, as depicted in Figure 13.

DOI: 10.1021/acs.chemrev.9b00395
Chem. Rev. 2020, 120, 3261−3295

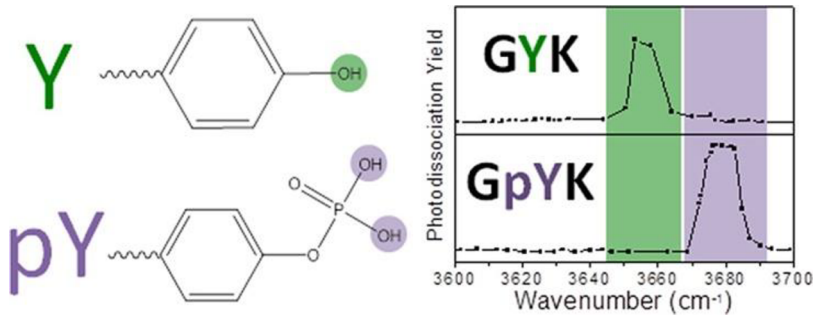

Figure 14. Excerpt of IRMPD spectra of noncovalent complexes of 18c6 with protonated GYK and GpYK peptides. Colored areas mark the range for phosphate OH stretches (purple) and phenol OH stretch (green). Reprinted from ref 159. Copyright 2012 American Chemical Society.

The consequence of phosphorylation is evident in the excerpt of IRMPD spectra of a modified and native tripeptide, GYK and GpYK, respectively, displayed in Figure 14.[159] The phosphate OH stretching in the 3665−3685 cm^{-1} range (purple area in Figure 14) replaces the phenol OH stretching of the native tyrosine residue that is active in the 3645−3665 cm^{-1} range (green area in Figure 14). The distinct wavenumber ranges for phosphate OH stretches (3665−3685 cm^{-1}), phenol/alcohol OH stretches (3640−3670 cm^{-1}), and carboxylic acid OH stretches (3550−3590 cm^{-1}) thus provide a potential means to reveal the occurrence of phosphorylation. Achievement of this goal is illustrated by the IRMPD spectra of representative native and phosphorylated tripeptides (Figure 15).[159] Notably, IRMPD spectra were recorded simultaneously for the peptide mixture in a multiplexed fashion and each peptide responded along the vibrational modes of respective functional groups.

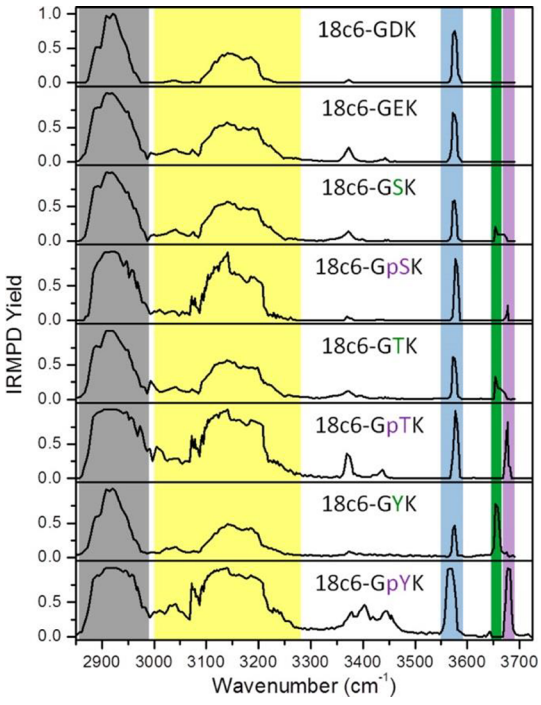

Figure 15. IRMPD spectra of the 18c6-adducted protonated peptides. Colored areas mark the wavenumber range for phosphate OH stretches (purple), phenol/alcohol OH stretch (green), carboxylic acid OH stretch (blue), $-NH_3^+$ stretches (yellow), and CH stretches (gray). Reprinted from ref 159. Copyright 2012 American Chemical Society.

The predictive power of this assay has been further successfully tested on an octapeptide (GAAAAAYK) and its Y-phosphorylated derivative (GAAAAApYK).[159] The presence (or absence) of phenol OH or phosphate OH stretching bands still provides a diagnostic feature. Sampling of OH stretching modes on other larger phosphorylated peptides, namely Ac-pYA_3SK, Ac-YA_3pSK, and Ac-YA_3pTK, by IR-UV double resonance spectroscopy confirms phosphorylation on tyrosine, unambiguously indicated by the OH stretch transition at 3670 cm^{-1}.[160] However, when the PTM involves the serine or threonine residue, one fails to detect any band in the 3665−3685 cm^{-1} region diagnostic for OH stretches of the phospho group. A likely explanation lies in this group being involved in hydrogen bonding which is known to induce red shift and broadening in the affected OH stretch absorption bands, making their detection problematic and likely lying beyond the inspected range.[160]

One may conclude that the general reliability of the OH stretching range for identifying characteristic features for the phosphorylation PTM needs to pass a preliminary test on model compounds prior to being used with novel analytes.

2.4. O-Sulfation

Sulfation is related to phosphorylation in that their differentiation by mass spectrometric analysis is challenging, due to the the nearly isobaric nature of the two $-PO_3H_2$ and $-SO_3H$ PTM groups, differing in mass by only 9.5 mDa.[161] As a consequence, formally equal fragmentation channels are observed by CID. Therefore, any possible discrimination by vibrational spectroscopy is particularly desirable. The phenol hydroxyl group of a Tyr residue in YG dipeptide may undergo both phosphorylation and sulfation, yielding pYG or sYG, respectively. Figure 16 displays IRMPD spectra in the OH stretching range showing a clear signature for the native and two modified pYG or sYG dipeptides. The native peptide is characterized by the phenol OH stretch at 3645 cm^{-1}, the pYG by the phospho OH stretch at 3670 cm^{-1}, and the sYG by the sulfate OH stretch at 3590 cm^{-1}.[162] Operating at fixed 3590 cm^{-1} wavenumber for analytical purposes, one would observe specific photofragmentation of the sulfated dipeptide, while operating at 3670 cm^{-1} only pYG would be found IRMPD active. Thus, monitoring photodissociation activity in correspondence with the two specific resonances may reveal which PTM (sulfation or phosphorylation) is in fact present in the assayed peptide. This finding is reported to hold also true for tripeptides bearing either sulfated or phosphorylated Tyr residues, mimicking a proteolytic digest. The same diagnostic bands can also be recognized when the two PTMs affect the neurotransmitter Leu-Enkephalin (YGGFL) which is promis-

DOI: 10.1021/acs.chemrev.9b00395
Chem. Rev. 2020, 120, 3261−3295

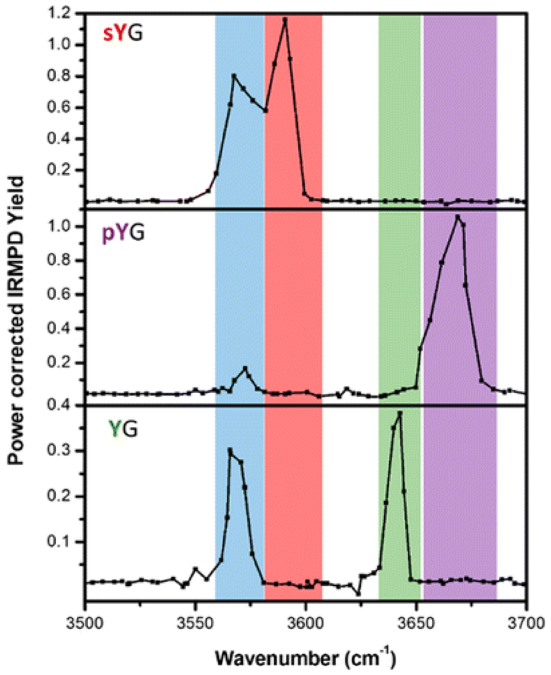

Figure 16. IRMPD spectra of protonated YG, pYG, and sYG. Colored areas mark the band position for phosphate OH stretch (purple), phenol/alcohol OH stretch (green), sulfate OH stretch (red), and carboxylic acid OH stretch (blue). Reprinted from ref 162. Copyright 2014 American Chemical Society.

ing evidence in view of an analytical exploitation of this criterion. Thus, it appears that the OH stretches pertaining to $-PO_3H_2$ and $-SO_3H$ groups in the modified peptides are not significantly sensitive to the nearby environment, at least in the reported cases. In particular, there seems to be not a major effect played by potential acceptor groups that could engage in H-bonding the sampled hydroxyls, shifting their diagnostic resonance. At least a significant fraction of the assayed peptide ions seems not to be perturbed by H-bonding. A contributing factor may be ascribed to the experiment being run at room temperature, hampering relatively weak noncovalent interactions. The characteristic OH stretch resonances at 3580–3600 cm^{-1} for sulfate and at 3655–3680 cm^{-1} for phosphate lend themselves to a semiquantitative estimate of the relative presence of the two PTMs in a mixture. In fact, exhaustive irradiation at each resonant frequency leads to complete depletion of the absorbing species, leaving the inert one unpertubed, so indicating the relative amount of each component. Complementary photofragmentation on the two individual wavenumber channels was successfully tested on weighted mixtures of pYG and sYG dipeptides.[162] In a quite similar way, the distinct OH stretch resonances have allowed to discriminate between isobaric sulfated and phosphated saccharides, presenting individual absorptions at 3595 and 3666 cm^{-1}, respectively.[163] The distinctive signature of the assayed OH stretching modes thus provides a reliable diagnostic for sulfated and phosphated biomolecules, rather independent from the specific molecular frame.

O-Sulfation applies also to alcoholic OH groups, such as the one on the side chain of Ser. The way this PTM affects structural motifs has been the topic of a thorough investigation by IRMPD spectroscopy on both protonated and deprotonated species of sulfated L-serine, $[sSer+H]^+$ and $[sSer-H]^-$, respectively.[129] Figures 17 and 18 show the IRMPD spectra of the sulfated ions, together with the ones of the corresponding native species, $[Ser+H]^+$ and $[Ser-H]^-$, as assayed by IRMPD spectroscopy.[133,154]

Dominant bands in the spectrum of $[Ser-H]^-$ are associated with the NH_2 scissor mode coupled with the antisymmetric (at 1610 cm^{-1}) and symmetric (at 1330 cm^{-1}) carboxylate stretches. Conversely, the C═O stretching mode absorbing at 1732 cm^{-1} in the spectrum of $[sSer-H]^-$ rather supports a neutral carboxylic functionality and deprotonation occurring at

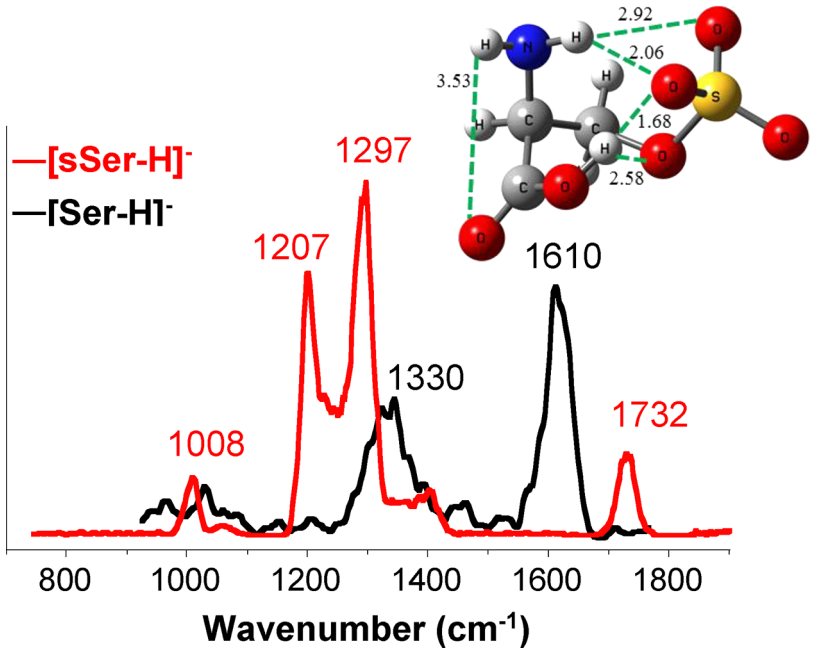

Figure 17. IRMPD spectra of $[sSer-H]^-$ (red profile) and $[Ser-H]^-$ (black profile) and optimized geometry for lowest energy isomer. Adapted from ref 129 with permission from the PCCP Owner Societies.

DOI: 10.1021/acs.chemrev.9b00395
Chem. Rev. 2020, 120, 3261–3295

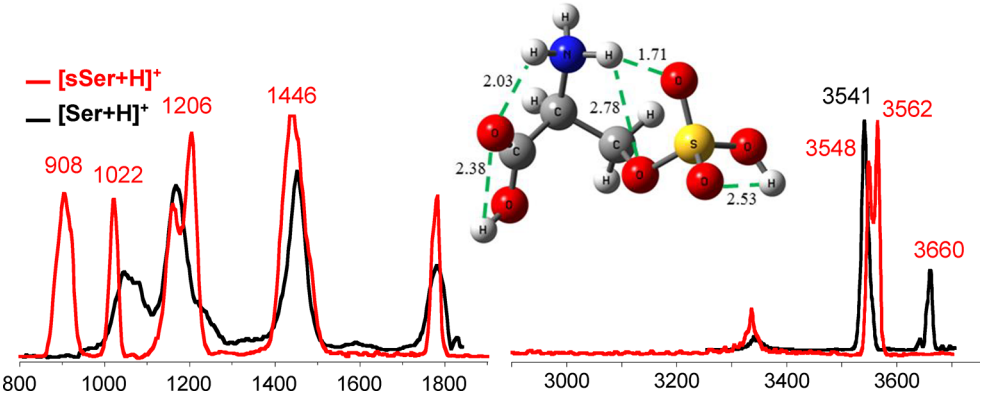

Figure 18. IRMPD spectra of $[sSer+H]^+$ (red profile) and $[Ser+H]^+$ (black profile) and optimized geometry for lowest energy isomer. Adapted from ref 129 with permission from the PCCP Owner Societies.

the sulfate group. Computed optimized structures for $[sSer-H]^-$ present a set of low energy conformers that are likely to collectively contribute to the sampled ion population. A representative rotamer displayed in Figure 17 shows the multiple hydrogen bonding network conferring a rather compact assembly, that is common to the whole family of structures. Vibrational analysis allows us to ascribe the pronounced IRMPD absorptions at 1207 and 1297 cm^{-1} to the highly active antisymmetric SO_3 stretch coupled to NH_2 twisting (at 1207 cm^{-1}) and antisymmetric SO_2 stretching (at 1297 cm^{-1}). Symmetric SO_3 stretchings contribute to the relatively weaker band at 1008 cm^{-1}. Active frequencies for symmetric and antisymmetric SO_3 stretching modes comply with the range reported for gaseous HSO_4^- water clusters.[164]

The IRMPD spectrum of $[sSer+H]^+$ displays two novel absorptions in the 800−1200 cm^{-1} range when viewed against the spectrum of native $[Ser+H]^+$, whereas comparable bands appear in the 1400−1800 cm^{-1} range (Figure 18).[129] In the OH stretching range O-sulfation generates a new band at 3562 cm^{-1}, replacing an absorbance of $[Ser+H]^+$ at 3660 cm^{-1}.[129]

According to calculations the favored protonation site of sSer is the N atom of the amino group, as in the native amino acid and in the phosphorylated derivative.[128,154] The most stable isomer, depicted in Figure 18, is characterized by a network of hydrogen bond motifs linking two ammonium hydrogens to the carbonyl oxygen, a sulfuryl oxygen, and the sulfoester oxygen. Vibrational analysis of the high energy portion of the spectrum shows the PTM to be responsible for silencing of the OH stretch of Ser side chain 3660 cm^{-1} and for the emerging feature at 3562 cm^{-1} due to sulfate OH stretch which provides a signature for the sulfation event. This resonance is partly merged with but still distinct from the carboxylic acid OH stretch, which remains active at about the same frequency also in the sulfate derivative. Vibrational modes due to sulfur bonding are found in the band at 908 cm^{-1} due to coupled SOH bending and S−OH stretching modes, while sulfate ester C−OS and CO−S stretches give rise to the conspicuous band at 1022 cm^{-1}.[129] The band at 1206 cm^{-1} involves a contribution of symmetric SO_2 stretch while antisymmetric SO_3 stretch is not resolved from the NH_3^+ umbrella mode in the broad band at 1446 cm^{-1}.

Notably, while $[sSer-H]^-$ displays an IRMPD spectrum that is well interpreted by an IR spectrum obtained from a Boltzmann averaged conformer population, accounting for the flexible arrangement of this species in comparably stable geometries, $[sSer+H]^+$ conforms to the vibrational features of the single most stable conformer. The localized positive charge on the ammonium group apparently imparts stiffness onto ionized sSer. According to the spectra reported in Figures 17 and 18, both protonated and deprotonated sSer display peculiar absorbances that are signatures of the sulfation PTM in IR ranges otherwise poorly active for the native amino acid.

2.5. S-Nitrosation

L-Cysteine is responsible for transport and storage of NO, paramount messenger molecule, via reversible S-nitrosation (also commonly named S-nitrosylation).[52,57,58] The S-nitrosation motif has been the focus of IRMPD spectroscopy on both protonated and deprotonated ions deriving from S-nitrosocysteine, $[SNOCys+H]^+$ and $[SNOCys-H]^-$.[165] The NO releasing activity of nitrosated cysteine and cysteine methyl ester is also testified by the facile (photo)fragmentation process of the protonated species, occurring by homolytic S−N bond cleavage and leading to the corresponding radical cation.[165,166] The comparison of the IRMPD spectra of $[SNOCys+H]^+$ and $[Cys+H]^+$,[167] in Figure 19, shows that the former has a distinct IR signature at 1783 cm^{-1}. IRMPD spectroscopy on the ^{15}N labeled species reveals that this band splits into two distinct features at 1718 and 1782 cm^{-1}. While the second absorption is associated with the carboxylic C═O stretching (see the corresponding band at 1761 cm^{-1} in the IRMPD spectrum of the native species), the band at 1718 cm^{-1} is ascribed to the red-shifted $^{15}N-O$ stretching mode. Thus, the NO oscillator does not provide an evident diagnostic signature in IR spectroscopy of unlabeled $[SNOCys+H]^+$ ions. Theoretical calculations succeed in interpreting the experimental spectrum by a convolution of IR frequencies and intensities reflecting the Maxwell−Boltzmann conformer distribution at the room temperature of the experiment. The lowest energy conformer is shown in Figure 19.

The IRMPD spectra of the deprotonated ions, $[Cys-H]^-$ and $[SNOCys-H]^-$, reported in Figure 20 are noticeably different from the ones of the positively charged counterparts.[165] The native amino acid diplays only two major bands.[133] The spectrum of $[SNOCys-H]^-$, however, displays in addition a clear IR signature at 1460−1488 cm^{-1}.[165] Once again the labeled species $[S^{15}NOCys-H]^-$ presents a frequency shift in the singular band in the mid range to 1418−1454 cm^{-1}. A red shift of about this size, ca. 30 cm^{-1} for ^{14}N to ^{15}N substitution on the NO oscillator, is also reported in IRMPD spectroscopy of inorganic complexes bearing a NO ligand.[168−170] The broad and composite character of this

DOI: 10.1021/acs.chemrev.9b00395
Chem. Rev. 2020, 120, 3261−3295

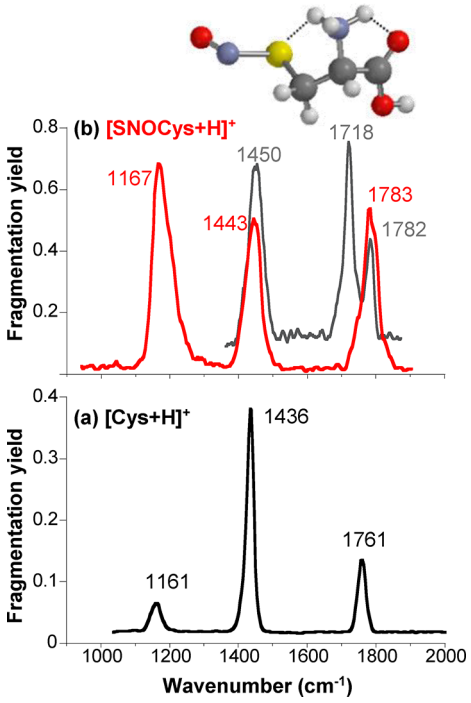

Figure 19. IRMPD spectra of $[Cys+H]^+$ (a) and of $[SNOCys+H]^+$ (b). The gray profile in panel (b) shows the effect of ^{15}N-labeling in $[S^{15}NOCys+H]^+$. The geometry of the lowest energy conformer of $[SNOCys+H]^+$ is shown. Adapted with permission from ref 165. Copyright 2012 Elsevier.

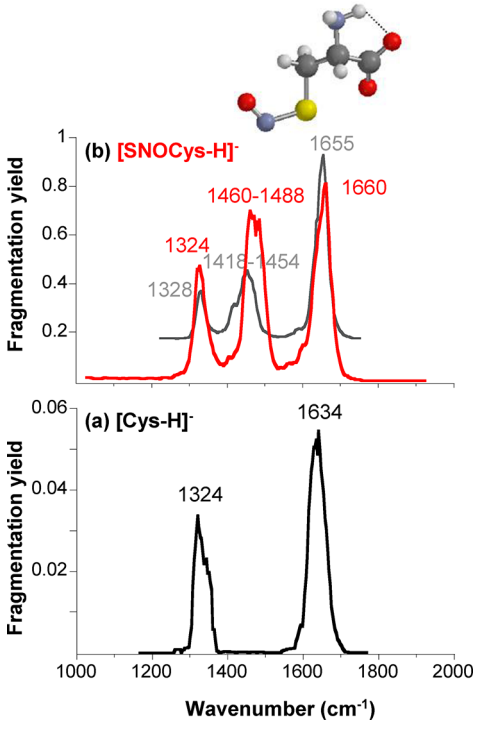

Figure 20. IRMPD spectra of $[Cys-H]^-$ (a) and of $[SNOCys-H]^-$ (b). The gray profile in panel (b) shows the impact of ^{15}N-labeling in $[S^{15}NOCys+H]^+$. The geometry of the lowest energy conformer of $[SNOCys-H]^-$ is also shown. Adapted with permission from ref 165. Copyright 2012 Elsevier.

band is accounted for by an array of comparably stable conformers contributing to the sampled ion population. The most stable one is shown on top of Figure 20. The most important conclusion is that the activity of the NO stretching mode appears in an otherwise nearly blank section of the IRMPD spectrum of native $[Cys-H]^-$, offering the chance to unambiguously reveal S-nitrosation of cysteine.

Transnitrosation reactions in biological systems are largely mediated by glutathione (GSH), where cysteine is inserted in a tripeptide (γ-GluCysGly), and S-nitroso glutathione (GSNO) performs as NO carrier.[59] Protonated GSNO, $[GSNO+H]^+$, has been assayed by IRMPD spectroscopy (Figure 21).[149]

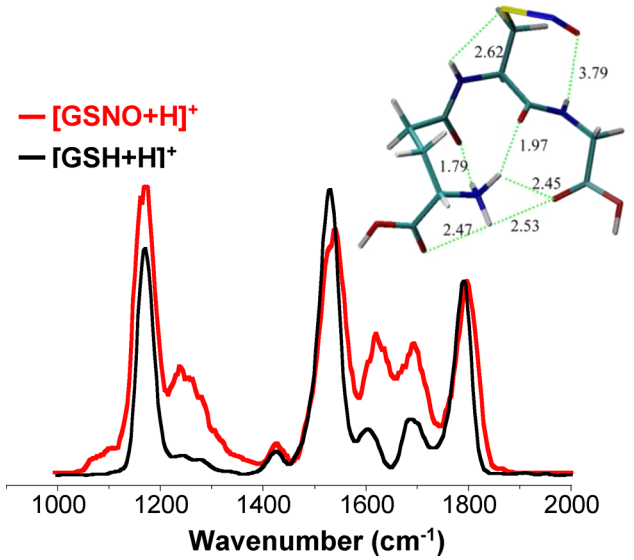

Figure 21. IRMPD spectra of $[GSH+H]^+$ (black profile) and of $[GSNO+H]^+$ (red profile). The lowest energy structure of $[GSNO+H]^+$ is depicted on top. Adapted from ref 149. Copyright 2014 American Chemical Society.

Analysis of IR features has relied on the combined information from IRMPD spectroscopy of $[GSH+H]^+$ and of ^{15}N labeled $[GS^{15}NO+H]^+$ together with an extensive computational inquiry of the potential energy surface for the two species. In particular, two independent approaches have been used to thoroughly explore the vast conformational space of both $[GSH+H]^+$ and $[GSNO+H]^+$. $[GSNO+H]^+$ ions are present as a thermally averaged mixture of multiple conformers, characterized by NO stretches mainly responsible for the pronounced bands at 1622 and 1690 cm^{-1}.[149] A common structural feature revealed by the spectroscopic and computational survey is the SNO group exposed on the periphery of the molecule, thus prone to perform the NO carrier function.

In view of the important role of SNO groups as nitric oxide reservoirs and donors, the S-nitroso derivative of a synthetic amino acid, L-captopril, used in the treatment of cardiovascular diseases, has been assayed by IRMPD spectroscopy. The NO stretching mode presents a neat band at 1716 cm^{-1} in the IRMPD spectrum of the protonated species, that is well interpreted by calculations.[171]

S-Nitrosation signatures obtained by IRMPD spectroscopy are listed in Table 4.

2.6. N-Nitrosation

The N atom in the heteroaromatic ring of tryptophan residues can also be a nitrosation target, depending on the cellular redox state, when the α-amino group is blocked. N-Nitrosotryptophan derivatives share similar properties as S-

DOI: 10.1021/acs.chemrev.9b00395
Chem. Rev. 2020, 120, 3261−3295

Table 4. Summary of Vibrational Signatures Associated to Nitrosation and Nitration[a]

Vibrational mode	ν(SN−O)	$\nu_{symm}(NO_2)$	$\nu_{asymm}(NO_2)$
$[SNOCys+H]^{+}$[b]	1783 (s)		
$[SNOCys-H]^{-}$[b]	1460−1488 (s)		
$[GSNO+H]^{+}$[c]	1622−1690 (m)		
$[NANT-H]^{-}$[d]	∼1463 (s)		
$[nitroTyr+H]^{+}$[e]		1330 (s)	1540 (m)

[a]Experimental features are reported as observed in IRMPD spectra, typically interpreted and substantiated by computational analysis. Qualitative scale of band activity: m (medium), s (strong). [b]Reference 165. [c]Reference 149. [d]$[NANT-H]^{-}$ is deprotonated *N*-acetyl-N^1-nitrosotryptophan. Reference 172. [e]$[nitroTyr+H]^{+}$ is protonated 3-nitrotyrosine. Reference 174.

nitrosothiols. This PTM has been assayed by IRMPD spectroscopy of the deprotonated species from N-acetyl-N^1-nitrosotryptophan, $[NANT-H]^{-}$.[172] The spectrum of $[NANT-H]^{-}$ has been analyzed by comparison with the one for deprotonated N-acetyltryptophan, $[NAT-H]^{-}$, and by the support of theoretical calculations. The experimental spectrum of $[NANT-H]^{-}$ appears more complex (Figure 22), showing in particular a prominent band at 1463 cm^{-1}, highly intense if compared with the corresponding band of $[NAT-H]^{-}$ at 1452 cm^{-1}. The remarkable activity and some sensitivity to ^{15}N substitution in the nitroso group, red shifting the maximum to 1445 cm^{-1}, suggest a major contribution of the NO stretching mode. Analysis the corresponding normal mode reveals that this band is an unresolved envelope of NH and indole CH bends, CH_2 scissor, and NO stretching modes. The relatively large bandwidth in the absorption features of both spectra in Figure 22 is once again dependent also on the contribution of several conformers of comparable energy in the sampled population. The structures of the most stable rotamer of $[NANT-H]^{-}$ and of $[NAT-H]^{-}$ are reported beside the IRMPD spectra in Figure 22. Both geometries present a H-bond interaction between a negatively charged carboxylate oxygen and the amide NH group.[172] One can thus conclude that irradiation at 1463 cm^{-1} would lead to the selective fragmentation of N-nitrosotryptophan containing molecular ions. The nitrosation signature is in the list reported in Table 4.

2.7. Nitration

Nitration may affect the aryl ring of tyrosine residues and is considered a sign of oxidative damage exerted by reactive

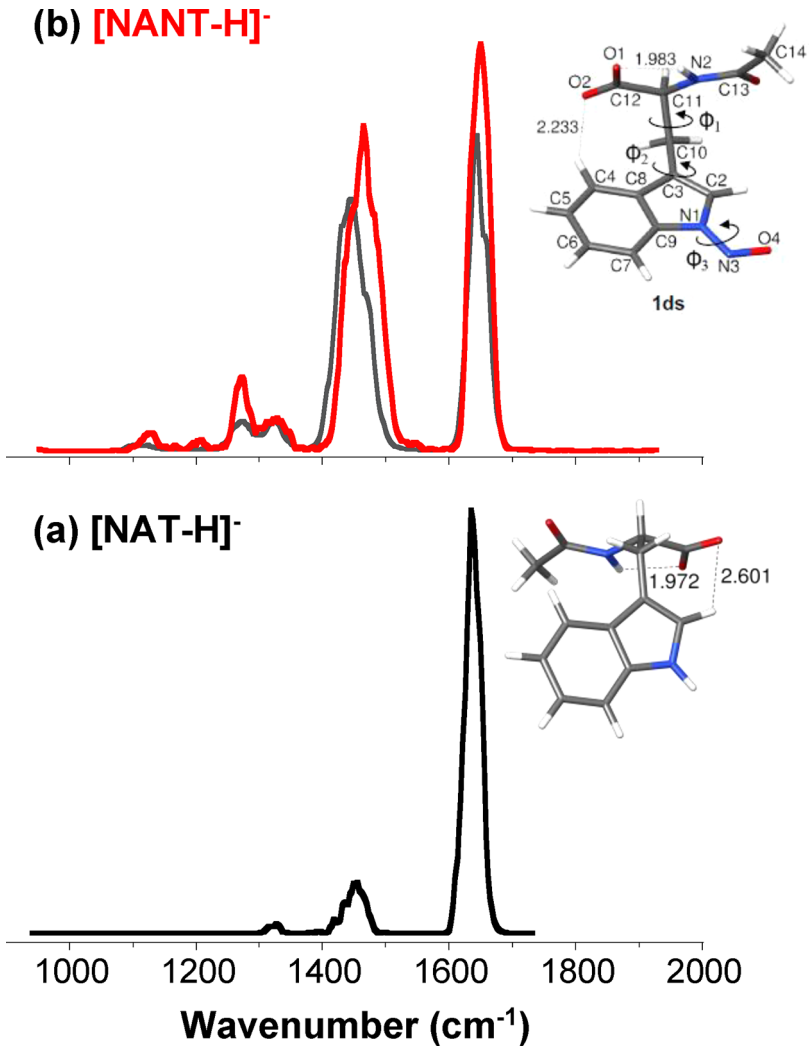

Figure 22. IRMPD spectra of $[NANT-H]^{-}$ (b, red profile), of ^{15}N labeled $[NANT-H]^{-}$ (b, gray profile), and $[NAT-H]^{-}$ (a). Geometries of the most stable conformer of $[NANT-H]^{-}$ and of $[NAT-H]^{-}$ are depicted along the corresponding spectrum. Adapted with permission from ref 172. Copyright 2013 Elsevier.

DOI: 10.1021/acs.chemrev.9b00395
Chem. Rev. 2020, 120, 3261−3295

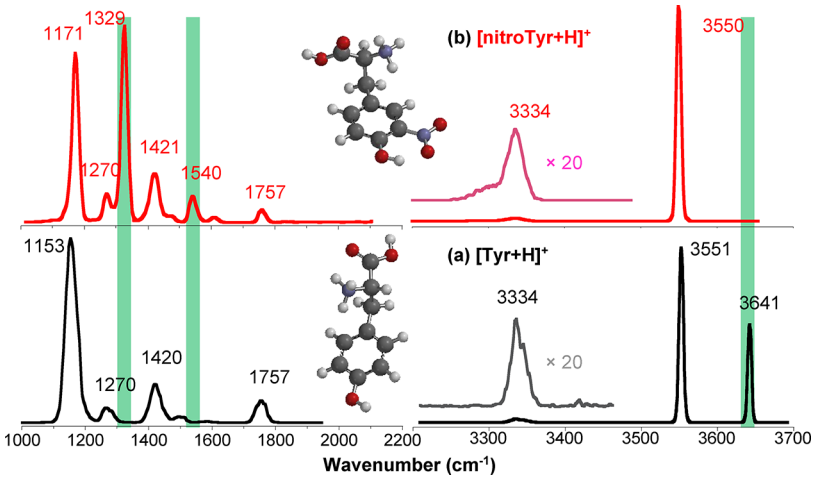

Figure 23. IRMPD spectra of $[Tyr+H]^+$ (a) and of $[nitroTyr+H]^+$ (b). Green areas mark the range of characteristic bands of the nitro derivative. Structures shown pertain to the most stable conformer of each species. Adapted with permission from ref 174. Copyright 2011 Elsevier.

oxygen and nitrogen species.[173] A remarkable effect due to the nitro group emerges from the IRMPD spectrum of protonated 3-nitrotyrosine (nitroTyr) when compared with the spectrum of the native species (Figure 23).[174] Theoretical calculations have delivered optimized geometries and IR spectra of the most stable structures for both $[Tyr+H]^+$ and $[nitroTyr+H]^+$ ions, and the lowest energy conformers are depicted in Figure 23.[174−176] All major bands which characterize $[Tyr+H]^+$ are present also in the spectrum of $[nitroTyr+H]^+$, including the dominant peak at 1153/1171 cm^{-1} associated with C−OH stretching and COH bending of the carboxylic group. Distinct features appearing only in the IRMPD spectrum of $[nitroTyr+H]^+$ are found at 1330 and 1540 cm^{-1} and are associated with strongly localized symmetric and asymmetric NO_2 stretching.[174] Their sizable activity is likely related to the polar NO_2 group imparting notable oscillator strength. These features (reported in Table 4) provide a clear marker for the nitration event on tyrosine. Also diagnostic to some extent is the spectrum in the OH stretching range (Figure 23). While the carboxylic OH stretching remains at 3550 cm^{-1} moving from $[Tyr+H]^+$ to $[nitroTyr+H]^+$, the ring OH stretching at 3641 cm^{-1} for $[Tyr+H]^+$ has apparently disappeared in the spectrum of $[nitroTyr+H]^+$, due to the strong H-bond with the ortho nitro group and ensuing large red shift.

Nitrobenzene radical anion has been the subject of an in depth investigation by IRMPD spectroscopy.[177] However, the strong perturbation due to electron attachment and weakening of the NO bonds does not allow a direct link with the properties of the electronically distant nitro group of $[nitroTyr+H]^+$.

When nitrotyrosine is part of a more complex environment, multiple additional noncovalent interactions may take place, altering and masking the diagnostic features just evidenced. This notion is already verified in the adducts of nitrotyrosine with halide ions, $[nitroTyr+X]^-$ (X = Cl, Br, I).[178] In the most favorable structures the halide ion interacts with tyrosine either via H-bonding to the ring hydroxyl or in a dual binding to a ring CH in the 2-position and to the carboxylic OH. The latter motif is also a preferred one for the nitrotyrosine complexes, while the ring OH preferentially interacts with the ortho nitro group hampering H-bonding to the halide. In addition, the π-acidic character of the nitro-substituted aryl ring favors a coordination geometry where the halide engages in H-bonding with both the carboxylic OH and an amino hydrogen and is also leaning toward the electron depleted π-system. The diverging pattern of conformational arrangements renders a direct probe of the nitration PTM here a more challenging task than in the above-discussed protonated species. Figure 24

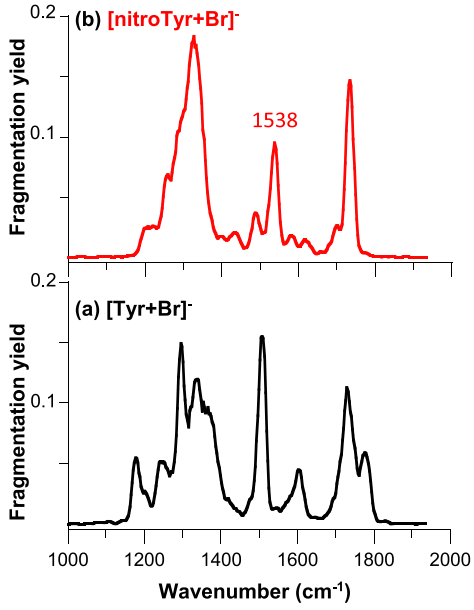

Figure 24. IRMPD spectra of $[Tyr+Br]^-$ (a) and of $[nitroTyr+Br]^-$ (b). Adapted from ref 178 with permission from the PCCP Owner Societies.

reports the IRMPD spectra of the bromide complexes where the asymmetric NO_2 stretching mode is assigned to the distinct IRMPD signature at 1538 cm^{-1} in the spectrum of $[nitroTyr+Br]^-$.[178]

2.8. Methylation

Methylation of lysine on the side chain amino group forming ε-*N*-methyllysine (Lys(Me)) converts a primary into a secondary amino functionality.[2,66,67] This PTM increases the hydrophobicity of the protein. The effect is pronounced also on the properties of the isolated amino acid, causing an increase of 16 kJ mol^{-1} in proton affinity.[179,180] IRMPD

DOI: 10.1021/acs.chemrev.9b00395
Chem. Rev. 2020, 120, 3261−3295

spectroscopy has been reported on protonated and alkali metal cationized Lys and Lys(Me). The presence of the additional methyl group does indeed allow us to discriminate between the two sets of ionic species as shown in Figure 25.[179] However,

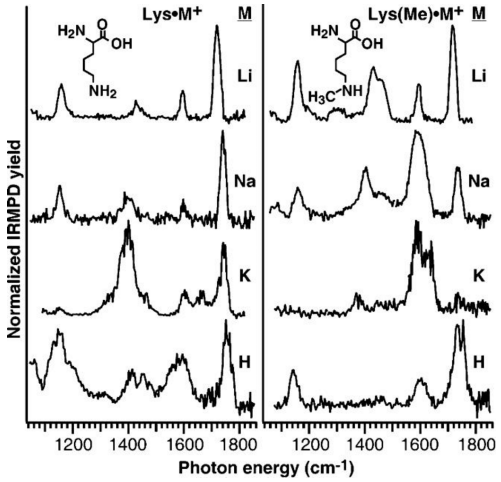

Figure 25. IRMPD spectra of $[Lys+M]^+$ and $[Lys(Me)+M]^+$ (M = H, Li, Na, K). Reprinted from ref 179. Copyright 2007 American Chemical Society.

this result is rather a reflection of the structural modifications induced by the increased basicity of the side chain amino group. In particular, $[Lys+M]^+$ and $[Lys(Me)+M]^+$ (M = H, Li, Na, K) ions comprise a population of low energy structures including zwitterionic and nonzwitterionic forms. The size of the metal ion and the basicity of the side chain amino group, that is the preferred protonation site in both $[Lys+H]^+$ and $[Lys(Me)+H]^+$, determine the balance between the two forms.

$[Lys+Li]^+$ and $[Lys+Na]^+$ present similar spectra, consistent with a nonzwitterionic structure characterized by a carboxylic C═O stretch at 1720 cm^{-1} and a NH_2 scissor at 1595 cm^{-1}. The spectrum of $[Lys+K]^+$ presents an additional major absorption at 1400 cm^{-1} assigned to COH bending involved in H-bonding to the N-terminal amino group in a novel structure presenting a dicoordinated rather than tricoordinated metal motif, though still nonzwitterionic. In contrast, in the spectrum of $[Lys(Me)+K]^+$ the absence of any band above 1700 cm^{-1} is a clear indication of prevailing zwitterionic forms, with the carboxylate group being responsible for the absorption at 1600 cm^{-1}. $[Lys(Me)+Na]^+$ presents features indicative of both zwitterion and nonzwitterion species while the litium complex is essentially nonzwitterionic. Overall, preferred structures of cationized Lys(Me) depend on a combination of factors including site specific proton affinity of the amino acid and size of the metal ion but also on metal ion solvation and hydrogen bonding.[179]

2.9. Deamidation

A process formally equivalent to a deamidation PTM may be realized and investigated in an isolated environment. To this end, proteinogenic Asn and Gln are released as naked protonated species and allowed to undergo NH_3 loss, corresponding to the spontaneous posttranslational protein modification and degradation.[181] However, cleavage of NH_3 from protonated Asn and Gln may involve either the amide function or the α-amino group, potentially yielding a variety of product ion structures.

IRMPD spectroscopy has allowed to conclusively clarify that NH_3 loss derives from the amido side chain of $[Asn+H]^+$ ions by nucleophilic displacement by the carbonyl oxygen leading to a cyclic 3-amino-succinic anhydride ion. The structure of the $[Asn+H-NH_3]^+$ product ion has been assayed by IRMPD spectroscopy and interpreted by theoretical calculations, confirming previously proposed mechanisms.[182]

The IRMPD assay of $[Asn+H]^+$ conforms to the calculated IR spectrum of the amino acid protonated on the terminal amino group.[183] However, loss of NH_3 is expected to occur through a side chain protonated intermediate, along the lowest activation energy pathway.[184] This hypothesis is confirmed by the experimental IRMPD spectrum reported in Figure 26A,

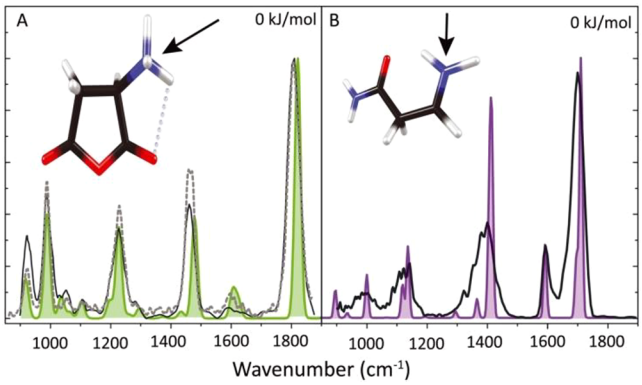

Figure 26. IRMPD spectrum of the $[Asn+H-NH_3]^+$ fragment ion and calculated IR spectrum of protonated 3-aminosuccinic anhydride (A). Panel B reports IRMPD and IR spectra of the $[Asn+H-(CO+H_2O)]^+$ fragment ion (in each panel, the protonation site is marked by an arrow). Reprinted with permission from ref 181. Copyright 2016 John Wiley and Sons.

showing good agreement with the calculated IR spectrum of the conceivably most stable species, namely N-protonated 3-aminosuccinic anhydride. In particular, the IR absorption at 1820 cm^{-1} is ascribed to the antisymmetric combination of C═O stretches in the succinic anhydride structure and the band at 1625 cm^{-1} is attributed to the NH bending mode. In addition to deamidation, loss of $CO+H_2O$ leads to an immonium product ion whose structure has also been ascertained by IRMPD spectroscopy (Figure 26B).[184]

As in the case of $[Asn+H]^+$, protonated glutamine, $[Gln+H]^+$, bears the additional proton on the α-amino group.[181] A fragmentation pathway similar to that of $[Asn+H]^+$, however, would lead to $[Gln+H-NH_3]^+$ with an unfavorable six-membered ring aminoglutaric anhydride ion. Instead, using IRMPD spectroscopy, the $[Gln+H-NH_3]^+$ structure is identified as an oxoproline structure protonated on the oxo-O atom.[181] In particular, an absorption at 1786 cm^{-1} is ascribed to the carboxylic C═O stretching and a band at 1687 cm^{-1} to lactam C−N stretching.

It can thus be concluded that IRMPD spectroscopy allows for the structural characterization of deaminated amino acids. Interestingly, the spectroscopic investigation has revealed that the product ions formed by H_2O cleavage from protonated aspartic and glutamic acid are similar to those formed from deamidation of protonated Asn and Gln.[181]

2.10. O-Glycosylation

Glycosylation is a rather common PTM affecting, inter alia, protein folding, recognition, stability, and immune response.

DOI: 10.1021/acs.chemrev.9b00395
Chem. Rev. 2020, 120, 3261−3295

Determining the number and localization of glycan moieties is a difficult task, particularly so for O-linked relative to N-linked glycopeptides.[185] IRMPD spectroscopy has been performed on an O-glycosylated peptide (named GP2), a nine residue sequence (Pro-Ser-Asp-Thr-Pro-Ile-Leu-Pro-Gln or PSDTPILPQ), with a galactose/N-acetylgalactosamine disaccharide unit O-linked to Ser (Galβ1−3GalNAcα1-).[185] IRMPD activity has been recorded in the 1050−1750 cm^{-1} range on both $[GP2+2H]^{2+}$ and $[GP2+H+Na]^{2+}$ ions, with the latter species presenting significantly lower photofragmentation efficiency.

Figure 27 shows the experimental spectra of $[GP2+2H]^{2+}$ and $[GP2+H+Na]^{2+}$, compared with the one of the native peptide $[PSDTPILPQ+2H]^{2+}$.

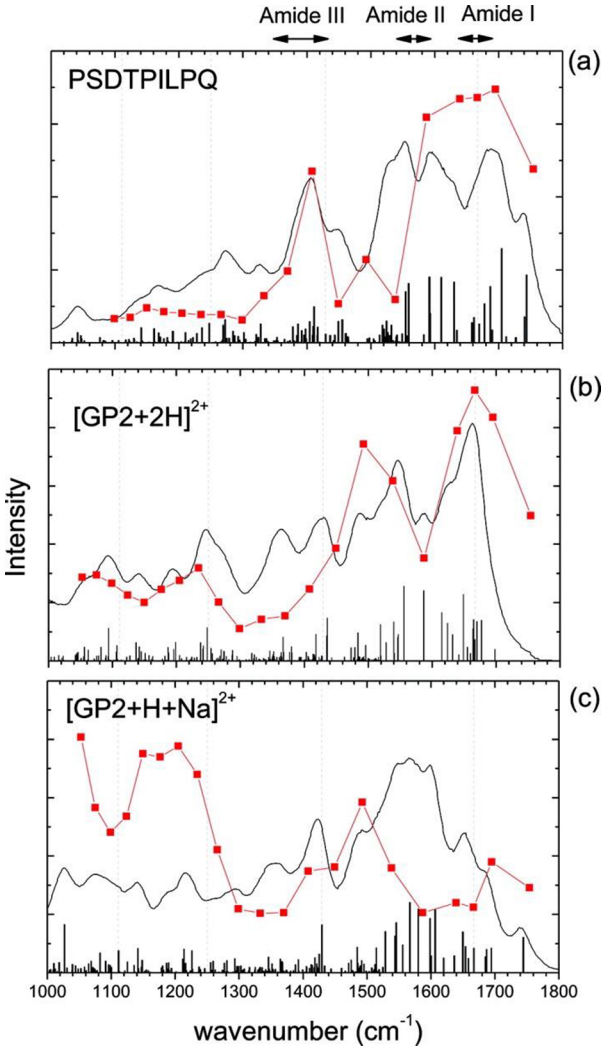

Figure 27. IRMPD spectra (in red) of $[PSDTPILPQ+2H]^{2+}$, $[GP2+2H]^{2+}$, and $[GP2+H+Na]^{2+}$, compared with respective calculated IR spectra. Reprinted from ref 185. Copyright 2012 American Chemical Society.

Computed IR spectra afford an indication of the major vibrational contribution. In both the native peptide and glycosylated derivative, dominant absorptions are due to amide I C═O stretching around 1660 cm^{-1} and to amide II N−H bending and C−N stretching of the backbone around 1550 cm^{-1}. The more pronounced activity of $[GP2 + 2H]^{2+}$ relative to the native peptide below 1300 cm^{-1} is ascribed to photoabsorption of saccharide units. This region pertains to highly coupled modes of oligosaccharides involving ring vibrations and stretching and bending in glycosyl bonds. The sodiated ion presents substantial discrepancy between IRMPD and calculated spectra ascribed to the multiphotonic character of the action spectroscopy and to incomplete intramolecular vibrational energy redistribution.[185]

3. IRMPD TO CHARACTERIZE FRAGMENTATION PRODUCTS FROM POSTTRANSLATIONALLY MODIFIED AMINO ACIDS AND PEPTIDES

IRMPD spectroscopy has played an invaluable role in providing insight into fragmentation mechanisms and evidence about fragment ion structures relevant to amino acid, peptide, and protein mass spectrometric behavior.[27,186] These results are particularly important because they establish the extent of information that may be attached to specific dissociation paths and products implicated in applications to peptide sequencing.[24,26,28,187]

IRMPD spectroscopy has been used to disclose the structure of fragment ions obtained from protonated tyrosine presenting a varying degree of iodination.[188] The dissociation processes are activated by ultraviolet photodissociation (UVPD). In the present case, efficient and specific homolytic cleavage of the C−I bond is observed in protonated iodotyrosine.[189] The so-formed radical site is prone to react to form a more stable species. Key fragmentation products obtained by UVPD from protonated 3-iodo- and 3,5-diiodotyrosine are thus probed by IRMPD spectroscopy in the hydrogen stretching range, together with a fragment ion from the native amino acid.[188] The structure of the sampled ions is clearly derived from the comparison with calculated IR spectra of plausible product ions (Figure 28). The closed shell product ion from native tyrosine, a reference species, is characterized by the O−H stretching at 3650 cm^{-1} and by asymm/symm NH_2 stretches at 3445/3250 cm^{-1}. On the other hand, the biradical intermediate from diiodotyrosine undergoes a dual hydrogen atom transfer process leading to a closed shell structure with highly delocalized positive charge. This feature confers electronic stabilization and is responsible for the red shift of the O−H stretch to 3600 cm^{-1}. The radical ion at m/z 135 presents IRMPD patterns which are best accounted for by a mixed population of ions formed by hydrogen atom transfer from either the methylene or the imino group on the side chain.[188]

The facile loss of H_3PO_4 from phosphorylated serine or threonine residues under low energy CID conditions often impairs sequence and site information about the occurrence of this PTM. IRMPD spectroscopy has allowed us to conclusively discriminate between the three putative isomers of the $[pSer+H-H_3PO_4]^+$ product ion, namely protonated 2-aminopropenoic acid (from a 1,2-β elimination process), protonated 2-carboxyaziridine (from nuclephilic attack by the amino nitrogen on the β-carbon), and a protonated β-lactone (from nucleophilic attack by the carbonyl oxygen on the β-carbon). As can be seen in Figure 29, the IRMPD spectrum (panel a) matches with the absorption spectrum predicted for the aziridine isomer. First, the IRMPD spectrum displays three carboxylic acid signatures at 1793 cm^{-1} (ν(C═O)), at 1167 cm^{-1} (ν(C−OH), β(COH)), and at 3540 cm^{-1} (ν(OH)). Second, three bands characteristic of the N-protonated aziridine ring were observed at 1010 cm^{-1} (wagging(NH_2)), 1530 cm^{-1} (scissor(NH_2)), and 3415 cm^{-1} (ν_{asymm}(NH_2)).[190]

DOI: 10.1021/acs.chemrev.9b00395
Chem. Rev. 2020, 120, 3261−3295

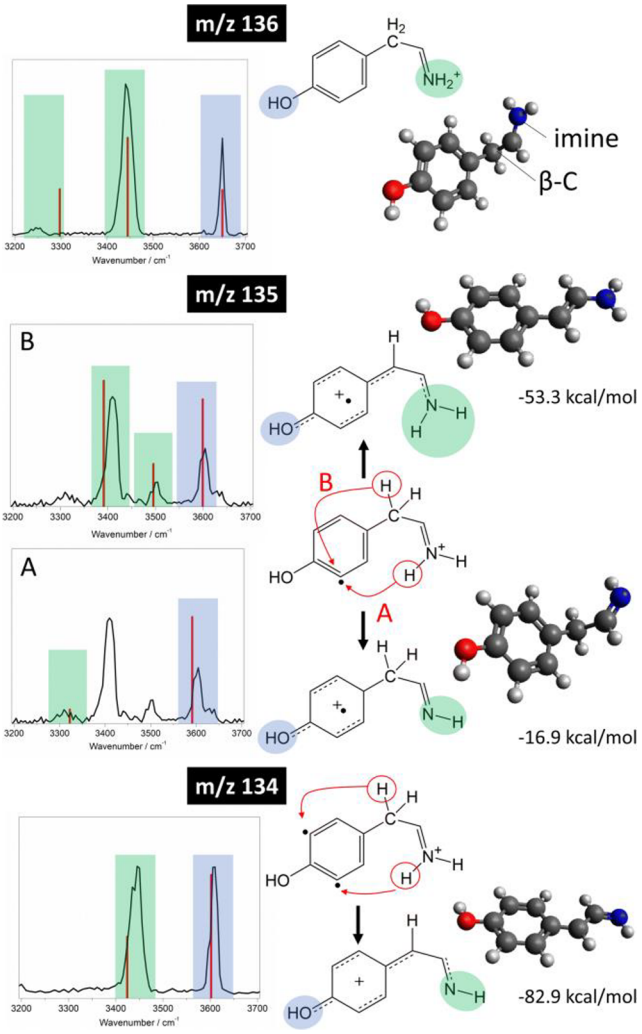

Figure 28. IRMPD spectra for UVPD product ions from protonated tyrosine (m/z 136), 3-iodotyrosine (m/z 135), and 3,5-diiodotyrosine (m/z 134) compared with calculated IR stick spectra of putative structures. Colored areas mark the active X-H (X = N, O) stretching mode(s). Reprinted with permission from ref 188. Copyright 2018 Springer Nature.

Notably, the global minimum corresponds to protonated 2-aminopropenoic acid (Figure 29b). The formation of the aziridine isomer (Figure 29c), lying 50 kJ mol^{-1} higher in energy, is rather under kinetic control, occurring via an intramolecular nucleophilic substitution reaction assisted by the vicinal amino group.[191] The observation of a kinetic rather than thermodynamic product is also consistent with computational studies, one on a phosphorylated peptide,[192] the other on the aziridine structure accounting for the dehydration product from protonated Ser and Thr.[193]

In comparison with phosphoserine, the sulfo analogue sSer, as well as sSer-containing peptides, have received much less attention. Major fragment ions from activated $[sSer+H]^+$ are formed by loss of 80 u and 98 u (i.e., cleavage of SO_3 and H_2SO_4).[194] Both ions have been probed by IRMPD spectroscopy. The IRMPD spectrum of $[sSer+H-SO_3]^+$ ions is very similar to the one of protonated Ser,[154,194] in both the fingerprint and in the OH/NH stretching ranges. These spectra well match with the computed IR spectrum of the lowest energy conformer of $[Ser+H]^+$ ions. The fragment ion

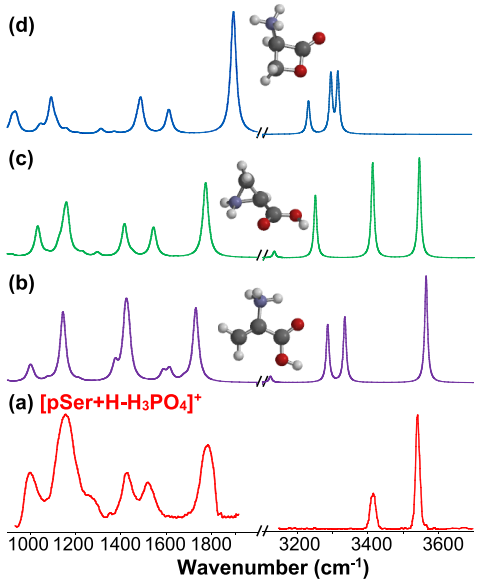

Figure 29. IRMPD spectrum of $[pSer+H-H_3PO_4]^+$ (a) and IR spectra of candidate structures (b–d). Adapted from ref 190 with permission from The Royal Society of Chemistry.

formed by cleavage of H_2SO_4, by far more likely than stepwise SO_3 and H_2O losses, yields an IRMPD spectrum reproducing the one recorded for $[pSer+H-H_3PO_4]^+$ and assigned to N-protonated 2-carboxyaziridine. Figure 30 shows the experimental spectrum of $[sSer+H-H_2SO_4]^+$ together with IR spectra of already purported plausible isomers, pointing to the presence of the carboxy aziridinium structure. Just as in the case of phosphoserine, the formation of a fragment ion that does not correspond to the lowest energy isomer is ascribed to this one being the product of the kinetically favored path.[194]

While protonated pSer and sSer undergo loss of H_3PO_4 and H_2SO_4, respectively, the primary fragment ion does not always correspond to the loss of PTM, as observed for protonated pYG and sYG.[162] The common fragment ions (m/z 216) were submitted to IRMPD spectroscopic assay, showing that the PTM is in fact retained. Their further photofragmentation abides by the expected 80 u loss.[162]

4. FIXED WAVELENGTH IRMPD IN ANALYTICAL APPLICATIONS

4.1. Excitation Efficiency of Molecular Ions Using a CO_2 Laser

As illustrated in the preceding sections, IRMPD spectroscopy is able to provide circumstantial identification of various types of PTMs. In fact, vibrational spectroscopy over an extended frequency range yields detailed structural information on the presence of functional groups, skeletal features, conformational arrangement, and noncovalent interactions. Backed by theoretical calculations, the molecular assignment does not necessarily need to be verified by comparison with a standard compound, being based on the evaluation of the experimental spectrum with computed IR spectra of all conceivable isomers for the assayed ion. Building on this, standard-free assignment of metabolite isomers has recently been proposed.[39,40]

The selectivity of IR activation for fast screening or high throughput analytical purpose has also been explored. In this perspective, the purpose is not to record the full scale IRMPD spectrum for each analyte within a complex mixture, but rather

DOI: 10.1021/acs.chemrev.9b00395
Chem. Rev. 2020, 120, 3261–3295

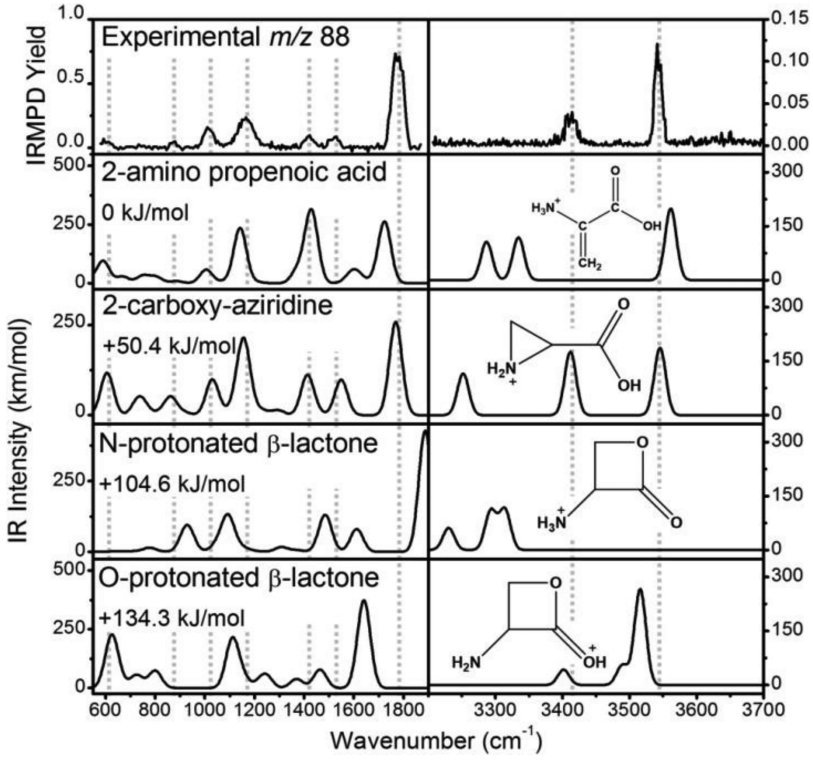

Figure 30. IRMPD spectrum of $[sSer+H-H_2SO_4]^+$ and IR spectra of candidate structures. Reprinted with permission from ref 194. Copyright 2015 Elsevier.

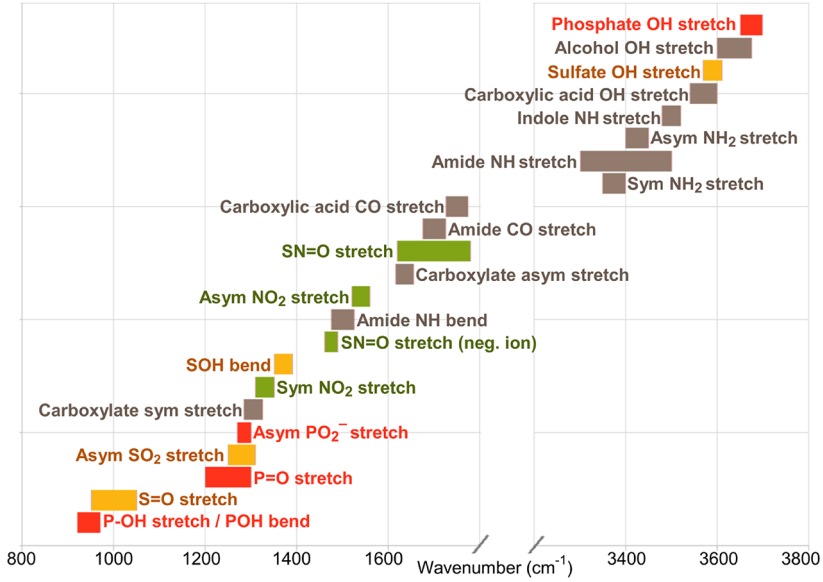

Figure 31. Typical ranges of selected vibrational modes characteristic of peptides and of some common PTMs.

to identify chemical classes of analytes. The idea relies on the wavelength-selective fragmentation of ions carrying a specific chemical moiety when the IR laser is on resonance with their IR absorption signatures. An overview of IR wavenumber ranges comprising functional groups characteristic of some major PTMs is provided in Figure 31. Obviously the various functionalities of either native or modified residues when embedded in a peptide carbon skeleton give rise to poorly structured broad bands, as depicted for example in the IRMPD spectra reported in Figures 12 and 21.

Applications of fixed wavelength IRMPD (fw-IRMPD) as an activation method to selectively detect biological molecules containing a specific chemical moiety have been covered in a number of excellent reviews, and only a general survey will be outlined here.[33,34,102,107,195] While recording an IR spectrum requires tunable IR lasers, mode selective IRMPD may be performed with a fixed-wavelength laser. Fixed wavelength (10.6 μm, i.e. 943 cm^{-1}) CO_2 lasers have been used. As outlined in section 1.3, the seminal experiment was reported in a landmark paper by Beauchamp and co-workers.[14] Commercially available high power and continuous wave (cw) CO_2

DOI: 10.1021/acs.chemrev.9b00395
Chem. Rev. 2020, 120, 3261−3295

lasers are well suited for driving the IRMPD process and can be easily integrated to marketed mass spectrometers. Incidentally, IR excitation of ions within a QIT succeeds in relieving the low mass cutoff limitation.[196,197] This effect restricts the CID performance within a QIT where high radiofrequency voltages are required to increase the ion kinetic energy. Using IRMPD as ion activation method, fragment ions formed in a primary IRMPD event may also undergo further IRMPD thus yielding a rich pattern of structurally informative fragmentation products.[198−200] This is an additional benefit of performing IRMPD in quadrupole ion trap systems where the overlap between the ion cloud and the IR laser is high.[102,107] Conversely, as already stated in section 1.3, the helium buffer gas (ca. 10^{-3} mbar), which is critical for confining the ions, also allows collisional deactivation and thus reduces the IRMPD efficiency.[201,202] While both spatial and temporal ion-laser overlap is not as efficient in an ICR cell as in a QIT, collisional cooling is not an issue at the low pressure (ca. 10^{-9} mbar) of the Penning trap. The superior performance of FT-ICR in terms of mass accuracy and mass resolving power provides an additional advantage for the identification of photofragmentation products.[16,21]

While most of the applications of fw-IRMPD for the detection of PTMs have been performed with FT-ICR or QIT, implementation of fw-IRMPD has been reported also on a hybrid quadrupole time-of-flight mass spectrometer, where protein ions are trapped in the radiofrequency only quadrupole, which is normally used as collision cell, and irradiated by a cw CO_2 laser. In this setup, efficient dissociation of posttranslationally modified proteins is verified in top-down analyses.[202]

4.2. Fast Differentiation between Modified and Unmodified Peptides and Proteins Using a CO_2 Laser

As discussed in section 2, some PTM motifs, such as phosphate and sufate groups, present a large IR absorption cross section just below 1000 cm^{-1}, i.e. near resonance with the CO_2 laser frequency. The exceptionally large photofragmentation yield of large biomolecules by a CO_2 laser had already been noted in 1994 in a leading reference on the application of IRMPD to probe multiply charged biomolecular ions.[16] This large absorbance is ascribed to the P−OH stretching and POH bending vibrations in the case of phosphate group. Also unmodified and large proteins can be efficiently excited using a cw CO_2 laser.[203] At low power settings, however, only modified peptides, such as phosphorylated peptides, may undergo efficient photodissociation and the process becomes highly structure selective.[204]

The phosphorylation PTM has thus represented a major test ground for fw-IRMPD. This is traced to the fact that identification of phosphopeptides by MS/MS has represented a challenging task. Difficulties arise from the low abundance of phosphopeptides relative to nonmodified counterparts and from the ion suppression effect attached to the presence of phosphate groups which severely reduce the ionization yield in MS analysis. Nevertheless, phosphorylation is readily revealed because modified peptides display efficient fw-IRMPD upon irradiation by a CO_2 laser, at variance with unphosphorylated peptides which remain intact when sampled under the same conditions.[205−207] This notion has been exploited to attain a rapid screening of phosphopeptides within a complex proteolytic digest.[205,206] Clear signature for phosphorylation is the increased extent of fragmentation displayed by phosphopeptides with increasing laser power, while the relative abundance of unphosphorylated peptides remains constant, together with the characteristic photofragmentation pattern.[205−208]

The ability of fw-IRMPD to discriminate between phosphorylated and unphosphorylated peptides has been implemented in various methods such as in a LC-IRMPD-MS strategy, probed in the analysis of complex proteolytic digests[209,210] while an assay of phosphopeptides has been used to test the performance of a dual pressure linear ion trap Orbitrap instrument, modified to permit infrared multiphoton dissociation.[211] There is no general agreement, though, about a distinct advantage of using fw-IRMPD for the analysis of phosphopeptides.[212]

The high absorption of the phosphate group at the emission frequency of the cw CO_2 laser has also been exploited to develop a cross-linker that incorporates a phosphate chromophore. The cross-linked peptides display magnified IRMPD which allows them to be easily distinguished from unmodified peptides.[213]

O-sulfation PTM detection is also amenable to fw-IRMPD. As the phosphate group, the sulfate group has a strong IR cross section at the frequency of the CO_2 laser, which can be ascribed to the C−O(SO_3) stretching and symmetrical SO_2 stretching modes.[129] Accordingly, fw-IRMPD provides extensive sequence coverage of sulfated peptides.[214] In a comparative assay, however, sulfate retention from a peptide containing sTyr was found to be smaller than phosphate retention from pTyr or pThr.[214] The reason may lie in a lower bond dissociation energy associated with the S−O bond or to exceedingly high efficient photon absorption by the sulfo PTM at the laser frequency.

Chemical derivatization has been used to obtain N-terminal sulfonated peptides. The pronounced absorbance of the cw CO_2 laser light by the SO_2 group, acting as a chromophore, is likely responsible for the optimized performance of fw-IRMPD compared with CID.[215] The reported result is a highly efficient photodissociation of N-terminal sulfonated peptides relative to the native compounds, which allowed to retrieve the most accurate sequence information from tryptic peptides.

N-Linked glycopeptides have also been investigated, and more particularly the influence of charge state, charge carrier, peptide composition, and glycan composition.[216] Each of these parameters plays a role in directing photodissociation. For example, at variance with multiply protonated glycopeptide ions yielding only glycan cleavage, singly protonated species containing a basic amino acid residue (Arg, for example) undergo mainly peptide backbone cleavage. Moving to the doubly protonated glycopeptide ion, fragmentation yields additional glycan fragments. This behavior is interpreted to be due to the first proton being tightly bound to the highly basic arginine while the second one enables additional fragmentation paths in either peptide or glycan units, in agreement with the mobile proton model for peptide dissociation.[217−219] In the absence of a highly basic amino acid residue, both glycan and peptide fragments are formed from the singly protonated ion, which is evidence for the greater proton mobility allowing more extensive glycan fragmentation. Sodium coordination, relative to proton attachment, results in an increased variety of fragment ions, and sodiated ions appear less sensitive to amino acid composition. Thus, the sodium adducts are seemingly a better choice for analytical IRMPD diagnosis of glycopeptides.

DOI: 10.1021/acs.chemrev.9b00395
Chem. Rev. 2020, 120, 3261−3295

Molecular modeling provides an explanation for the observed dissociation behavior showing multidentate coordination to the metal mainly by hydroxyl groups of the glycan portion in multiple low energy structures, releasing preferentially glycan containing fragments.[216] To summarize, sodiated ions yield fragmentation regarding the glycan while protonated species deliver information about both glycan and peptide sequence. Similar fragmentation patterns are reported for both N- and O-glycopeptides.[216,220]

The differentiation of peptides containing cysteine based oxidative modifications has been addressed by fw-IRMPD only relatively recently. As already discussed in section 2, the S−O bond presents strong IR activity near the cw CO_2 laser emission frequency, providing an efficient chromophore and behaving in a similar way as a phosphate functionality. Selective activation at this wavelength has been exploited to discriminate oxidized peptides in complex mixtures and obtain clear identification of peptides containing cysteine sulfonic acid.[221] As shown in Figure 32, the extent of dissociation

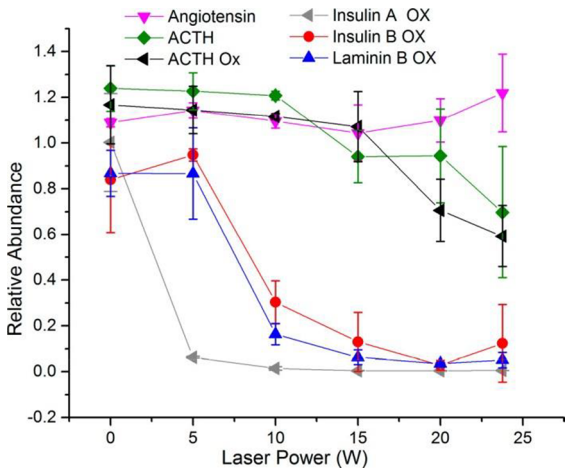

Figure 32. Relative abundances of precursor peptide ions submitted to IR irradiation of varying laser power for 0.15 s in an FT-ICR cell. Only Insulin chain A Ox, Insulin chain B Ox, and Laminin β Ox possess cysteine sulfonic acid residue(s), and the abundance of their parent ion is remarkably depleted upon laser irradiation at >5 W. Reprinted from ref 221. Copyright 2017 American Chemical Society.

induced by IR irradiation in peptides containing cysteine sulfonic acid is remarkably higher when compared with unmodified peptides. Furthermore, the analysis of photofragmentation products provides sequence information allowing to localize the PTM on the specific residue(s).[221] Modified peptides can be discriminated from unmodified ones in a mixture also along a liquid chromatography (LC) run. To this end, the laser light is admitted during alternate scans, allowing one to collect both MS and IRMPD spectra in the same run. Ion chromatograms recorded with and without laser irradiation yield direct information about the sensitivity of each peptide to IRMPD.

Disulfide bond formation is an oxidative PTM of cysteine residues. Acknowledging the presence of disulfide bond bridges is required for a thorough understanding of a protein structure and function.[51,52] The extent to which S−S bond cleavage is involved in the fragmentation of multiply positively charged peptide ions is dependent on the type of ion activation method in a frequently nonpredictable way. In contrast, IRMPD is found to consistently favor S−S and C−S bond cleavages in negatively charged peptide ions, in a similar way as electron detachment dissociation.[222]

Loss of weakly bound PTMs may occur easily upon IR excitation and be favored over backbone cleavage. As discussed in section 2, preferential cleavage of H_3PO_4 by β-elimination of the phosphate ester group from pSer and pThr residues and loss of HPO_3 from pTyr are observed. Loss of a phosphate group from phosphorylated serine residues is pronounced from small polypeptides and represents a drawback in determining phosphorylation sites.[208,209] However, serine phosphorylation is largely retained in IRMPD experiments performed on multiply charged ions of a protein such as bovine α-casein. Possible factors tending to decrease phosphate loss under IRMPD are traced to the size of the protein ion and increased positive charge, with the underlying reason being the stabilization of the phosphate group by hydrogen bonding to basic residues.[202]

4.3. Combining Fixed-Wavelength IR and Electron Transfer or UV Activation Modes

PTM retention upon fragmentation is a particularly important issue in the context of mass-spectrometry-based approaches applied to proteomics where peptide sequence information is derived from fragmentation mass spectra. Depending on the excitation mode of protonated peptides, for example, different fragmentation spectra are observed. Upon slow heating fragmentation, i.e. CID or IRMPD, peptidic bond cleavage occurs and series of the so-called b and y type ions are observed (Figure 33).[16,102,107] Upon electron transfer ex-

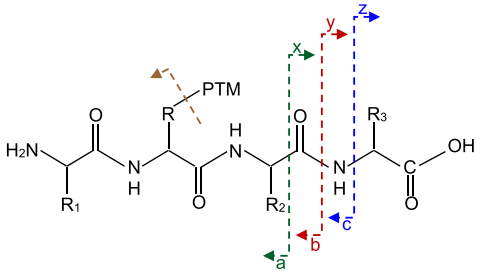

Figure 33. Backbone peptide bond cleavage at C_α−C, C−N, and N−C bonds occurring upon ion activation, leading to x, y, or z fragments or a, b, or c fragments depending on the localization of the charge.[223,224] Rearrangement and prevailing PTM loss (indicated in brown color) are typically favored over C−N cleavage under low energy CID conditions, hampering clear identification of the modification site.

citation, specific radical driven fragmentation chemistry occurs, and the peptide backbone is cleaved at the N−C_α bonds, leading to the so-called c and z ions (Figure 33). More importantly, PTMs are retained.

Combined application of ECD and IRMPD techniques in FT-ICR mass spectrometry has thus proven particularly fruitful, providing large sequence coverage and unveiling features and location of modifications.[95,97] This combination has allowed to characterize the phosphorylation of protein kinase A and to identify the PTM site in three tryptic phosphopeptides.[225]

The recent coupling of fw-IRMPD with ETD has resulted in a hybrid fragmentation technique named activated ion ETD (AI-ETD).[226−228] In this fragmentation method, peptide ions are activated by fw-IRMPD during the ETD reaction because the two processes may overlap in place and time. The well

DOI: 10.1021/acs.chemrev.9b00395
Chem. Rev. 2020, 120, 3261−3295

ascertained efficiency of fw-IRMPD by phosphorylated peptides concurred to greatly enhance their fragmentation in b/y ions in comparison with nonmodified peptides. The slow heating of ions delivered by the absorption of several low energy (ca. 0.1 eV per photon) photons over a relatively long activation time ensured the highest extent of neutral losses, as underlined in a recent comparative survey of ECD/ETD-based techniques applied to phosphopeptide fragmentation and site localization.[226] While HCD remains the benchmark dissociation technique in phosphoproteomics, AI-ETD yielded the highest coverage of phosphopeptide identification among ETD based methods.[228]

N-Linked glycosylation regards asparagine residues and is largely widespread in nature.[229] fw-IRMPD used in conjunction with ECD has provided complementary information on the structure of an N-glycosylated peptide from an unfractionated tryptic digest analyzed in FT-ICR MS. Cleavage of multiply protonated glycopeptide ions by ECD yields c and z ions providing sequence information while maintaining intact saccharide binding. Conversely, CO_2 activation succeeds in breaking the glycan moieties providing information on the nature of the monosaccharide components and branching. Clarifying the glycan components and branching is particularly relevant in view of the microheterogeneity of N-linked glycoproteins, namely the occurrence of different glycans at a particular N-glycosylation site.[230,231] The fragmentation of glycans upon CO_2-laser excitation has been thoroughly reviewed.[232]

Protein nitration occurs selectively at specific tyrosine residues. Mass shifts of the peptides from proteolytic digests reveal the presence of nitrotyrosine but dissociation experiments are required to localize the PTM on the protein backbone. Dissociation experiments are needed also in the alternative top-down characterization of the modified protein,[233] starting from intact protein ions which are subsequently fragmented and analyzed by MS. Different dissociation methods, namely ECD, CID, and IRMPD, have been comparatively tested in the top-down mass analysis of protein tyrosine nitration.[234] ECD appears less effective in the proximity of the sites of nitration, probably an effect of the high electron affinity of the nitro group. IRMPD shows superior performance in producing abundant cleavages in the important region within few residues next to the PTM. It is found to successfully induce fragmentation between two nitrotyrosines in bis-nitrated lysozyme and cytochrome c, while ECD fails in this task.[234]

Protein deamidation has also been probed using a combination of CO_2 laser activation and ECD. As mentioned in section 4.1, cw CO_2 laser provides an efficient excitation means of large biomolecular ions under FT-ICR conditions.[203] This slow heating process can be used to induce protein unfolding through hydrogen bond disruption, as evidenced by the increased ECD efficiency observed when proteins are first heated using a CO_2 laser.[235] The result is that the protein ion becomes more susceptible to interact with thermal electrons, allowing the backbone chain to be extensively sampled by ECD. In deamidation an uncharged asparagine residue is converted into a negatively charged one (aspartic or isoaspartic acid) so that the hydrogen bonding pattern is different in the modified and native protein. This difference has an impact on the laser power required to achieve unfolding which in turn has an effect on the ECD fragment intensities as a function of the linear increase of the laser power. An increased fragmentation yield at low laser power was observed around heavily deamidated regions of the proteins.[235]

Fragmentation patterns observed upon UV excitation are also different from those observed under slow heating as with a CO_2 laser. Combination of these two activation modes are thus of interest, and a combined photodissociation method has been devised, bringing together IRMPD with UV photodissociation (UVPD), named HiLoPD (high-low photodissociation).[214,236] The experiment is conducted in the HDC cell of a hybrid quadrupole Orbitrap mass spectrometer[214] allowing simultaneous irradiation by the 10.6 μm CO_2 laser and UV laser at 213 nm. The performance of the method, merging the action of IR and UV photons, has been verified in characterizing phospho-, sulfo-, and glycopeptides. A comparative assay by IRMPD and by HiLoPD has invested an O-glycosylated peptide holding a GalNAc-Ser residue. IRMPD shows fair PTM retention efficiency in the fragment ions and allows extensive sequence coverage and PTM localization. HiLoPD displays higher PTM retention in comparison to both IRMPD and UV photodissociation.[236]

5. PRESENT AND FUTURE DIRECTIONS: CRYOGENIC VIBRATIONAL SPECTROSCOPY AND INTEGRATION OF ION MOBILITY SPECTROMETRY

Improving both the sensitivity and the spectral resolution of IRMPD spectroscopy is mandatory for the characterization of the nature, localization, and structural role of PTMs on large peptides and proteins. Among the most fruitful and promising achievements realized in this context, one should acknowledge cryogenic vibrational spectroscopy.[32,237−240] As initially proposed by Gerlich,[241] most of the setups are based on a cryogenically cooled multipole ion trap. Molecular ions are cooled through multiple collisions with a buffer gas,[242−244] thus reducing the thermal energy distribution of the sampled ionic species and thereby improving the spectroscopic resolution. Sensitivity improvement is achieved using the "messenger technique".[18,112−115] This technique relies on the formation of weakly bound ion-neutral complexes, where the neutral species, also called tag, is typically a rare gas or H_2. The corresponding binding energy is such that one IR photon succeeds in releasing the tag and in revealing the resonant IR active modes of the nearly unperturbed molecular ions.

Rotationally resolved vibrational spectra of small ions formed upon electron ionization, of astrophysical interest especially, have been obtained.[114] Other external ion sources, in particular electrospray and nanoelectrospray sources, can be used allowing for the spectroscopic study of large biolomolecular ions. Peptide ions encompassing proteinogenic as well as synthetic amino acid residues have been thoroughly characterized based on double laser interaction stages,[245,246] which may anticipate promising extension toward investigating posttranslationally modified peptides. Finally, the neat dissociation process, dismissing the tag, lends itself to a multiplexed kind of experiment which may become advantageous in sampling complex mixtures.[247]

As discussed in section 4, under MS/MS conditions, the combination of two selective activation techniques such as IR and electron transfer is of interest for deriving the peptide sequence and PTM localization. Integration of ion mobility spectrometry (IMS) provides an additional dimension to mass spectrometry analysis,[248,249] and fragmentation spectra of mobility-selected ions obtained upon IR activation can be of high interest for both fundamental and analytical applications.

DOI: 10.1021/acs.chemrev.9b00395
Chem. Rev. 2020, 120, 3261−3295

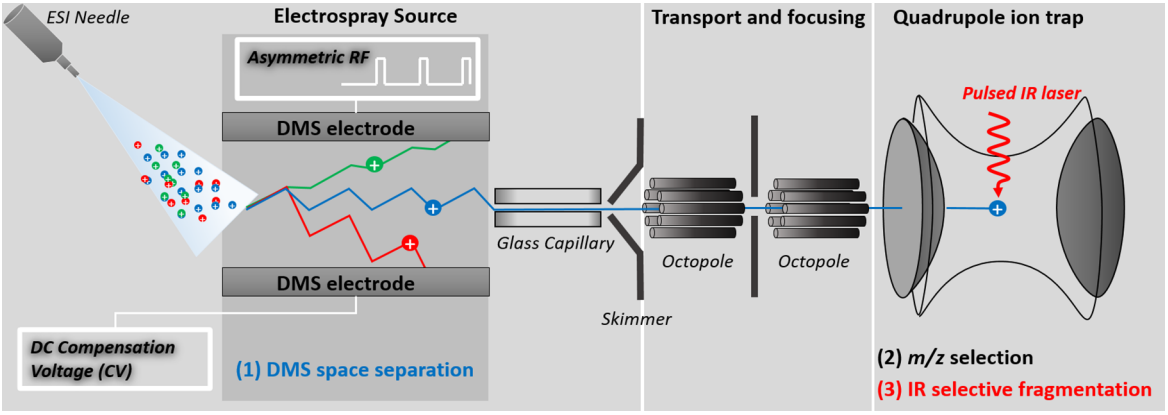

Figure 34. Schematic of the integrated DMS ion space separation in a Paul trap based tandem mass spectrometer allowing for IRMPD activation of DMS- and mass-selected molecular ions. The DMS device (1) holding the two DMS electrodes is inserted between the ESI needle and the transfer glass capillary in the ambient pressure source region. DMS-selected ions are then transferred in the quadrupole ion trap where they are mass-selected and subjected to IRMPD activation.

From a fundamental point of view, time separation of molecular ions in a drift tube under a relatively low electric field in a buffer gas allows for the derivation of collision cross sections which are directly related to the shape of the molecular ion. Nevertheless, especially for large biomolecular ions,[250] the structural assignment might be difficult. Combinations of IMS and other probes sensitive to the different levels of structuration are required for detailed conformation studies. In this context, IRMPD spectroscopy can provide additional structural descriptors based on specific band shifts, for example. Thus the combination of these two orthogonal approaches is a remarkably powerful tool to investigate the structure of biomolecular ions.[251]

Mobility-selected IRMPD spectroscopy has been gained on isomeric peptides.[252] In a protonated polyalanine peptide, arranged in stable α-helices, a systematic modification has been inserted by amide to ester substitution, whereby the H-bond donor group NH is replaced by an O atom. The resulting so-called depsi peptides have been scrutinized for conformational changes possibly imparted by the changing pattern of H-bonding along the peptide chain. Removal of a single backbone H-bond resulted to have only minor influence on the stability of the α-helix. Such well designed experiments provide a neat example of the valuable information that may be accessed on variously posttranslationally modified peptides by the combined use of IMS and IRMPD spectroscopy backed by molecular dynamics simulations.[252] Depsi peptides are in fact found in marine and microbial natural products and studied for the structural and functional consequences of an amide-to-ester substitution.[253]

Recently developed ultrahigh resolution IMS also known as "structures for lossless ion manipulations" (SLIM)[254] opens the door for the resolution of conformational families, which could be of high interest to interrogate posttranslationally modified peptides. The first coupling of SLIM with cryogenic IR spectroscopy of the analysis of glycan mixtures has recently appeared.[255]

Space separation as performed with field-asymmetric ion mobility spectrometry (FAIMS) or differential mobility spectrometry (DMS) is an alternative for the separation of isobaric and isomeric ions. Due to nonlinear mobility behaviors at high electric field, no direct structural information can be retrieved from FAIMS or DMS. Nevertheless, these small devices present high ion transmission and are found to be more orthogonal than drift tube IMS to tandem mass spectrometry. They can thus be used as ion filter for analytical purposes. For instance, a commercial FAIMS source has been used in conjunction with cryogenic ion spectroscopy to interrogate the doubly charged ions of bradychinin, a nine amino acid peptide.[251]

Analytical workflows based on IRMPD activation of DMS- and mass-selected ions can also be envisioned. As illustrated in Figure 34, electrosprayed isomeric ions can be space separated by inserting a DMS- or FAIMS-device within the ion source. As a result, mobility- and mass-selected isomeric ions can be interrogated using an IR laser. This approach has been applied to the separation and identification of sarcosine, a biomarker candidate of prostate cancer, from isomeric ions.[256] Sarcosine (*N*-methylglycine) is formed from glycine by the enzyme glycine-*N*-methyl transferase and is found in bodily tissues and fluids. The protonated ion when assayed by CID displays the same fragment ions as the isomeric α-alanine. DMS resolution drastically depends on the composition of the buffer gas. Using N_2 (Figure 35), an unresolved broad DMS peak is observed.

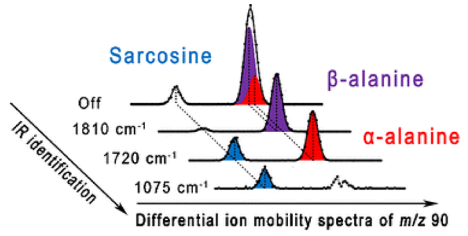

Figure 35. Differential ion mobility spectra of ions at m/z 90 corresponding to protonated sarcosine and α- and β-alanine recorded with no IR laser or with IR irradiation at the selected wavenumbers. Reprinted with permission from ref 256. Copyright 2018 Springer Nature.

With the addition of so-called modifier gases such as alcohols,[256] however, three peaks were observed for the equimolar mixture of sarcosine, α-alanine, and β-alanine. Figure 35 illustrates in a compact way the type of bidimensional experiments that result when scans are recorded where DMS- and mass-selected isomers are active at fixed wavelength. Specific depletion of protonated α-alanine and β-alanine is

DOI: 10.1021/acs.chemrev.9b00395
Chem. Rev. 2020, 120, 3261−3295

observed at 1810 and 1720 cm^{-1}, respectively, thus allowing for the resolution of the broadband. Conversely, the third peak (sarcosine) is the only one remaining intact at 1075 cm^{-1}. DMS peak assignment could be made based on the calculated IR absorption spectra.

6. CONCLUSIONS

Vibrational spectroscopy of gaseous species accessed by means of IRMPD ion spectroscopy is still a largely unexplored realm. IRMPD spectroscopy has to date concerned only selected types of PTMs which characterize amino acids and small peptides, demonstrating individual vibrational signatures and also revealing the way a PTM may intervene in constitutional isomerism and conformational features. Providing detailed structural information on the species isolated in the gas phase, as naked ion or in carefully controlled microsolvated state, IRMPD spectroscopy well integrates the structural assay of biomolecules and reactive intermediates in combination with X-ray crystallography and NMR spectroscopy. Each technique for determining molecular structure has its own strengths and limitations but can together concur in elucidating the relationship between structure and biological function in the actual environment.

The survey of the IR spectrum in an extended frequency range has revealed individual absorptions due to specific PTMs which are exploited to selectively activate posttranslationally modified peptide and protein ions. IRMPD is a valuable extension to the conventional collision-induced dissociation method used to obtain structurally diagnostic information in mass spectrometry. The wealth of already documented analytical applications of IRMPD is likely only an anticipation of the expanding performance of methods based on IR photon−gaseous ion interaction in a variety of problems.

APPENDIX

Amino acid abbreviations are listed in Table 5.

Table 5. Amino Acid Abbreviations[a]

amino acid	3-letter abbreviation	1-letter abbreviation
Alanine	Ala	A
Arginine	Arg	R
Asparagine	Asn	N
Aspartic acid	Asp	D
Cysteine	Cys	C
Glutamic acid	Glu	E
Glutamine	Gln	Q
Glycine	Gly	G
Histidine	His	H
Isoleucine	Ile	I
Leucine	Leu	L
Lysine	Lys	K
Methionine	Met	M
Phenylalanine	Phe	F
Proline	Pro	P
Serine	Ser	S
Threonine	Thr	T
Tryptophan	Trp	W
Tyrosine	Tyr	Y
Valine	Val	V

[a]Please note that pAA and sAA are meant to indicate the amino acid modified by phosphorylation or O-sulfation, respectively.

AUTHOR INFORMATION

Corresponding Authors

*E-mail: philippe.maitre@u-psud.fr. Tel. No.: +33 (0)1-69153250.
*E-mail: simonetta.fornarini@uniroma1.it. Tel. No.: +39 (0)6-49913510.

ORCID

Philippe Maitre: 0000-0003-2924-1054
Debora Scuderi: 0000-0003-3931-8481
Davide Corinti: 0000-0001-8064-3492
Barbara Chiavarino: 0000-0002-1585-7061
Maria Elisa Crestoni: 0000-0002-0991-5034
Simonetta Fornarini: 0000-0002-6312-5738

Notes

The authors declare no competing financial interest.

Biographies

Philippe Maitre, CNRS research director, is currently the director of the institute of physical chemistry at the University Paris-Sud (France). He started his career as a quantum chemist, with a Ph.D. in Chemistry at University Paris-Sud on Valence Bond theory. As a Postdoc in 1992−94, he worked in the group of C. W. Bauschlicher Jr. (NASA Ames) and then M. T. Bowers (UCSB) on theoretical studies of hypo-coordinated metal cations. He then moved to experiments and developed a platform for infrared spectroscopy of mass-selected molecular ions at infrared free electron laser of Orsay. His current interests range from fundamental developments for separation and characterization of isomeric ions to applications to analyses of complex mixtures using a combination of infrared activation and differential ion mobility spectrometry.

Debora Scuderi received her "laurea" degree in Chemistry in 2000 under the supervision of Prof. Anna Giardini and obtained her Ph.D. in 2003 at the Università di Roma "La Sapienza". She was a postdoctoral fellow in the laboratory of Applied Optics in Ensta - Ecole Polytechnique in France under the direction of Jean Etchepare in 2003-2005, and she began her independent scientific career in 2005 as assistant professor of Physical Chemistry at Université Paris Sud. Her current research, at the Free Electron Laser facility in Orsay, is focussed on IR and UV spectroscopy of mass-selected ions in the gas phase. She is mainly involved in studying energetics, structure, and reactivity of molecules of biological interest in the gas phase by using mass-spectrometry-based methods such as IRMPD and UVPD spectroscopies combined to DFT calculations.

Davide Corinti attended Università di Roma "La Sapienza", where he completed his undergraduate studies in 2014 and his Ph.D. degree in 2018 under the supervision of Prof. S. Fornarini. During his graduate studies he was hosted for a few months in the laboratories of Prof. Perdita Barran at the Manchester Institute of Biotechnology. His research work is addressed to the study of intrinsic properties of nutrients and biologically active compounds using mass spectrometry coupled with IRMPD spectroscopy and quantum chemical calculations. He was recipient of an award by the Lake Louise tandem MS conference in 2017 and of the International Journal of Mass Spectrometry − Best Student Paper Award 2018.

Barbara Chiavarino is associate professor of Inorganic Chemistry in the faculty of Pharmacy and Medicine at the Università di Roma "La Sapienza". She obtained her "laurea" degree in Pharmaceutical chemistry and technology in 1992 and her Ph.D. degree in Pharmaceutical sciences in 1996 from the same university. After postdoctoral work at the Faculté des Sciences et Techniques de

DOI: 10.1021/acs.chemrev.9b00395
Chem. Rev. 2020, 120, 3261−3295

l'Université de Nantes and at Eurofins Scientific France, in 1998 she became research associate at the Università di Roma "La Sapienza". Her research interests are directed on the structure and reactivity of ionic species in the gas phase and on the application of mass-spectrometry-based methods (using various analyzers such as FT-ICR, triple quadrupole, and ion trap, also coupled with IRMPD spectroscopy combined to DFT calculations) to address issues in medicinal and food chemistry.

Maria Elisa Crestoni is currently professor of chemistry. She obained her Ph.D. degree in 1991 from the Università di Roma "La Sapienza" working in the group of prof. Fulvio Cacace and then pursued postdoctoral studies with Prof. H.-F. Grützmacher at the University of Bielefeld in Germany and with Prof. J. R. Eyler at the University of Florida in U.S.A. She has been principal investigator of numerous national research projects and of several projects at the CLIO (Centre Laser Infrarouge d'Orsay) European centre centre and several times visiting professor at Ecole Polytechnique (Palaiseau) and Université Paris Sud (Orsay). Her research interests are in the structure and reactivity of gaseous (bio)inorganic systems by means of mass spectrometry and infrared ion spectroscopy.

Simonetta Fornarini is professor of chemistry in the faculty of Pharmacy and Medicine at the Università di Roma "La Sapienza". She received her "laurea" degree at the same university and then moved to the University of California, Santa Cruz under the Fulbright exchange program. After a period at the laboratory of Nuclear chemistry of the Italian National Research Council, she became research associate at the Università di Roma "La Sapienza". She has been an invited lecturer by national and international academic institutions and has published over 170 publications, including chapters and reviews. Her research interests focus on reactive intermediates and molecular interactions using mass-spectrometry-based methods, such as ion–molecule kinetics and vibrational spectroscopy of trapped ions.

ACKNOWLEDGMENTS

The authors acknowledge financial support by the Italian Ministry for Education, University and Research - Dipartimenti di Eccellenza - L. 232/2016, by the EU Horizon 2020 Programme (CALIPSOPlus and EU_FT-ICR_MS, under grant numbers 730872 and 731077, respectively), and the RTRA "Triangle de la Physique" contract (Project N°2013-0562-T, Chiraux IRUV).

ABBREVIATIONS

AIETD	activated ion ETD
CID	collision-induced dissociation
cw	continuous wave
DFT	density functional theory
DMS	differential mobility spectrometry
DNA	deoxyribonucleic acid
ECD	electron capture dissociation
ETD	electron transfer dissociation
FAIMS	field-asymmetric ion mobility spectrometry
FEL	free electron laser
FT-ICR	Fourier transform ion cyclotron resonance
fw-IRMPD	fixed wavelength IRMPD
GSH	glutathione
GS-Me	*S*-methylglutathione
GSNO	*S*-nitrosated glutathione
HCD	high-energy collisional dissociation
HiLoPD	high-low photodissociation
Hyp	(2*S*,4*R*)-4-hydroxyproline
hyp	(2*S*,4*S*)-4-hydroxyproline
IMS	ion mobility spectrometry
IR	infrared
IRMPD	infrared multiple photon dissociation
LC	liquid chromatography
MD	molecular dynamics
MS	mass spectrometry
MS/MS	tandem mass spectrometry
NMR	nuclear magnetic resonance
PTM	posttranslational modification
QIT	quadrupole ion trap
RNA	ribonucleic acid
SLIM	structures for lossless ion manipulations
UV	ultraviolet
UVPD	UV photodissociation
18c6	crown ether 18-crown-6

REFERENCES

(1) Walsh, C. T. *Posttranslational Modifications of Proteins: Expanding Nature's Inventory*; Roberts and Co.: Greenwood Village, CO, 2006.
(2) Walsh, C. T.; Garneau-Tsodikova, S.; Gatto, G. J., Jr. Protein Posttranslational Modifications: the Chemistry of Proteome Diversifications. *Angew. Chem., Int. Ed.* **2005**, *44*, 7342–7372.
(3) Mnatsakanyan, R.; Shema, G.; Basik, M.; Batist, G.; Borchers, C. H.; Sickmann, A.; Zahedi, R. P. Detecting Post-Translational Modification Signatures as Potential Biomarkers in Clinical Mass Spectrometry. *Expert Rev. Proteomics* **2018**, *15*, 515–535.
(4) Buuh, Z. Y.; Lyu, Z.; Wang, R. E. Interrogating the Roles of Post-Translational Modifications of Non-Histone Proteins. *J. Med. Chem.* **2018**, *61*, 3239–3252.
(5) Hirano, A.; Fu, Y.-H.; Ptáek, L. J. The Intricate Dance of Post-Translational Modifications in the Rhythm of Life. *Nat. Struct. Mol. Biol.* **2016**, *23*, 1053–1060.
(6) Venne, A. S.; Kollipara, L.; Zahedi, R. P. The Next Level of Complexity: Crosstalk of Posttranslational Modifications. *Proteomics* **2014**, *14*, 513–524.
(7) Seo, J.; Lee, K.-J. Post-Translational Modifications and their Biological Functions: Proteomic Analysis and Systematic Approaches. *J. Biochem. Mol. Biol.* **2004**, *37*, 35–44.
(8) Bowers, W. D.; Delbert, S. S.; Hunter, R. L.; McIver, R. T. Fragmentation of Oligopeptide Ions Using Ultraviolet-Laser Radiation and Fourier-Transform Mass-Spectrometry. *J. Am. Chem. Soc.* **1984**, *106*, 7288–7289.
(9) van der Hart, W. J. Photodissociation of Trapped Ions. *Mass Spectrom. Rev.* **1989**, *8*, 237–268.
(10) Williams, E. R.; Furlong, J. J. P.; McLafferty, F. W. Efficiency of Collisionally Activated Dissociation and 193-nm Photodissociation of Peptide Ions in Fourier-Transform Mass-Spectrometry. *J. Am. Soc. Mass Spectrom.* **1990**, *1*, 288–294.
(11) Dunbar, R. C. Photodissociation of Trapped Ions. *Int. J. Mass Spectrom.* **2000**, *200*, 571–589.
(12) Antoine, R.; Lemoine, J.; Dugourd, P. Electron Photodetachment Dissociation for Structural Characterization of Synthetic and Bio-Polymer Anions. *Mass Spectrom. Rev.* **2014**, *33*, 501–522.
(13) Wetzel, D. M.; Brauman, J. I. Electron Photodetachment Spectroscopy of Trapped Negative Ions. *Chem. Rev.* **1987**, *87*, 607–622.
(14) Woodin, R. L.; Bomse, D. S.; Beauchamp, J. L. Multi-Photon Dissociation of Molecules with Low-Power Continuous Wave Infrared-Laser Radiation. *J. Am. Chem. Soc.* **1978**, *100*, 3248–3250.
(15) Rosenfeld, R. N.; Jasinski, J. M.; Brauman, J. I. The Infrared Photodissociation of CH_3OHF^-. *J. Am. Chem. Soc.* **1979**, *101*, 3999–4000.
(16) Little, D. P.; Speir, J. P.; Senko, M. W.; O'Connor, P. B.; McLafferty, F. W. Infrared Multiphoton Dissociation of Large Multiply Charged Ions for Biomolecule Sequencing. *Anal. Chem.* **1994**, *66*, 2809–2815.

DOI: 10.1021/acs.chemrev.9b00395
Chem. Rev. 2020, 120, 3261–3295

(17) McLuckey, S. A.; Goeringer, D. E. Slow Heating Methods in Tandem Mass Spectrometry. *J. Mass Spectrom.* **1997**, *32*, 461−474.
(18) Lisy, J. M. Infrared Studies of Ionic Clusters: The Influence of Yuan T. Lee. *J. Chem. Phys.* **2006**, *125*, 132302/1−19.
(19) Yeh, L. I.; Okumura, M.; Myers, J. D.; Price, J. M.; Lee, Y. T. Vibrational Spectroscopy of the Hydrated Hydronium Cluster Ions H_3O^+ $(H_2O)_n$ (n = 1, 2, 3). *J. Chem. Phys.* **1989**, *91*, 7319−7330.
(20) Lemaire, J.; Boissel, P.; Heninger, M.; Mauclaire, G.; Bellec, G.; Mestdagh, H.; Simon, A.; Le Caer, S.; Ortega, J. M.; Glotin, F.; Maitre, P. Gas Phase Infrared Spectroscopy of Selectively Prepared Ions. *Phys. Rev. Lett.* **2002**, *89*, 273002−273004.
(21) Valle, J. J.; Eyler, J. R.; Oomens, J.; Moore, D. T.; van der Meer, A. F. G.; von Helden, G.; Meijer, G.; Hendrickson, C. L.; Marshall, A. G.; Blakney, G. T. Free Electron Laser-Fourier Transform Ion Cyclotron Resonance Mass Spectrometry Facility for Obtaining Infrared Multiphoton Dissociation Spectra of Gaseous Ions. *Rev. Sci. Instrum.* **2005**, *76*, 023103/1−7.
(22) Oomens, J.; Sartakov, B. G.; Meijer, G.; von Helden, G. Gas-Phase Infrared Multiple Photon Dissociation Spectroscopy of Mass-Selected Molecular Ions. *Int. J. Mass Spectrom.* **2006**, *254*, 1−19.
(23) MacAleese, L.; Maitre, P. Infrared Spectroscopy of Organometallic Ions in the Gas Phase: from Model to Real World Complexes. *Mass Spectrom. Rev.* **2007**, *26*, 583−605.
(24) Polfer, N. C.; Oomens, J. Reaction Products in Mass Spectrometry Elucidated with Infrared Spectroscopy. *Phys. Chem. Chem. Phys.* **2007**, *9*, 3804−3817.
(25) Maitre, P.; Lemaire, J.; Scuderi, D. Structural Characterization under Tandem Mass Spectrometry Conditions: Infrared Spectroscopy of Gas Phase Ions. *Phys. Scr.* **2008**, *78*, 058111/1−6.
(26) Fridgen, T. D. Infrared Consequence Spectroscopy of Gaseous Protonated and Metal Ion Cationized Complexes. *Mass Spectrom. Rev.* **2009**, *28*, 586−607.
(27) Eyler, J. R. Infrared Multiple Photon Dissociation Spectroscopy of Ions in Penning Traps. *Mass Spectrom. Rev.* **2009**, *28*, 448−467.
(28) Polfer, N. C.; Oomens, J. Vibrational Spectroscopy of Bare and Solvated Ionic Complexes of Biological Relevance. *Mass Spectrom. Rev.* **2009**, *28*, 468−494.
(29) Baer, T.; Dunbar, R. C. Ion Spectroscopy: Where Did it Come from; Where is it Now; and Where is it Going? *J. Am. Soc. Mass Spectrom.* **2010**, *21*, 681−693.
(30) Polfer, N. C. Infrared Multiple Photon Dissociation Spectroscopy of Trapped Ions. *Chem. Soc. Rev.* **2011**, *40*, 2211−2221.
(31) Roithovà, J. Characterization of Reaction Intermediates by Ion Spectroscopy. *Chem. Soc. Rev.* **2012**, *41*, 547−559.
(32) Asmis, K. R.; Neumark, D. M. Vibrational Spectroscopy of Microhydrated Conjugate Base Anions. *Acc. Chem. Res.* **2012**, *45*, 43−52.
(33) Polfer, N. C.; Stedwell, C. N. Infrared Photodissociation of Biomolecular Ions. In *Laser Photodissociation and Spectroscopy of Mass-Separated Biomolecular Ions*; Polfer, N. C., Dugourd, P., Eds.; Lecture Notes in Chemistry, Vol. *83*; Springer: Switzerland, 2013; pp 93−116.
(34) Stedwell, C. N.; Galindo, J. F.; Roitberg, A. E.; Polfer, N. C. Structures of Biomolecular Ions in the Gas Phase Probed by Infrared Light Sources. *Annu. Rev. Anal. Chem.* **2013**, *6*, 267−285.
(35) Rijs, A. M.; Oomens, J. IR Spectroscopic Techniques to Study Isolated Biomolecules. In *Gas Phase IR Spectroscopy and Structure of Biological Molecules*; Rijs, A. M., Oomens, J., Eds.; Topics in Current Chemistry, Vol. *364*; Springer: Berlin, 2015; pp 1−42.
(36) Dunbar, R. C. In the Beginning Was H_2^+: Mass Spectrometry and the Molecular Spectroscopy of Gas-Phase Ions. *Int. J. Mass Spectrom.* **2015**, *377*, 159−171.
(37) Jasiková, L.; Roithová, J. Infrared Multiphoton Dissociation Spectroscopy with Free-Electron Lasers: On the Road from Small Molecules to Biomolecules. *Chem. - Eur. J.* **2018**, *24*, 3374−3390.
(38) Madsen, J. A.; Brodbelt, J. S. Comparison of Infrared Multiphoton Dissociation and Collision-Induced Dissociation of Supercharged Peptides in Ion Traps. *J. Am. Soc. Mass Spectrom.* **2009**, *20*, 349−358.
(39) Martens, J.; Berden, G.; Bentlage, H.; Coene, K. L. M.; Engelke, U. F.; Wishart, D.; van Scherpenzeel, M.; Kluijtmans, L. A. J.; Wevers, R. A.; Oomens, J. Unraveling the Unknown Areas of the Human Metabolome: the Role of Infrared Ion Spectroscopy. *J. Inherited Metab. Dis.* **2018**, *41*, 367−377.
(40) Cismesia, A. P.; Bell, M. R.; Tesler, L. F.; Alves, M.; Polfer, N. C. Infrared Ion Spectroscopy: an Analytical Tool for the Study of Metabolites. *Analyst* **2018**, *143*, 1615−1623.
(41) Kalume, D. E.; Molina, H.; Pandey, A. Tackling the Phosphoproteome: Tools and Strategies. *Curr. Opin. Chem. Biol.* **2003**, *7*, 64−69.
(42) Johnson, L. N.; Lewis, R. J. Structural Basis for Control by Phosphorylation. *Chem. Rev.* **2001**, *101*, 2209−2242.
(43) Temporini, C.; Calleri, E.; Massolini, G.; Caccialanza, G. Integrated Analytical Strategies for the Study of Phosphorylation and Glycosylation in Proteins. *Mass Spectrom. Rev.* **2008**, *27*, 207−236.
(44) Engholm-Keller, K.; Røssel Larsen, M. Technologies and Challenges in Large-Scale Phosphoproteomics. *Proteomics* **2013**, *13*, 910−931.
(45) Blume-Jensen, P.; Hunter, T. Oncogenic Kinase Signaling. *Nature* **2001**, *411*, 355−365.
(46) Sasaki, N. Current Status and Future Prospects for Research on Tyrosine Sulfation. *Curr. Pharm. Biotechnol.* **2012**, *13*, 2632−2641.
(47) Watson, E. E.; Liu, X.; Thompson, R. E.; Ripoll-Rozada, J.; Wu, M.; Alwis, I.; Gori, A.; Loh, C.-T.; Parker, B. J.; Otting, G.; et al. Mosquito-Derived Anophelin Sulfoproteins Are Potent Antithrombotics. *ACS Cent. Sci.* **2018**, *4*, 468−476.
(48) Stone, M. J.; Payne, R. J. Homogeneous Sulfopeptides and Sulfoproteins: Synthetic Approaches and Applications to Characterize the Effects of Tyrosine Sulfation on Biochemical Function. *Acc. Chem. Res.* **2015**, *48*, 2251−2261.
(49) Medzihradszky, K. F.; Darula, Z.; Perlson, E.; Fainzilber, M.; Chalkley, R. J.; Ball, H.; Greenbaum, D.; Bogyo, M.; Tyson, D. R.; Bradshaw, R. A.; et al. Mass Spectrometric Detection and Characterization of a New Posttranslational Modification in Diverse Proteins throughout the Eukaryotes. *Mol. Cell. Proteomics* **2004**, *3*, 429−440.
(50) Shoulders, M. D.; Raines, R. T. Collagen Structure and Stability. *Annu. Rev. Biochem.* **2009**, *78*, 929−958.
(51) Fass, D.; Thorpe, C. Chemistry and Enzymology of Disulfide Cross-Linking in Proteins. *Chem. Rev.* **2018**, *118*, 1169−1198.
(52) Couvertier, S. M.; Zhou, Y.; Weerapana, E. Chemical-Proteomic Strategies to Investigate Cysteine Posttranslational Modifications. *Biochim. Biophys. Acta, Proteins Proteomics* **2014**, *1844*, 2315−2330.
(53) Davies, M. J. Protein Oxidation and Peroxidation. *Biochem. J.* **2016**, *473*, 805−825.
(54) Chung, H. S.; Wang, S.-B.; Venkatraman, V.; Murray, C. I.; Van Eyk, J. E. Cysteine Oxidative Posttranslational Modifications: Emerging Regulation in the Cardiovascular System. *Circ. Res.* **2013**, *112*, 382−392.
(55) Roos, G.; Messens, J. Protein Sulfenic Acid Formation: from Cellular Damage to Redox Regulation. *Free Radical Biol. Med.* **2011**, *51*, 314−326.
(56) Zhong, F.; Pletneva, E. V. Ligation and Reactivity of Methionine-Oxidized Cytochrome *c*. *Inorg. Chem.* **2018**, *57*, 5754−5766.
(57) Seth, D.; Stamler, J. S. The SNO-Proteome: Causation and Classifications. *Curr. Opin. Chem. Biol.* **2011**, *15*, 129−136.
(58) Schulman, I. H.; Hare, J. M. Regulation of Cardiovascular Cellular Processes by S-Nitrosylation. *Biochim. Biophys. Acta, Gen. Subj.* **2012**, *1820*, 752−762.
(59) Moldogazieva, N. T.; Mokhosoev, I. M.; Feldman, N. B.; Lutsenko, S. V. ROS and RNS Signalling: Adaptive Redox Switches through Oxidative/Nitrosative Protein Modifications. *Free Radical Res.* **2018**, *52*, 507−543.
(60) López-Sánchez, L. M.; López-Pedrera, C.; Rodriguez-Ariza, A. Proteomic Approaches to Evaluate Protein S-Nitrosylation in Disease. *Mass Spectrom. Rev.* **2014**, *33*, 7−20.

DOI: 10.1021/acs.chemrev.9b00395
Chem. Rev. 2020, 120, 3261−3295

(61) Bryan, N. S.; Rassaf, T.; Maloney, R. E.; Rodriguez, C. M.; Saijo, F.; Rodriguez, J. R.; Feelisch, M. Cellular Targets and Mechanisms of Nitros(Yl)Ation: An Insight into their Nature and Kinetics in Vivo. *Proc. Natl. Acad. Sci. U. S. A.* **2004**, *101*, 4308−4313.
(62) Ferrer-Sueta, G.; Campolo, N.; Trujillo, M.; Bartesaghi, S.; Carballal, S.; Romero, N.; Alvarez, B.; Radi, R. Biochemistry of Peroxynitrite and Protein Tyrosine Nitration. *Chem. Rev.* **2018**, *118*, 1338−1408.
(63) Abello, N.; Kerstjens, H. A.; Postma, D. S.; Bischoff, R. Protein Tyrosine Nitration: Selectivity, Physicochemical and Biological Consequences, Denitration, and Proteomics Methods for the Identification of Tyrosine-Nitrated Proteins. *J. Proteome Res.* **2009**, *8*, 3222−3238.
(64) Choudhary, C.; Kumar, C.; Gnad, F.; Nielsen, M. L.; Rehman, M.; Walther, T. C.; Olsen, J. V.; Mann, M. Lysine Acetylation Targets Protein Complexes and Co-Regulates Major Cellular Functions. *Science* **2009**, *325*, 834−840.
(65) Shahbazian, M. D.; Grunstein, M. Functions of Site-Specific Histone Acetylation and Deacetylation. *Annu. Rev. Biochem.* **2007**, *76*, 75−100.
(66) Zhang, X.; Wen, H.; Shi, X. Lysine Methylation: Beyond Histones. *Acta Biochim. Biophys. Sin.* **2012**, *44*, 14−27.
(67) Black, J. C.; Whetstine, J. R. Tipping the Lysine Methylation Balance in Disease. *Biopolymers* **2013**, *99*, 127−135.
(68) Niwa, T. Mass Spectrometry for the Study of Protein Glycation in Disease. *Mass Spectrom. Rev.* **2006**, *25*, 713−723.
(69) Khoury, G. A.; Baliban, R. C.; Floudas, C. A. Proteome-Wide Post-Translational Modification Statistics: Frequency Analysis and Curation of the Swiss-Prot Database. *Sci. Rep.* **2011**, *1*, article no. 90. DOI: 10.1038/srep00090
(70) Spiro, R. G. Protein glycosylation: Nature, Distribution, Enzymatic Formation, and Disease Implications of Glycopeptides Bonds. *Glycobiology* **2002**, *12*, 43R−56R.
(71) Van den Steen, P.; Rudd, P. M.; Dwek, R. A.; Opdenakker, G. Concepts and Principles of O-Linked Glycosylation. *Crit. Rev. Biochem. Mol. Biol.* **1998**, *33*, 151−208.
(72) Robinson, N. E. Protein Deamidation. *Proc. Natl. Acad. Sci. U. S. A.* **2002**, *99*, 5283−5288.
(73) Yang, H.; Zubarev, R. A. Mass Spectrometric Analysis of Asparagine Deamidation and Aspartate Isomerization in Polypeptides. *Electrophoresis* **2010**, *31*, 1764−1772.
(74) Dedieu, A.; Gaillard, J.-C.; Pourcher, T.; Darrouzet, E.; Armengaud, J. Revisiting Iodination Sites in Thyroglobulin with an Organ-Oriented Shotgun Strategy. *J. Biol. Chem.* **2011**, *286*, 259−269.
(75) Dunford, H. B.; Ralston, I. M. On the Mechanism of Iodination of Tyrosine. *Biochem. Biophys. Res. Commun.* **1983**, *116*, 639−643.
(76) Liu, T.; Zhang, W.; Zhang, Z.; Chen, M.; Wang, J.; Qian, X.; Qin, W. Sensitive Western-Blot Analysis of Azide-Tagged Protein Post Translational Modifications Using Thermoresponsive Polymer Self-Assembly. *Anal. Chem.* **2018**, *90*, 2186−2192.
(77) Xiao, H.; Sun, F.; Suttapitugsakul, S.; Wu, R. Global and Site-Specific Analysis of Protein Glycosylation in Complex Biological Systems with Mass Spectrometry. *Mass Spectrom. Rev.* **2019**, *38*, 1−24.
(78) Chicooree, N.; Unwin, R. D.; Griffiths, J. R. The Application of Targeted Mass Spectrometry-Based Strategies to the Detection and Localization of Post-Translational Modifications. *Mass Spectrom. Rev.* **2015**, *34*, 595−626.
(79) Butterfield, D. A.; Gu, L.; Di Domenico, F.; Robinson, R. A. S. Mass Spectrometry and Redox Proteomics: Applications in Disease. *Mass Spectrom. Rev.* **2014**, *33*, 277−301.
(80) Aebersold, R.; Mann, M. Mass-Spectrometric Exploration of Proteome Structure and Function. *Nature* **2016**, *537*, 347−355.
(81) Witze, E. S.; Old, W. M.; Resing, K. A.; Ahn, N. G. Mapping Protein Post-Translational Modifications with Mass Spectrometry. *Nat. Methods* **2007**, *4*, 798−806.
(82) Jensen, O. N. Modification-Specific Proteomics: Characterization of Post-Translational Modifications by Mass Spectrometry. *Curr. Opin. Chem. Biol.* **2004**, *8*, 33−41.
(83) Kertesz, V.; Connelly, H. M.; Erickson, B. K.; Hettich, R. L. PTMSearchPlus: Software Tool for Automated Protein Identification and Post-Translational Modification Characterization by Integrating Accurate Intact Protein Mass and Bottom-Up Mass Spectrometric Data Searches. *Anal. Chem.* **2009**, *81*, 8387−8395.
(84) Gnad, F.; de Godoy, L. M. F.; Cox, J.; Neuhauser, N.; Ren, S.; Olsen, J. V.; Mann, M. High-Accuracy Identification and Bioinformatic Analysis of in Vivo Protein Phosphorylation Sites in Yeast. *Proteomics* **2009**, *9*, 4642−4652.
(85) Zhan, X.; Wang, X.; Desiderio, D. M. Mass Spectrometry Analysis of Nitrotyrosine-Containing Proteins. *Mass Spectrom. Rev.* **2015**, *34*, 423−448.
(86) Palumbo, A. M.; Smith, S. A.; Kalcic, C. L.; Dantus, M.; Stemmer, P. M.; Reid, G. E. Tandem Mass Spectrometry Strategies for Phosphoproteome Analysis. *Mass Spectrom. Rev.* **2011**, *30*, 600−625.
(87) Wang, T.; Tran, T. T. N.; Andreazza, H. J.; Bilusich, D.; Brinkworth, C. S.; Bowie, J. H. Negative Ion Cleavages of $(M-H)^-$ Anions Of Peptides. Part 3. Post-Translational Modifications. *Mass Spectrom. Rev.* **2018**, *37*, 3−21.
(88) Ryan, C. M.; Souda, P.; Bassilian, S.; Ujwal, R.; Zhang, J.; Abramson, J.; Ping, P.; Durazo, A.; Bowie, J. U.; Hasan, S. S.; et al. Post-Translational Modifications of Integral Membrane Proteins Resolved by Top-Down Fourier Transform Mass Spectrometry with Collisionally Activated Dissociation. *Mol. Cell. Proteomics* **2010**, *9*, 791−803.
(89) Yin, S.; Loo, J. A. Top-Down Mass Spectrometry of Supercharged Native Protein-Ligand Complexes. *Int. J. Mass Spectrom.* **2011**, *300*, 118−122.
(90) Xu, F.; Xu, Q.; Dong, X.; Guy, M.; Guner, H.; Hacker, T. A.; Ge, Y. Top-Down High-Resolution Electron Capture Dissociation Mass Spectrometry for Comprehensive Characterization of Post-Translational Modifications in *Rhesus* Monkey Cardiac Troponin I. *Int. J. Mass Spectrom.* **2011**, *305*, 95−102.
(91) Silva, A. M. N.; Vitorino, R.; Domingues, M. R. M.; Spickett, C. M.; Domingues, P. Post-Translational Modifications and Mass Spectrometry Detection. *Free Radical Biol. Med.* **2013**, *65*, 925−941.
(92) Sze, S. K.; Ge, Y.; Oh, H.; McLafferty, F. W. Top-Down Mass Spectrometry of a 29-kDa Protein for Characterization of any Posttranslational Modification to within one Residue. *Proc. Natl. Acad. Sci. U. S. A.* **2002**, *99*, 1774−1779.
(93) Zubarev, R. A.; Kelleher, N. L.; McLafferty, F. W. Electron Capture Dissociation of Multiply Charged Protein Cations. A non Ergodic Process. *J. Am. Chem. Soc.* **1998**, *120*, 3265−3266.
(94) Cooper, H. J.; Hakansson, K.; Marshall, A. G. The Role of Electron Capture Dissociation in Biomolecular Analysis. *Mass Spectrom. Rev.* **2005**, *24*, 201−222.
(95) Zubarev, R. A. Electron-Capture Dissociation Tandem Mass Spectrometry. *Curr. Opin. Biotechnol.* **2004**, *15*, 12−16.
(96) Zubarev, R. A. Reactions of Polypeptide Ions with Electrons in the Gas Phase. *Mass Spectrom. Rev.* **2003**, *22*, 57−77.
(97) Tsybin, Y. O.; Ramström, M.; Witt, M.; Baykut, G.; Hakansson, P. Peptide and Protein Characterization by High-Rate Electron Capture Dissociation Fourier Transform Ion Cyclotron Resonance Mass Spectrometry. *J. Mass Spectrom.* **2004**, *39*, 719−729.
(98) Syka, J. E. P.; Coon, J. J.; Schroeder, M. J.; Shabanowitz, J.; Hunt, D. F. Peptide and Protein Sequence Analysis by Electron Transfer Dissociation Mass Spectrometry. *Proc. Natl. Acad. Sci. U. S. A.* **2004**, *101*, 9528−9533.
(99) Wiesner, J.; Premsler, T.; Sickmann, A. Application of Electron Transfer Dissociation (ETD) for the Analysis of Post Translational Modifications. *Proteomics* **2008**, *8*, 4466−4483.
(100) Zhurov, K. O.; Fornelli, L.; Wodrich, M. D.; Laskay, U. A.; Tsybin, Y. O. Principles of Electron Capture and Transfer Dissociation Mass Spectrometry Applied to Peptide and Protein Structure Analysis. *Chem. Soc. Rev.* **2013**, *42*, 5014−5030.
(101) Olsen, J. V.; Macek, B.; Lange, O.; Makarov, A.; Horning, S.; Mann, M. Higher-Energy C-Trap Dissociation for Peptide Modification Analysis. *Nat. Methods* **2007**, *4*, 709−712.

DOI: 10.1021/acs.chemrev.9b00395
Chem. Rev. 2020, 120, 3261−3295

(102) Brodbelt, J. S. Photodissociation Mass Spectrometry: New Tools for Characterization of Biological Molecules. *Chem. Soc. Rev.* **2014**, *43*, 2757−2783.
(103) Kim, T.-Y.; Reilly, J. P. Time-Resolved Observation of Product Ions Generated by 157 nm Photodissociation of Singly Protonated Phosphopeptides. *J. Am. Soc. Mass Spectrom.* **2009**, *20*, 2334−2341.
(104) Fort, K. L.; Dyachenko, A.; Potel, C. M.; Corradini, E.; Marino, F.; Barendregt, A.; Makarov, A. A.; Scheltema, R. A.; Heck, A. J. R. Implementation of Ultraviolet Photodissociation on a Benchtop Q Exactive Mass Spectrometer and its Application to Phosphoproteomics. *Anal. Chem.* **2016**, *88*, 2303−2310.
(105) Robinson, M. R.; Taliaferro, J. M.; Dalby, K. N.; Brodbelt, J. S. 193 nm Ultraviolet Photodissociation Mass Spectrometry for Phosphopeptide Characterization in the Positive and Negative Ion Modes. *J. Proteome Res.* **2016**, *15*, 2739−2748.
(106) Oka, T. Observation of the Infrared Spectrum of H_3^+. *Phys. Rev. Lett.* **1980**, *45*, 531−534.
(107) Brodbelt, J. S.; Wilson, J. J. Infrared Multiphoton Dissociation in Quadrupole Ion Traps. *Mass Spectrom. Rev.* **2009**, *28*, 390−424.
(108) Gaumann, T.; Riveros, J. M.; Zhu, Z. The Infrared Multiphoton Dissociation Spectra of Bromopropene Isomeric Cations. *Helv. Chim. Acta* **1990**, *73*, 1215−1218.
(109) Okumura, M.; Yeh, L. I.; Lee, Y. T. The Vibrational Predissociation Spectroscopy of Hydrogen Cluster Ions. *J. Chem. Phys.* **1985**, *83*, 3705−3706.
(110) Shin, J.-W.; Hammer, N. I.; Diken, E. G.; Johnson, M. A.; Walters, R. S.; Jaeger, T. D.; Duncan, M. A.; Christie, R. A.; Jordan, K. D. Infrared Signature of Structures Associated with the $H^+(H_2O)_n$ (n = 6 to 27) clusters. *Science* **2004**, *304*, 1137−1140.
(111) Headrick, J. M.; Diken, E. G.; Walters, R. S.; Hammer, N. I.; Christie, R. A.; Cui, J.; Myshakin, E. M.; Duncan, M. A.; Johnson, M. A.; Jordan, K. D. Spectral Signatures of Hydrated Proton Vibrations in Water Clusters. *Science* **2005**, *308*, 1765−1769.
(112) Duncan, M. A. Infrared Laser Spectroscopy of Mass-Selected Carbocations. *J. Phys. Chem. A* **2012**, *116*, 11477−11491.
(113) Kamrath, M. Z.; Relph, R. A.; Guasco, T. L.; Leavitt, C. M.; Johnson, M. A. Vibrational Predissociation Spectroscopy of the H_2-Tagged Mono- and Dicarboxylate Anions of Dodecanedioic Acid. *Int. J. Mass Spectrom.* **2011**, *300*, 91−98.
(114) Bieske, E. J.; Dopfer, O. High Resolution Spectroscopy of Cluster Ions. *Chem. Rev.* **2000**, *100*, 3963−3998.
(115) Ebata, T.; Fujii, A.; Mikami, N. Vibrational Spectroscopy of Small-Sized Hydrogen-Bonded Clusters and their Ions. *Int. Rev. Phys. Chem.* **1998**, *17*, 331−361.
(116) Elias, L. R.; Fairbank, W. M.; Madey, J. M. J.; Schwettman, H. A.; Smith, T. I. Observation of Stimulated Emission of Radiation by Relativistic Electrons in a Spatially Periodic Transverse Magnetic-Field. *Phys. Rev. Lett.* **1976**, *36*, 717−720.
(117) Oepts, D.; Van der Meer, A. F. G.; Van Amersfoort, P. W. The Free-Electron-Laser User Facility Felix. *Infrared Phys. Technol.* **1995**, *36*, 297−308.
(118) Prazeres, R.; Glotin, F.; Insa, C.; Jaroszynski, D. A.; Ortega, J. M. Two-Color Operation of a Free-Electron Laser and Applications in the Mid-Infrared. *Eur. Phys. J. D* **1998**, *3*, 87−93.
(119) Mac Aleese, L.; Simon, A.; McMahon, T. B.; Ortega, J. M.; Scuderi, D.; Lemaire, J.; Maitre, P. Mid-IR Spectroscopy of Protonated Leucine Methyl Ester Performed with an FTICR or a Paul Type Ion-Trap. *Int. J. Mass Spectrom.* **2006**, *249*, 14−20.
(120) Remes, P. M.; Glish, G. L. Mapping the Distribution of Ion Positions as a Function of Quadrupole Ion Trap Mass Spectrometer Operating Parameters to Optimize Infrared Multiphoton Dissociation. *J. Phys. Chem. A* **2009**, *113*, 3447−3454.
(121) Bakker, J. M.; Besson, T.; Lemaire, J.; Scuderi, D.; Maitre, P. Gas-Phase Structure of a π-Allyl-Palladium Complex: Efficient Infrared Spectroscopy in a 7 T Fourier Transform Mass Spectrometer. *J. Phys. Chem. A* **2007**, *111*, 13415−13424.
(122) Hernandez, O.; Paizs, B.; Maitre, P. Rearrangement Chemistry of a_n Ions Probed by IR Spectroscopy. *Int. J. Mass Spectrom.* **2015**, *377*, 172−178.
(123) Oomens, J.; Moore, D. T.; Meijer, G.; von Helden, G. Infrared Multiple Photon Dynamics and Spectroscopy of Cationic PABA and its Dehydroxylated Fragment Ion. *Phys. Chem. Chem. Phys.* **2004**, *6*, 710−718.
(124) Prell, J. S.; O'Brien, J. T.; Williams, E. R. IRPD Spectroscopy and Ensemble Measurements: Effects of Different Data Acquisition and Analysis Methods. *J. Am. Soc. Mass Spectrom.* **2010**, *21*, 800−809.
(125) Becke, A. D. Density Functional Thermochemistry. The Role of Exact Exchange. *J. Chem. Phys.* **1993**, *98*, 5648−5652.
(126) Stephens, P. J.; Devlin, F. J.; Chabalowski, C. F.; Frisch, M. J. Ab Initio Calculation of Vibrational Absorption and Circular Dichroism Spectra Using Density Functional Force Fields. *J. Phys. Chem.* **1994**, *98*, 11623−11627.
(127) Halls, M. D.; Velkovski, J.; Schlegel, H. B. Harmonic Frequency Scaling Factors for Hartree-Fock, S-VWN, B-LYP, B3-LYP, B3-PW91 and MP2 with the Sadlej pVTZ Electric Property Basis Set. *Theor. Chem. Acc.* **2001**, *105*, 413−421.
(128) Correia, C. F.; Balaj, P.; Scuderi, D.; Maitre, P.; Ohanessian, G. Vibrational Signatures of Protonated, Phosphorylated Amino Acids in the Gas Phase. *J. Am. Chem. Soc.* **2008**, *130*, 3359−370.
(129) Paciotti, R.; Coletti, C.; Re, N.; Scuderi, D.; Chiavarino, B.; Fornarini, S.; Crestoni, M. E. Serine O-Sulfation Probed by IRMPD Spectroscopy. *Phys. Chem. Chem. Phys.* **2015**, *17*, 25891−25904.
(130) Nei, Y.-w.; Hallowita, N.; Steill, J. D.; Oomens, J.; Rodgers, M. T. Infrared Multiple Photon Dissociation Action Spectroscopy of Deprotonated DNA Mononucleotides: Gas-Phase Conformations and Energetics. *J. Phys. Chem. A* **2013**, *117*, 1319−1335.
(131) Ignasiak, M.; Scuderi, D.; De Oliveira, P.; Pedzinski, T.; Rayah, Y.; Houée Levin, C. Characterization by Mass Spectrometry and IRMPD Spectroscopy of the Sulfoxide Group in Oxidized Methionine and Related Compounds. *Chem. Phys. Lett.* **2011**, *502*, 29−36.
(132) Scuderi, D.; Bodo, E.; Chiavarino, B.; Fornarini, S.; Crestoni, M. E. Amino Acid Oxidation: A Combined Study of Cysteine Oxo Forms by IRMPD Spectroscopy and Simulations. *Chem. - Eur. J.* **2016**, *22*, 17239−17250.
(133) Oomens, J.; Steill, J. D.; Redlich, B. Gas-Phase IR Spectroscopy of Deprotonated Amino Acids. *J. Am. Chem. Soc.* **2009**, *131*, 4310−4319.
(134) Lanucara, F.; Chiavarino, B.; Crestoni, M. E.; Scuderi, D.; Sinha, R. K.; Maitre, P.; Fornarini, S. S-Nitrosation of Cysteine as Evidenced by IRMPD Spectroscopy. *Int. J. Mass Spectrom.* **2012**, *330*−*332*, 160−167.
(135) Sinha, R. K.; Scuderi, D.; Maitre, P.; Chiavarino, B.; Crestoni, M. E.; Fornarini, S. Elusive Sulfurous Acid: Gas Phase Basicity and IR Signature of the Protonated Species. *J. Phys. Chem. Lett.* **2015**, *6*, 1605−1610.
(136) Yacovitch, T. I.; Heine, N.; Brieger, C.; Wende, T.; Hock, C.; Neumark, D. M.; Asmis, K. R. Vibrational Spectroscopy of Bisulfate/Sulfuric Acid/Water Clusters: Structure, Stability, and Infrared Multiple-Photon Dissociation Intensities. *J. Phys. Chem. A* **2013**, *117*, 7081−7090.
(137) Macaluso, V.; Scuderi, D.; Crestoni, M. E.; Fornarini, S.; Corinti, D.; Dalloz, E.; Martínez-Núñez, E.; Hase, W.; Spezia, R. L-Cysteine Modified by S-Sulfation: Consequence on Fragmentation Processes Elucidated by Tandem Mass Spectrometry and Chemical Dynamics Simulations. *J. Phys. Chem. A* **2019**, *123*, 3685−3696.
(138) Sinha, R. K.; Chiavarino, B.; Fornarini, S.; Lemaire, J.; Maitre, P.; Crestoni, M. E. Protonated Sulfuric Acid: Vibrational Signatures of the Naked Ion in the Near- and Mid-IR. *J. Phys. Chem. Lett.* **2010**, *1*, 1721−1724.
(139) Ignasiak, M.; De Oliveira, P.; Levin, C. H.; Scuderi, D. Oxidation of Methionine-Containing Peptides by˙OH Radicals: Is Sulfoxide the Only Product? Study by Mass Spectrometry and IRMPD Spectroscopy. *Chem. Phys. Lett.* **2013**, *590*, 35−40.

DOI: 10.1021/acs.chemrev.9b00395
Chem. Rev. 2020, 120, 3261−3295

(140) Scuderi, D.; Ignasiak, M. T.; Serfaty, X.; De Oliveira, P.; Houée Levin, C. Tandem Mass Spectrometry and Infrared Spectroscopy as a Tool to Identify Peptide Oxidized Residues. *Phys. Chem. Chem. Phys.* **2015**, *17*, 25998−26007.
(141) Gregori, B.; Guidoni, L.; Crestoni, M. E.; de Oliveira, P.; Houée-Levin, C.; Scuderi, D. One-Electron Oxidation of Methionine-Containing Dipeptides of Reverse Sequence: Sulfur versus Sulfoxide Characterized by IRMPD Spectroscopy and Static and Dynamics DFT Simulations. *J. Phys. Chem. B* **2017**, *121*, 2083−2094.
(142) Di Stefano, S.; Mazzonna, M.; Bodo, E.; Mandolini, L.; Lanzalunga, O. Photoinversion of Sulfoxides as a Source of Diversity in Dynamic Combinatorial Chemistry. *Org. Lett.* **2011**, *13*, 142−145.
(143) Scuderi, D.; Le Barbu-Debus, K.; Zehnacker, A. The Role of Weak Hydrogen Bonds in Chiral Recognition. *Phys. Chem. Chem. Phys.* **2011**, *13*, 17916−17929.
(144) Sunahori, F. X.; Yang, G.; Kitova, E. N.; Klassen, J. S.; Xu, Y. Chirality Recognition of the Protonated Serine Dimer and Octamer by Infrared Multiphoton Dissociation Spectroscopy. *Phys. Chem. Chem. Phys.* **2013**, *15*, 1873−1886.
(145) Lepere, V.; Le Barbu-Debus, K.; Clavaguera, C.; Scuderi, D.; Piani, G.; Simon, A.; Chirot, F.; MacAleese, L.; Dugourd, P.; Zehnacker, A. Chirality-Dependent Structuration of Protonated or Sodiated Polyphenylalanines: IRMPD and Ion Mobility Studies. *Phys. Chem. Chem. Phys.* **2016**, *18*, 1807−1817.
(146) Alata, I.; Perez-Melor, A.; Ben-Nasr, F.; Scuderi, D.; Steinmetz, V.; Gobert, F.; Jaidane, N.-E.; Zehnacker-Rentien, A. Does the Residues Chirality Modify the Conformation of a Cyclo-Dipeptide? Vibrational Spectroscopy of Protonated Cyclo-Diphenylalanine in the Gas Phase. *J. Phys. Chem. A* **2017**, *121*, 7130−7138.
(147) Scuderi, D.; Bergès, J.; de Oliveira, P.; Houée-Levin, C. Methionine One-Electron Oxidation: Coherent Contributions from Radiolysis, IRMPD Spectroscopy, DFT Calculations and Electrochemistry. *Radiat. Phys. Chem.* **2016**, *128*, 103−111.
(148) Filipiak, P.; Hug, G. L.; Bobrowski, K.; Pedzinski, T.; Kozubek, H.; Marciniak, B. Sensitized Photooxidation of S-Methylglutathione in Aqueous Solution: Intramolecular (S∴O) and (S∴N) Bonded Species. *J. Phys. Chem. B* **2013**, *117*, 2359−2368.
(149) Gregori, B.; Guidoni, L.; Chiavarino, B.; Scuderi, D.; Nicol, E.; Frison, G.; Fornarini, S.; Crestoni, M. E. Vibrational Signatures of S-Nitroso Glutathione as Gaseous, Protonated Species. *J. Phys. Chem. B* **2014**, *118*, 12371−12382.
(150) Coates, J. Interpretation of Infrared Spectra, A Practical Approach. In *Encyclopedia of Analytical Chemistry*; Meyers, R. A., Ed.; John Wiley & Sons Ltd: Chichester, 2000; pp 10815−10837.
(151) Crestoni, M. E.; Chiavarino, B.; Scuderi, D.; Di Marzio, A.; Fornarini, S. Discrimination of 4-Hydroxyproline Diastereomers by Vibrational Spectroscopy of the Gaseous Protonated Species. *J. Phys. Chem. B* **2012**, *116*, 8771−8779.
(152) Stearns, J. A.; Mercier, S.; Seaiby, C.; Guidi, M.; Boyarkin, O. V.; Rizzo, T. R. Conformation-Specific Spectroscopy and Photodissociation of Cold, Protonated Tyrosine and Phenylalanine. *J. Am. Chem. Soc.* **2007**, *129*, 11814−11820.
(153) Scuderi, D.; Bakker, J. M.; Durand, S.; Maitre, P.; Sharma, A.; Martens, J. K.; Nicol, E.; Clavaguera, C.; Ohanessian, G. Structure of Singly Hydrated, Protonated Phospho-Tyrosine. *Int. J. Mass Spectrom.* **2011**, *308*, 338−347.
(154) Wu, R. H.; McMahon, T. B. An Investigation of Protonation Sites and Conformations of Protonated Amino Acids by IRMPD Spectroscopy. *ChemPhysChem* **2008**, *9*, 2826−2835.
(155) Correia, C. F.; Clavaguera, C.; Erlekam, U.; Scuderi, D.; Ohanessian, G. IRMPD Spectroscopy of a Protonated, Phosphorylated Dipeptide. *ChemPhysChem* **2008**, *9*, 2564−2573.
(156) Turecek, F.; Moss, C. L.; Pikalov, I.; Pepin, R.; Gulyuz, K.; Polfer, N. C.; Brown, J.; Williams, J.; Richardson, K. Gas-Phase Structures of Phosphopeptide Ions: A difficult case. *Int. J. Mass Spectrom.* **2013**, *354*−*355*, 249−256.
(157) Scuderi, D.; Correia, C. F.; Balaj, O. P.; Ohanessian, G.; Lemaire, J.; Maitre, P. Structural Characterization by IRMPD Spectroscopy and DFT Calculations of Deprotonated Phosphorylated Amino Acids in the Gas Phase. *ChemPhysChem* **2009**, *10*, 1630−1641.
(158) Fales, B. S.; Fujamade, N. O.; Nei, Y.-W.; Oomens, J.; Rodgers, M. T. Infrared Multiple Photon Dissociation Action Spectroscopy and Theoretical Studies of Diethyl Phosphate Complexes: Effects of Protonation and Sodium Cationization on Structure. *J. Am. Soc. Mass Spectrom.* **2011**, *22*, 81−92.
(159) Stedwell, C. N.; Patrick, A. L.; Gulyuz, K.; Polfer, N. C. Screening for Phosphorylated and Nonphosphorylated Peptides by Infrared Photodissociation Spectroscopy. *Anal. Chem.* **2012**, *84*, 9907−9912.
(160) Kopysov, V.; Nagornova, N. S.; Boyarkin, O. V. Identification of Tyrosine-Phosphorylated Peptides Using Cold Ion Spectroscopy. *J. Am. Chem. Soc.* **2014**, *136*, 9288−9291.
(161) Bossio, R. E.; Marshall, A. G. Baseline Resolution of Isobaric Phosphorylated and Sulfated Peptides and Nucleotides by Electrospray Ionization FTICR MS: Another Step toward Mass Spectrometry-Based Proteomics. *Anal. Chem.* **2002**, *74*, 1674−1679.
(162) Patrick, A. L.; Stedwell, C. N.; Polfer, N. C. Differentiating Sulfopeptide and Phosphopeptide Ions via Resonant Infrared Photodissociation. *Anal. Chem.* **2014**, *86*, 5547−5552.
(163) Schindler, B.; Joshi, J.; Allouche, A.-R.; Simon, D.; Chambert, S.; Brites, V.; Gaigeot, M.-P.; Compagnon, I. Distinguishing Isobaric Phosphated and Sulfated Carbohydrates by Coupling of Mass Spectrometry with Gas Phase Vibrational Spectroscopy. *Phys. Chem. Chem. Phys.* **2014**, *16*, 22131−22138.
(164) Yacovitch, T. I.; Wende, T.; Jiang, L.; Heine, N.; Meijer, G.; Neumark, D. M.; Asmis, K. R. Infrared Spectroscopy of Hydrated Bisulfate Anion Clusters: $HSO_4^-(H_2O)_{1-16}$. *J. Phys. Chem. Lett.* **2011**, *2*, 2135−2140.
(165) Lanucara, F.; Chiavarino, B.; Crestoni, M. E.; Scuderi, D.; Sinha, R. K.; Maitre, P.; Fornarini, S. S-Nitrosation of Cysteine as Evidenced by IRMPD Spectroscopy. *Int. J. Mass Spectrom.* **2012**, *330*−*332*, 160−167.
(166) Osburn, S.; Steill, J. D.; Oomens, J.; O'Hair, R. A. J.; van Stipdonk, M.; Ryzhov, V. Structure and Reactivity of the Cysteine Methyl Ester Radical Cation. *Chem. - Eur. J.* **2011**, *17*, 873−879.
(167) Citir, M.; Stennett, E. M. S.; Oomens, J.; Steill, J. D.; Rodgers, M. T.; Armentrout, P. B. Infrared Multiple Photon Dissociation Spectroscopy of Cationized Cysteine: Effects of Metal Cation Size on Gas-Phase Conformation. *Int. J. Mass Spectrom.* **2010**, *297*, 9−17.
(168) Lanucara, F.; Scuderi, D.; Chiavarino, B.; Fornarini, S.; Maitre, P.; Crestoni, M. E. IR Signature of NO Binding to a Ferrous Heme Center. *J. Phys. Chem. Lett.* **2013**, *4*, 2414−2417.
(169) Lanucara, F.; Chiavarino, B.; Crestoni, M. E.; Scuderi, D.; Sinha, R. K.; Maitre, P.; Fornarini, S. Naked Five-Coordinate FeIII(NO) Porphyrin Complexes: Vibrational and Reactivity Features. *Inorg. Chem.* **2011**, *50*, 4445−4452.
(170) Chiavarino, B.; Crestoni, M. E.; Fornarini, S.; Lanucara, F.; Lemaire, J.; Maitre, P.; Scuderi, D. Direct Probe of NO Vibration in the Naked Ferric Heme Nitrosyl Complex. *ChemPhysChem* **2008**, *9*, 826−828.
(171) Coletti, C.; Re, N.; Scuderi, D.; Maitre, P.; Chiavarino, B.; Fornarini, S.; Lanucara, F.; Sinha, R. K.; Crestoni, M. E. IRMPD Spectroscopy of Protonated S-Nitrosocaptopril, a Biologically Active, Synthetic Amino Acid. *Phys. Chem. Chem. Phys.* **2010**, *12*, 13455−13467.
(172) Crestoni, M. E.; Lanucara, F.; Chiavarino, B.; Fornarini, S. N-Nitrosation of N-Acetyltryptophan Probed by IR Spectroscopy of the Gaseous Anion. *Chem. Phys. Lett.* **2013**, *588*, 215−219.
(173) Rubbo, H.; Radi, R. Protein and Lipid Nitration: Role in Redox Signaling and Injury. *Biochim. Biophys. Acta, Gen. Subj.* **2008**, *1780*, 1318−1324.
(174) Sinha, R. K.; Chiavarino, B.; Crestoni, M. E.; Scuderi, D.; Fornarini, S. Tyrosine Nitration as Evidenced by IRMPD Spectroscopy. *Int. J. Mass Spectrom.* **2011**, *308*, 209−216.
(175) Gronert, S.; Simpson, D. C.; Conner, K. M. A Reevaluation of Computed Proton Affinities for the Common Alpha-Amino Acids. *J. Am. Soc. Mass Spectrom.* **2009**, *20*, 2116−2123.

DOI: 10.1021/acs.chemrev.9b00395
Chem. Rev. 2020, 120, 3261−3295

(176) Bouchoux, G.; Bourcier, S.; Blanc, V.; Desaphy, S. Gas Phase Protonation Thermochemistry of Phenylalanine and Tyrosine. *J. Phys. Chem. B* **2009**, *113*, 5549−5562.
(177) Steill, J. D.; Oomens, J. Spectroscopically Resolved Competition between Dissociation and Detachment from Nitrobenzene Radical Anion. *Int. J. Mass Spectrom.* **2011**, *308*, 239−252.
(178) Corinti, D.; Gregori, B.; Guidoni, L.; Scuderi, D.; McMahon, T.; Chiavarino, B.; Fornarini, S.; Crestoni, M. E. Complexation of Halide Ions to Tyrosine: Role of Non-Covalent Interactions Evidenced by IRMPD Spectroscopy. *Phys. Chem. Chem. Phys.* **2018**, *20*, 4429−4441.
(179) Bush, M. F.; Forbes, M. W.; Jockusch, R. A.; Oomens, J.; Polfer, N. C.; Saykally, R. J.; Williams, E. R. Infrared Spectroscopy of Cationized Lysine and ε-N-Methyllysine in the Gas Phase: Effects of Alkali-Metal Ion Size and Proton Affinity on Zwitterion Stability. *J. Phys. Chem. A* **2007**, *111*, 7753−7760.
(180) Lemoff, A. S.; Bush, M. F.; O'Brien, J. T.; Williams, E. R. Structures of Lithiated Lysine and Structural Analogues in the Gas Phase: Effects of Water and Proton Affinity on Zwitterionic Stability. *J. Phys. Chem. A* **2006**, *110*, 8433−8442.
(181) Kempkes, L. J. M.; Martens, J. K.; Grzetic, J.; Berden, G.; Oomens, J. Deamidation Reactions of Protonated Asparagine and Glutamine Investigated by Ion Spectroscopy. *Rapid Commun. Mass Spectrom.* **2016**, *30*, 483−490.
(182) Heaton, A. L.; Armentrout, P. B. Thermodynamics and Mechanism Of Protonated Asparagine Decomposition. *J. Am. Soc. Mass Spectrom.* **2009**, *20*, 852−866.
(183) Heaton, A. L.; Bowman, V. N.; Oomens, J.; Steil, J. D.; Armentrout, P. B. Infrared Multiple Photon Dissociation Spectroscopy of Cationized Asparagine: Effects of Metal Cation Size on Gas-Phase Conformation. *J. Phys. Chem. A* **2009**, *113*, 5519−5530.
(184) Rogalewicz, F.; Hoppilliard, Y.; Ohanessian, G. Fragmentation Mechanisms of Alpha-Amino Acids Protonated under Electrospray Ionization. A Collision Activation and ab Initio Theoretical Study. *Int. J. Mass Spectrom.* **2000**, *195/196*, 565−590.
(185) Fukui, K.; Takahashi, K. Infrared Multiple Photon Dissociation Spectroscopy and Computational Studies of O-Glycosylated Peptides. *Anal. Chem.* **2012**, *84*, 2188−2194.
(186) Patrick, A. L.; Polfer, N. C. Peptide Fragmentation Products in Mass Spectrometry Probed by Infrared Spectroscopy. *Top. Curr. Chem.* **2014**, *364*, 153−182.
(187) Polfer, N. C.; Oomens, J.; Suhai, S.; Paizs, B. Spectroscopic and Theoretical Evidence for Oxazolone Ring Formation in Collision-Induced Dissociation of Peptides. *J. Am. Chem. Soc.* **2005**, *127*, 17154−17155.
(188) Ranka, K.; Zhao, N.; Yu, L.; Stanton, J. F.; Polfer, N. C. Radical Rearrangement Chemistry in Ultraviolet Photodissociation of Iodotyrosine Systems: Insights from Metastable Dissociation, Infrared Ion Spectroscopy, and Reaction Pathway Calculations. *J. Am. Soc. Mass Spectrom.* **2018**, *29*, 1791−1801.
(189) Sun, Q.; Yin, S.; Loo, J. A.; Julian, R. R. Radical Directed Dissociation for Facile Identification of Iodo- Tyrosine Residues using ESI-MS. *Anal. Chem.* **2010**, *82*, 3826−3833.
(190) Lanucara, F.; Chiavarino, B.; Scuderi, D.; Maitre, P.; Fornarini, S.; Crestoni, M. E. Kinetic Control in the CID-Induced Elimination of H_3PO_4 from Phosphorylated Serine Probed by IRMPD Spectroscopy. *Chem. Commun.* **2014**, *50*, 3845−3848.
(191) Reid, G. E.; Simpson, R. J.; O'Hair, R. A. J. Leaving Group and Gas Phase Neighboring Group Effects in the Side Chain Losses from Protonated Serine and its Derivatives. *J. Am. Soc. Mass Spectrom.* **2000**, *11*, 1047−1060.
(192) Rozman, M. Modelling of the Gas-Phase Phosphate Group Loss and Rearrangement in Phosphorylated Peptides. *J. Mass Spectrom.* **2011**, *46*, 949−955.
(193) O'Hair, R. A. J.; Reid, G. E. Does Side Chain Water Loss from Protonated Threonine Yield N-Protonated Dehydroamino-2-Butyric Acid? *Rapid Commun. Mass Spectrom.* **1998**, *12*, 999−1002.
(194) Patrick, A. L.; Stedwell, C. N.; Schindler, B.; Compagnon, I.; Berden, G.; Oomens, J.; Polfer, N. C. Insights into the Fragmentation Pathways of Gas-Phase Protonated Sulfoserine. *Int. J. Mass Spectrom.* **2015**, *379*, 26−32.
(195) Laskin, J.; Futrell, J. H. Activation of Large Ions in FT-ICR Mass Spectrometry. *Mass Spectrom. Rev.* **2005**, *24*, 135−167.
(196) Stephenson, J. L.; Booth, M. M.; Shalosky, J. A.; Eyler, J. R.; Yost, R. A. Infrared Multiple Photon Dissociation in the Quadrupole Ion Trap via a Multipass Optical Arrangement. *J. Am. Soc. Mass Spectrom.* **1994**, *5*, 886−893.
(197) Gardner, M. A.; Ledvina, A. R.; Smith, S.; Madsen, J.; Schwartz, G. C.; Stafford, G. C.; Coon, J. J.; Brodbelt, J. S. Infrared Multiphoton Dissociation of Peptide Cations in a Dual Pressure Linear Ion Trap Mass Spectrometer. *Anal. Chem.* **2009**, *81*, 8109−8118.
(198) Goolsby, B. J.; Brodbelt, J. S. Analysis of Protonated and Alkali Metal Cationized Aminoglycoside Antibiotics by Collision-Activated Dissociation and Infrared Multi-Photon Dissociation in the Quadrupole Ion Trap. *J. Mass Spectrom.* **2000**, *35*, 1011−1024.
(199) Goolsby, B. J.; Brodbelt, J. S. Tandem Infrared Multiphoton Dissociation and Collisionally Activated Dissociation Techniques in a Quadrupole Ion Trap. *Anal. Chem.* **2001**, *73*, 1270−1276.
(200) Chiavarino, B.; Crestoni, M. E.; Fornarini, S.; Dopfer, O.; Lemaire, J.; Maitre, P. IR Spectroscopic Features of Gaseous $C_7H_7O^+$ Ions: Benzylium versus Tropylium Ion Structures. *J. Phys. Chem. A* **2006**, *110*, 9352−9360.
(201) Payne, A. H.; Glish, G. L. Thermally Assisted Infrared Multiphoton Photodissociation in a Quadrupole Ion Trap. *Anal. Chem.* **2001**, *73*, 3542−3548.
(202) Raspopov, S. A.; El-Faramawy, A.; Thomson, B. A.; Siu, K. W. M. IRMPD in Quadrupole Time-of-Flight Mass Spectrometry: Top-Down Characterization of Proteins. *Anal. Chem.* **2006**, *78*, 4572−4577.
(203) Freitas, M. A.; Hendrickson, C. L.; Marshall, A. G. Determination of Relative Ordering of Activation Energies for Gas-Phase Ion Unimolecular Dissociation by Infrared Radiation for Gaseous Multiphoton Energy Transfer. *J. Am. Chem. Soc.* **2000**, *122*, 7768−7775.
(204) Polfer, N. C.; Stedwell, C. N. UV-Visible Activation of Biomolecular Ions. In *Laser Photodissociation and Spectroscopy of Mass-separated Biomolecular Ions*; Polfer, N. C., Dugourd, P., Eds.; Lecture Notes in Chemistry, Vol. *83*; Springer: Switzerland, 2013; pp 71−92.
(205) Flora, J. W.; Muddiman, D. C. Selective, Sensitive, and Rapid Phosphopeptide Identification in Enzymatic Digests Using ESI-FTICR-MS with Infrared Multiphoton Dissociation. *Anal. Chem.* **2001**, *73*, 3305−3311.
(206) Flora, J. W.; Muddiman, D. C. Determination of the Relative Energies of Activation for the Dissociation of Aromatic versus Aliphatic Phosphopeptides by ESI-FTICR-MS and IRMPD. *J. Am. Soc. Mass Spectrom.* **2004**, *15*, 121−127.
(207) Flora, J. W.; Muddiman, D. C. Gas-Phase Ion Unimolecular Dissociation for Rapid Phosphopeptide Mapping by IRMPD in a Penning Ion Trap: An Energetically Favored Process. *J. Am. Chem. Soc.* **2002**, *124*, 6546−6547.
(208) DeGnore, J. P.; Qin, J. Fragmentation of Phosphopeptides in an Ion Trap Mass Spectrometer. *J. Am. Soc. Mass Spectrom.* **1998**, *9*, 1175−1188.
(209) Crowe, M. C.; Brodbelt, J. S. Infrared Multiphoton Dissociation (IRMPD) and Collisionally Activated Dissociation of Peptides in a Quadrupole Ion Trap with Selective IRMPD of Phosphopeptides. *J. Am. Soc. Mass Spectrom.* **2004**, *15*, 1581−1592.
(210) Crowe, M. C.; Brodbelt, J. S. Differentiation of Phosphorylated and Unphosphorylated Peptides by HP-LC-ESI-IRMPD in a Quadrupole Ion Trap. *Anal. Chem.* **2005**, *77*, 5726−5734.
(211) Vasicek, L. A.; Ledvina, A. R.; Shaw, J.; Griep-Raming, J.; Westphall, M. S.; Coon, J. J.; Brodbelt, J. S. Implementing Photodissociation in an Orbitrap Mass Spectrometer. *J. Am. Soc. Mass Spectrom.* **2011**, *22*, 1105−1108.
(212) Stingl, C.; Ihling, C.; Ammerer, G.; Sinz, A.; Mechtler, K. Application of Different Fragmentation Techniques for the Analysis of Phosphopeptides Using a Hybrid Linear Ion Trap-FTICR Mass

DOI: 10.1021/acs.chemrev.9b00395
Chem. Rev. 2020, 120, 3261−3295

Spectrometer. *Biochim. Biophys. Acta, Proteins Proteomics* **2006**, *1764*, 1842−1852.
(213) Gardner, M. W.; Vasicek, L. A.; Shabbir, S.; Anslyn, E. V.; Brodbelt, J. S. Chromogenic Cross-Linker for the Characterization of Protein Structure by Infrared Multiphoton Dissociation Mass Spectrometry. *Anal. Chem.* **2008**, *80*, 4807−4819.
(214) Halim, M. A.; MacAleese, L.; Lemoine, J.; Antoine, R.; Dugourd, P.; Girod, M. Ultraviolet, Infrared, and High-Low Energy Photodissociation of Post-Translationally Modified Peptides. *J. Am. Soc. Mass Spectrom.* **2018**, *29*, 270−283.
(215) Wilson, J. J.; Brodbelt, J. S. Infrared Multiphoton Dissociation for Enhanced de Novo Sequence Interpretation of N-Terminal Sulfonated Peptides in a Quadrupole Ion Trap. *Anal. Chem.* **2006**, *78*, 6855−6862.
(216) Seipert, R. R.; Dodds, E. D.; Clowers, B. H.; Beecroft, S. M.; German, J. B.; Lebrilla, C. B. Factors that Influence Fragmentation Behavior of N-Linked Glycopeptide Ions. *Anal. Chem.* **2008**, *80*, 3684−3692.
(217) Paizs, B.; Suhai, S. Fragmentation Pathways of Protonated Peptides. *Mass Spectrom. Rev.* **2005**, *24*, 508−548.
(218) Cox, K. A.; Gaskell, S. J.; Morris, M.; Whiting, A. Role of the Site of Protonation in the Low-Energy Decompositions of Gas-Phase Peptide Ions. *J. Am. Soc. Mass Spectrom.* **1996**, *7*, 522−531.
(219) Dongre, A. R.; Jones, J. L.; Somogyi, A.; Wysocki, V. H. Influence of Peptide Composition, Gas-Phase Basicity, and Chemical Modification on Fragmentation Efficiency: Evidence for the Mobile Proton Model. *J. Am. Chem. Soc.* **1996**, *118*, 8365−8374.
(220) Seipert, R. R.; Dodds, E. D.; Lebrilla, C. B. Exploiting Differential Dissociation Chemistries of O-Linked Glycopeptide Ions for the Localization of Mucin-Type Protein Glycosylation. *J. Proteome Res.* **2009**, *8*, 493−501.
(221) Borotto, N. B.; McClory, P. J.; Martin, B. R.; Hakansson, K. Targeted Annotation of S-Sulfonylated Peptides By Selective Infrared Multiphoton Dissociation Mass Spectrometry. *Anal. Chem.* **2017**, *89*, 8304−8310.
(222) Kalli, A.; Hakansson, K. Preferential Cleavage of S-S and C-S Bonds in Electron Detachment Dissociation and Infrared Multiphoton Dissociation of Disulfide-Linked Peptide Anions. *Int. J. Mass Spectrom.* **2007**, *263*, 71−81.
(223) Biemann, B. Nomenclature for Peptide Fragment Ions (Positive Ions). *Methods Enzymol.* **1990**, *193*, 886−887.
(224) Chu, I. K.; Siu, C.-K.; Lau, J. K.-C.; Tang, W. K.; Mu, X.; Lai, C. K.; Guo, X.; Wang, X.; Li, N.; Xia, Y.; et al. Proposed Nomenclature for Peptide Ion Fragmentation. *Int. J. Mass Spectrom.* **2015**, *390*, 24−27.
(225) Chalmers, M. J.; Hakansson, K.; Johnson, R.; Smith, R.; Shen, J.; Emmett, M. R.; Marshall, A. G. Protein Kinase A phosphorylation Characterized by Tandem Fourier Transform Ion Cyclotron Resonance Mass Spectrometry. *Proteomics* **2004**, *4*, 970−981.
(226) Potel, C. M.; Lemeer, S.; Heck, A. J. R. Phosphopeptide Fragmentation and Site Localization by Mass Spectrometry: An Update. *Anal. Chem.* **2019**, *91*, 126−141.
(227) Riley, N. M.; Westphall, M. S.; Hebert, A. S.; Coon, J. J. Implementation of Activated Ion Electron Transfer Dissociation on a Quadrupole-Orbitrap-Linear Ion Trap Hybrid Mass Spectrometer. *Anal. Chem.* **2017**, *89*, 6358−6366.
(228) Riley, N. M.; Hebert, A. S.; Dürnberger, G.; Stanek, F.; Mechtler, K.; Westphall, M. S.; Coon, J. J. Phosphoproteomics with Activated Ion Electron Transfer Dissociation. *Anal. Chem.* **2017**, *89*, 6367−6376.
(229) Ruhaak, L. R.; Xu, G.; Li, Q.; Goonatilleke, E.; Lebrilla, C. B. Mass Spectrometry Approaches to Glycomic and Glycoproteomic Analyses. *Chem. Rev.* **2018**, *118*, 7886−7930.
(230) Hakansson, K.; Cooper, H. J.; Emmett, M. R.; Costello, C. E.; Marshall, A. G.; Nilsson, C. L. Electron Capture Dissociation and Infrared Multiphoton Dissociation MS/MS of an N-Glycosylated Tryptic Peptide to Yield Complementary Sequence Information. *Anal. Chem.* **2001**, *73*, 4530−4536.
(231) Hakansson, K.; Chalmers, M. J.; Quinn, J. P.; McFarland, M. A.; Hendrickson, C. L.; Marshall, A. G. Combined ECD and IRMPD for Multistage MS/MS in a FTICR Mass Spectrometer. *Anal. Chem.* **2003**, *75*, 3256−3262.
(232) An, H. J.; Lebrilla, C. B. Structure Elucidation of Native N- and O-Linked Glycans by Tandem Mass Spectrometry. *Mass Spectrom. Rev.* **2011**, *30*, 560−578.
(233) Lanucara, F.; Eyers, C. E. Top-Down Mass Spectrometry for the Analysis of Combinatorial Post-Translational Modifications. *Mass Spectrom. Rev.* **2013**, *32*, 27−42.
(234) Mikhailov, V. A.; Iniesta, J.; Cooper, H. J. Top-Down Mass Analysis of Protein Tyrosine Nitration: Comparison of Electron Capture Dissociation with "Slow-Heating" Tandem Mass Spectrometry Methods. *Anal. Chem.* **2010**, *82*, 7283−7292.
(235) Soulby, A. J.; Heal, J. W.; Barrow, M. P.; Roemer, R. A.; O'Connor, P. B. Does Deamidation Cause Protein Unfolding? A Top-Down Tandem Mass Spectrometry Study. *Protein Sci.* **2015**, *24*, 850−860.
(236) Halim, M. A.; Girod, M.; MacAleese, L.; Lemoine, J.; Antoine, R.; Dugourd, P. Combined Infrared Multiphoton Dissociation with Ultraviolet Photodissociation for Ubiquitin Characterization. *J. Am. Soc. Mass Spectrom.* **2016**, *27*, 1435−1442.
(237) Schwarz, H.; Asmis, K. R. Identification of Active Sites and Structural Characterization of Reactive Ionic Intermediates by Cryogenic Ion Trap Vibrational Spectroscopy. *Chem. - Eur. J.* **2019**, *25*, 2112−2126.
(238) Roithovà, J.; Gray, A.; Andris, E.; Jasik, J.; Gerlich, D. Helium Tagging Infrared Photodissociation Spectroscopy of Reactive Ions. *Acc. Chem. Res.* **2016**, *49*, 223−230.
(239) Rizzo, T. R.; Boyarkin, O. V. Cryogenic Methods for the Spectroscopy of Large, Biomolecular Ions. In *Gas Phase IR Spectroscopy and Structure of Biological Molecules*; Rijs, A. M., Oomens, J., Eds.; Topics in Current Chemistry, Vol. *364*; Springer: Berlin, 2015; pp 43−97.
(240) Redwine, J. G.; Davis, Z. A.; Burke, N. L.; Oglesbee, R. A.; McLuckey, S. A.; Zwier, T. S. A Novel Ion Trap Based Tandem Mass Spectrometer for the Spectroscopic Study of Cold Gas Phase Polyatomic Ions. *Int. J. Mass Spectrom.* **2013**, *348*, 9−14.
(241) Gerlich, D.; Borodi, G. Buffer Gas Cooling of Polyatomic Ions in rf Multielectrode Traps. *Faraday Discuss.* **2009**, *142*, 57−72.
(242) Tesler, L. F.; Cismesia, A. P.; Bell, M. R.; Bailey, L. S.; Polfer, N. C. Operation and Performance of a Mass-Selective Cryogenic Linear Ion Trap. *J. Am. Soc. Mass Spectrom.* **2018**, *29*, 2115−2124.
(243) Gunther, A.; Nieto, P.; Muller, D.; Sheldrick, A.; Gerlich, D.; Dopfer, O. BerlinTrap: a New Cryogenic 22-Pole Ion Trap Spectrometer. *J. Mol. Spectrosc.* **2017**, *332*, 8−15.
(244) Schlemmer, S.; Kuhn, T.; Lescop, E.; Gerlich, D. Laser Excited N_2^+ in a 22-Pole Ion Trap: Experimental Studies of Rotational Relaxation Processes. *Int. J. Mass Spectrom.* **1999**, *187*, 589−602.
(245) Wolk, A. B.; Leavitt, C. M.; Garand, E.; Johnson, M. A. Cryogenic Ion Chemistry and Spectroscopy. *Acc. Chem. Res.* **2014**, *47*, 202−210.
(246) Rizzo, T. R.; Stearns, J. A.; Boyarkin, O. V. Spectroscopic Studies of Cold, Gas-Phase Biomolecular Ions. *Int. Rev. Phys. Chem.* **2009**, *28*, 481−515.
(247) Cismesia, A. P.; Bailey, L. S.; Bell, M. R.; Tesler, L. F.; Polfer, N. C. Making Mass Spectrometry See the Light: The Promises and Challenges of Cryogenic Infrared Ion Spectroscopy as a Bioanalytical Technique. *J. Am. Soc. Mass Spectrom.* **2016**, *27*, 757−766.
(248) Lapthorn, C.; Pullen, F.; Chowdhry, B. Z. Ion Mobility Spectrometry - Mass Spectrometry (IMS-MS) of Small Molecules: Separating and Assigning Structures to Ions. *Mass Spectrom. Rev.* **2013**, *32*, 43−71.
(249) Schneider, B. B.; Nazarov, E. G.; Londry, F.; Vouros, P.; Covey, T. R. Differential Mobility Spectrometry/Mass Spectrometry History, Theory, Design Optimization, Simulations, and Applications. *Mass Spectrom. Rev.* **2016**, *35*, 687−737.

DOI: 10.1021/acs.chemrev.9b00395
Chem. Rev. 2020, 120, 3261−3295

(250) Daly, S.; MacAleese, L.; Dugourd, P.; Chirot, F. Combining Structural Probes in the Gas Phase - Ion Mobility-Resolved Action-FRET. *J. Am. Soc. Mass Spectrom.* **2018**, *29*, 133−139.
(251) Kamrath, M. Z.; Rizzo, T. R. Combining Ion Mobility and Cryogenic Spectroscopy for Structural and Analytical Studies of Biomolecular Ions. *Acc. Chem. Res.* **2018**, *51*, 1487−1495.
(252) Hoffmann, W.; Marianski, M.; Warnke, S.; Seo, J.; Baldauf, C.; von Helden, G.; Pagel, K. Assessing the Stability of Alanine-Based Helices by Conformer-Selective IR Spectroscopy. *Phys. Chem. Chem. Phys.* **2016**, *18*, 19950−19954.
(253) Valiyaveetil, F. I.; Sekedat, M.; MacKinnon, R.; Muir, W. Structural and Functional Consequences of an Amide-to-Ester Substitution in the Selectivity Filter of a Potassium Channel. *J. Am. Chem. Soc.* **2006**, *128*, 11591−11599.
(254) Chouinard, C. D.; Nagy, G.; Webb, I. K.; Shi, T.; Baker, E. S.; Prost, S. A.; Liu, T.; Ibrahim, Y. M.; Smith, R. D. Improved Sensitivity and Separations for Phosphopeptides Using Online Liquid Chromotography Coupled with Structures for Lossless Ion Manipulations Ion Mobility−Mass Spectrometry. *Anal. Chem.* **2018**, *90*, 10889−10896.
(255) Faleh, A. B.; Warnke, S.; Rizzo, T. R. Combining Ultrahigh-Resolution Ion-Mobility Spectrometry with Cryogenic Infrared Spectroscopy for the Analysis of Glycan Mixtures. *Anal. Chem.* **2019**, *91*, 4876−4882.
(256) Berthias, F.; Maatoug, B.; Glish, G. L.; Moussa, F.; Maitre, P. Resolution and Assignment of Differential Ion Mobility Spectra of Sarcosine and Isomers. *J. Am. Soc. Mass Spectrom.* **2018**, *29*, 752−760.

DOI: 10.1021/acs.chemrev.9b00395
Chem. Rev. 2020, 120, 3261−3295